Investigation of Alkali-Silica Reactions in Different Cement Systems by Thermodynamic Modelling

By

Haoliang Jin

Supervisors:

Professor John L. Provis

Dr. Hajime Kinoshita

A thesis submitted in total fulfilment of the requirements for the degree of

Doctor of Philosophy

Department of Materials Science and Engineering

The University of Sheffield

March 2024

Abstract

Alkali silica reaction (ASR) is a crucial concrete durability problem that causes swelling and degradation in the process of service. It involves the chemical reaction between the reactive silica content of aggregates used in concrete, and alkali sources in the pore solution or from the aggregate itself. This problem, also named as “concrete cancer”, has been reported for more than 80 years with respect to its mechanism and mitigation methods. However, due to the variable material compositions and different testing conditions and duration time, controversy between opinions is always presented in the literature. Therefore, the aim of this study is to use thermodynamic modelling instead of experimental methods to investigate ASR, eliminating the effects of variabilities mentioned above.

Thermodynamic parameters of shlykovite-type ASR products, which have similar microstructure and chemistry to field-observed ASR products, were firstly refined and built up in this study. New pH values of two shlykovite products gained from GEM-Selektor v.3 software were implemented and used in the calculation of solubility products. Other thermodynamic parameters were also introduced through a correlation based on formula unit volumes. Binary phase diagrams were used to show the relationship between oxide concentrations and phases formed. Without alkali ions, only C-S-H and amorphous silica were found. Increasing the concentration of alkalis leads to the formation of shlykovite-type products. However, there is a maximum concentration of alkalis that enables the formation of ASR products due to the suppression of calcium solubility.

The well-agreed method to mitigate ASR is the incorporation of supplementary cementitious materials (SCMs). The study here systematically selected four types of SCMs (ground granulated blast furnace slag (GGBFS), silica fume (SF), metakaolin (MK) and fly ash (FA)) and explained each role in mitigating ASR via thermodynamic modelling. A newly-designed two-step modelling method was used to separate the process of hydration and ASR, to establish the relationship among amount of portlandite, alkali contents in the pore solution, and the volume of ASR products formed for the first time.

The simulation results indicated that the consumption of $Ca(OH)_2$ and the reduction of alkali content in the pore solution decrease the volume of K- and Na-shlykovite products formed. The former aspect is responsible for the hydration via latent hydraulic or pozzolanic reactions, while

the latter is attributed to a dilution effect and formation of more of the alkali-bearing end-member of the C-S-H solid solution. However, Al-rich SCMs (MK and FA) have weaker ASR-resisting performance based on the modelling outcomes, which contrasts with experiments. This does not mean that this modelling fails to work in these materials. Rather, this indirectly supports the idea that the role of Al is to slow the dissolution of reactive silica from aggregates, rather than forming Al-bearing zeolites.

Lastly, by changing the types, dosages, and modulus of activators (NaOH, Na_2SO_4, Na_2CO_3, Na_2SiO_3), the thesis investigates ASR in alkali-activated slag cements. Compared with Portland cement, there is no K-shlykovite and much less Na-shlykovite predicted to form in the simulations of alkali activated cements. Na-shlykovite was formed only with 0.5-2% and 8% equivalent Na_2O added as NaOH, and only formed at the lowest dosage simulated (2%) for the rest of the activators. For waterglass activation, the volume of ASR products increases when increasing the waterglass modulus. Combining the results of solution chemistry and phase assemblages, the higher concentration of Ca in the pore solution after hydration is the main reason for forming Na-shlykovite. Even though there is a much higher concentration of alkali in the pore solution of alkali-activated cement, less portlandite was found and this avoids triggering the process of ASR.

The results shown in this study prove that it is plausible to observe and analyse the formation of ASR products and reaction process by using thermodynamic modelling. The improved thermodynamic database for shlykovite-type products at ambient temperature fills in gaps because of the lack of the understanding about ASR products, and improves the accuracy of ASR simulation. The thesis provides new thermodynamic insights into the mechanism by which SCMs enhance concrete durability against ASR. Raw materials with unknown compositions may also have a new and time-saving way to predict expansion, instead of depending on slow laboratory testing methods. This advantage is also reflected in different cement systems.

Acknowledgments

First of all, I would like to extend my sincerest gratitude to my supervisor, Professor John L. Provis, whose guidance, expertise, and unwavering support have been indispensable throughout my doctoral journey, especially during the COVID-19 pandemic when all our interactions shifted online. Despite the challenges posed by the unprecedented circumstances, he provided unwavering guidance and encouragement, which enabled the smooth progress of my research work. His insightful feedback and advice have been instrumental in my growth throughout my doctoral journey.

I am also deeply thankful for my supervisor's care and assistance during the final stages of my PhD. Despite not being physically present on campus due to work commitments, he remained fully engaged in the editing process of my thesis, offering meticulous revisions and constructive feedback for each chapter. His dedication and expertise have significantly contributed to the enhancement of the academic quality of my thesis, ensuring its adherence to the highest standards.

I want to extend my heartfelt appreciation to my postdoctoral supervisor Dr. Sam Ghazizadeh, who has been an unwavering source of support and guidance throughout my academic journey. We first met during my master's studies, where his encouragement played a pivotal role in shaping my research interests. During my doctoral studies, he continued to mentor and support me, akin to a trusted friend. Together, we navigated through software intricacies and meticulously edited every word of my thesis. Even after completing his postdoctoral project and transitioning to the company, he continued to offer his guidance without interruption. Many of our discussions extended into late-night hours, underscoring his dedication to my academic and personal growth.

Lastly, I am profoundly grateful to my family for their unwavering support and sacrifice throughout my academic pursuits. My parents provided financial assistance that enabled me to pursue my doctoral studies in the UK. Their unwavering belief in my abilities and their selfless dedication to my education have been instrumental in my success.

I also owe a debt of gratitude to my wife Ning Mao, who stood by my side despite the challenges of a long-distance relationship spanning three years. Her unwavering support, patience, and encouragement served as a constant source of motivation, propelling me forward in the face of adversity. Her enduring commitment to our relationship and her belief in my dreams have been a guiding light throughout my doctoral journey.

Contents

List of Figures

List of Tables

Chapter 1 . INTRODUCTION

Concrete plays an indispensable role in the infrastructure and construction industries, and for now its demand still increases with the development of society. The side effects raised by this, such as increasing emission of CO_2 and the need to dispose of construction wastes from demolishing old or low-quality buildings are worth the consideration of each cement researcher. Improving the long-term performance of concrete by dealing with durability problems is an efficient way to alleviate the impacts mentioned above. One of the most severe endogenous issues is the alkali silica reaction (ASR).

Investigation of the alkali silica reaction in concrete has been reported extensively since the 1940s. Due to the chemical reaction between alkali sources, mainly from the pore fluid of cement, and reactive silica dissolved from aggregates, expansive products form and can thus cause expansion and cracks in the concrete, which reduce the life service of concrete or spend money repairing or replacing structures. In order to identify this damage before it happens, petrographic examination and criteria for reactivity of unknown aggregates were presented in major documents such as RILEM recommendations and BRE Digest 330. However, some countries such as Canada, Iceland and Brazil inevitably use local highly reactive aggregates. More attention was thus paid to mitigation methods recently, such as the incorporation of supplementary cementitious materials (SCMs) and lithium compounds.

Despite experiments performed in recent papers showing that less ASR expansion is generated with the addition of SCMs, it depends on the composition of materials. In other words, contradictory results are gained from various research studies with different cementitious compositions, via different testing methods. In addition, the conditions of formation of ASR products remain unknown, as limited studies elaborate the relationship among the concentration of calcium, the alkali contents in the pore solution, and the precipitation of expansive products. The mechanism of the limited expansion caused in alkali-activated cement is also unclear.

One of the most important factors that restricts the application of thermodynamics in the study of ASR is the lack of an appropriate database describing the thermodynamics of the likely products of ASR.

Therefore, the main aim of this thesis is to qualitatively analyse the condition of the formation of ASR products via thermodynamic approaches, and then compare these findings with experimental results shown in the literature. The objectives are shown as follows:

- Two synthetic shlykovite-type ASR products at 80 °C were selected to represent the field ASR products, and their thermodynamic parameters at ambient temperature are refined and established. This can provide an accurate database for further modelling performed in the real cement systems.
- The formation of ASR products and other hydrates is predicted in the $(Na,K)_2O$-CaO–SiO_2-H_2O system. Binary phase diagrams are presented to show solubility curves and corresponding phase formation regions.
- A two-stage (time-separated) thermodynamic modelling approach is used to separate cement hydration and ASR process, to probe questions related to the potential formation of ASR products in cements blended with different SCMs. Combining phase assemblage and solution chemistry results, the role of each SCM in mitigating ASR is explained.
- The same method is applied to observe the volume of ASR products formed in slag-based alkali-activated materials (AAMs), considering different types and dosages of activators. The differences between the two types of cement systems with respect to the formation of ASR products is discussed.

Experimental-based papers mainly measure the expansion caused by ASR instead of measuring the amount of ASR products formed, because the latter needs more advanced measurement and equipment. Also, the reasons for ASR expansion are not only from the formation of ASR products, but also depend on other factors, for example, the porosity of the cement. However, it is meaningful to use these modelling results to compare with experimental expansion outcomes, which can help better understand the precipitation conditions and avoid it. The more

knowledge about different types and composition of ASR product can be generated, and the more complete the thermodynamic database is, the better the modelling results are.

Chapter 2 presents a literature review about the mechanisms of ASR and factors that affect the process of ASR. A series of reactions when ASR happens includes the dissolution of reactive aggregates, the formation of ASR products, and the resultant swelling, which affects by alkalis sources, reactive aggregates and moisture. Mitigation methods for ASR are also discussed, with a focus on the use of supplementary cementitious materials (SCMs) and other strategies. This chapter also covers the fundamental basis of thermodynamic modelling. The potential of thermodynamic modelling in studying ASR is also discussed.

Chapter 3 discusses the estimation of thermodynamic parameters of two shlykovite-type ASR products which have similar structures compared with those found in field concretes. They are used as potential reaction products for prediction of phase formation in the $(Na,K)_2O$-CaO–SiO_2-H_2O system. Beginning with an introduction outlining the incompleteness of the existing thermodynamic database, the chapter details the refinement of it by replacing new concentration of hydroxyl ion and the estimation of thermodynamic parameters for ASR products. Results of thermodynamic modelling considering different concentrations of elements and temperatures are presented, and the conditions that lead to formation of ASR products are discussed. Data of solution chemistry for corresponding points in the binary phase diagram are used to further explain the interaction between reactants and the aqueous solution.

Based on the newly built-up database for shlykovite-type products, Chapter 4 applies thermodynamic modelling in real cement systems with the potential to show ASR. Different SCMs including GGBFS, SF, MK, and FA are used to discuss the role of each in mitigating ASR. A newly-designed two-stage modelling method is introduced to separate the cement hydration and ASR process. The phase assemblage and solution chemistry in the cement hydration stage are analysed to find the triggering factors of ASR. The role of Al is discussed to explain its better performance in inhibiting ASR.

The work described in Chapter 5 is intended to apply this modelling method into alkali activated cement and investigate the volume of ASR products formed. Ground granulated blast furnace slag is used as an aluminosilicate precursor. The simulation considers four activators that are extensively used in AAM, with different dosages from 2% to 8% of equivalent Na_2O. For silicate activators, different modulus values from 0.5 to 2 are also considered. As for the Portland cement blends in Chapter 4, the phase assemblage and solution chemistry in the cement hydration stage are also analysed. The aim of this chapter is to investigate ASR in AAM and then compare with the processes observed in Portland cement, and the results show that expansion caused in AAMs is less than in Portland cement, although the former has more alkalis.

Lastly, Chapter 6 summarises the main conclusions from this study and also gives some recommendations for further work on developing the database for other types of ASR products, and the modelling for classifying reactive aggregates and filtering useful SCMs to mitigate ASR, rather than depending on experiments only.

Chapter 2 . LITERATURE REVIEW

2.1 Introduction

2.1.1 Alkali-silica reaction

Achieving an increase in the lifespan of concrete, and thus in the efficiency of use of natural non-renewable resources, requires improving the durability of concrete. This includes enhancing the response of concrete to chemical attack and solving internal detrimental problems, for example, alkali-silica reaction (ASR). This phenomenon was first found by Stanton in the 1940s (Stanton et al., 1942) and almost 90 years of investigation has shown that this involves the chemical reaction between the reactive silica content of aggregate used in concrete, and alkali sources in the pore solution or from the aggregate itself. The resulting gel-like products swell when exposed to moisture in the process of service, which causes internal pressure and leads to the formation of cracks and degradation of the concrete structure over time (Diamond, 1975, 1976).

Hydraulic structures such as dams, bridges, and undersea tunnels that suffered from harmful ASR problems have been reported all around the world, especially for those coastal countries such as Australia and northern countries such as Iceland, Canada and the United States (Bérubé & Fournier, 1993; Shayan et al., 1988; Gudmundsson & Olafsson, 1999), as this issue is largely triggered by some additional factors, for example using high-alkali cement, exposure to moist environments, and inevitably using local reactive aggregates. In addition, South Africa has reported some cracking incidents in concrete structures associated with ASR (Oberholster et al., 1978). Therefore, in order to inhibit detrimental damage taking place in structures and to prolong their service life, methods such as using low alkali cements and incorporating supplemental cementitious materials and lithium compounds were implemented.

2.1.1.1 Mechanism of ASR

A series of continuous steps representing a relatively well-agreed ASR mechanism was proposed by Figueira et al. (Figueira et al., 2019), as shown in Figure 2-1: (1) dissolution of

silica; (2) formation of silica sol and further gel, and (3) swelling of the gel. Each step will be described as follows.

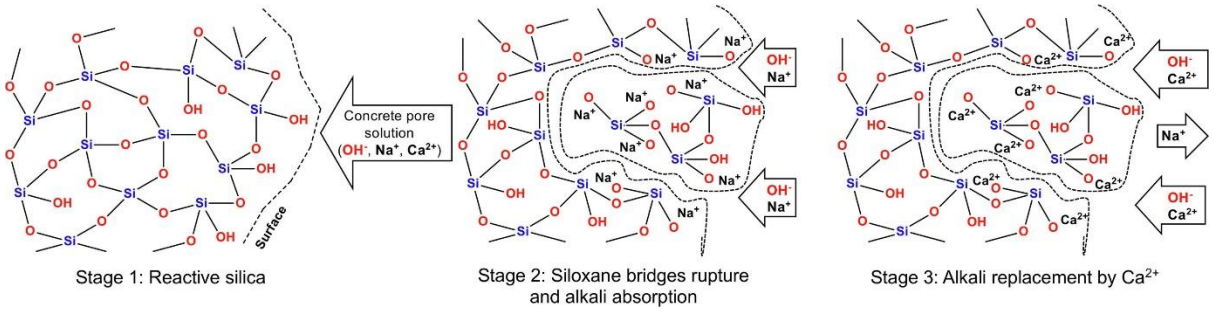

Figure 2-1 Schematic representation of the possible process of alkali-silica reaction (ASR) happening in the aggregate in concrete. Reactive silica from the aggregate is dissolved by hydroxyl ions and reacts with alkali ions, resulting in the formation of expansive ASR gel, thus causing cracks inside the aggregate. Adapted from (Figueira et al., 2019).

Dissolution of silica

Aggregates in concrete are often comprised of different types of silica and/or silicate, and they are considered as sources of Si as claimed by the definition of ASR. Two categories divided according to different degree of chemical ordering are shown in Figure 2-2, and this determines the process and rate of dissolution (Diamond, 1976). Uniformly sized silica rings make up the first one (Figure 2-2a) which is a form of crystalline solid silica where each oxygen atom in Si tetrahedral units (silicon atoms with four oxygen atoms) acts as a bridging oxygen and directly connect with other Si tetrahedral units (Zachariasen, 1932). Quartz is a typical example of this. Another type (Figure 2-2b), for example, silicate glasses, is amorphous or disordered. Some bonds involving oxygens are occupied by alkali metal or calcium ions, which forms so-called non-bridging oxygen sites. The starting point of ASR is the dissolution of these silica structures from the aggregate into solution.

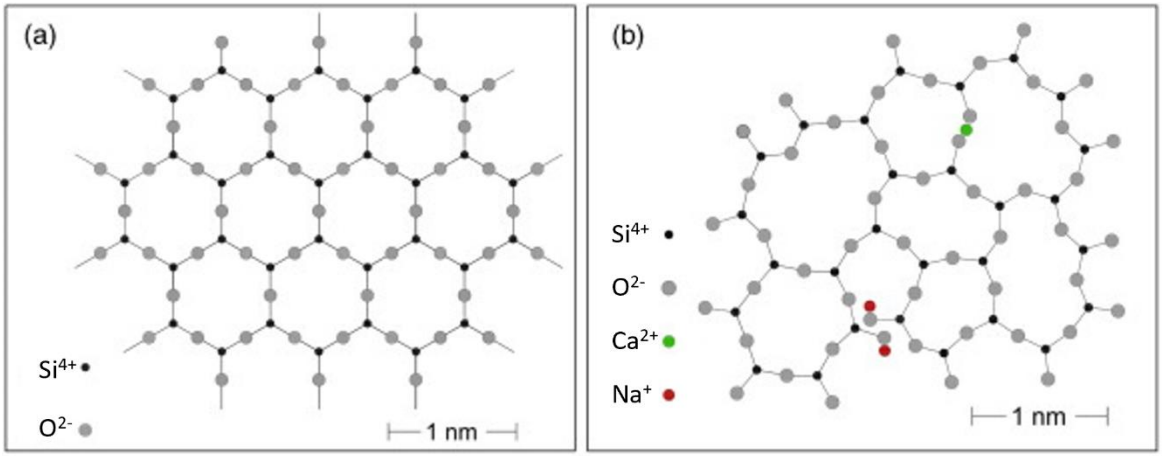

Figure 2-2 Ball-and-stick representation showing two types of silica structure. a: crystalline solid silica with uniformly sized ring structure, b: an amorphous solid silicate which contains bridging oxygen and non-bridging oxygen connected with alkali and calcium ions, adapted from (Rajabipour et al., 2015)

Overall, the rate of dissolution of silica in neutral water at ambient temperature is quite slow, regardless of the different types of crystal or amorphous structure [3]. However, the pore solution in cements, with a high pH, has a great effect on this progress (Maraghechi, 2014; Sjöberg, 1996). For crystalline solid silica, the dissolution caused by hydroxyl ions is rather slow because the large bond energy barrier between silicon atoms and bridging oxygen is difficult to overcome for the bond to be broken (Dent Glasser & Kataoka, 1981). An equation representing this reaction is shown in Eq.2-1, where ≡Si-O-Si≡ is a siloxane group in the interior of the silica. On the other hand, in poorly crystalline structures with more lattice defects, or etch pits, hydroxyl ions and alkali ions in the cement system can more easily break the bond structure, thus triggering dissolution reactions [4]. Eq. 2-2 shows this process. Here ≡Si-OH represents the silanol group at the surface of silica interacting with solution (Powers & Steinour, 1955). In addition, breakage of the silanol group in turn opens more space for attack on other siloxane groups, which provides more opportunities to aggravate the dissolution and repeat the reaction shown in Eq. 2-1, inside the aggregate (Walther & Helgeson, 1977).

$$\equiv Si - O - Si \equiv + 2OH^- \rightarrow 2 \equiv Si - O^- + H_2O \qquad \textbf{Eq.2-1}$$

$$\equiv Si - OH + OH^- \rightarrow \equiv Si - O^- + H_2O \qquad \textbf{Eq.2-2}$$

Formation of silica sol and further gel

Negatively charged products shown on the right side of Eq. 2-1 and Eq. 2-2 inhibit gelation reactions and result in the suppression of the dissolution when solution reaches the Si solubility limit (Dent Glasser & Kataoka, 1981). However, a gel is developed in the presence of alkali ions such as sodium and potassium ions present in the pore fluid resulting from cement hydration. They penetrate into "broken" structures through sites created from previous dissolution processes and balance the negative charge, as shown in Eq. 2-3 where M^+ indicates alkali metal ions and … means that this type of bond may be strong Van der Waals bonding (Rajabipour et al., 2015). Wang and Gillott (Wang & Gillott, 1991) noted that alkali ions can also exchange the protons of the silanol group in the left side of Eq. 2-2 directly, and produce alkali-silica complexes at the surface of aggregates.

$$\equiv Si - O^- + M^+ \rightarrow \equiv Si - O \ldots M \qquad \textbf{Eq.2-3}$$

This reaction reduces the pH of the pore fluid, thus potentially reducing the further dissolution of silica. However, Portland cement contains adequate calcium ions that accelerate the further reaction. Calcium hydroxide forms around the aggregate in the interfacial transition zone, and its lower solubility than alkali ions, particularly at high pH, means that the alkalis first penetrate into silica structure (Wang & Gillott, 1991). As pH reduces when forming an alkali silica sol, calcium hydroxide starts to dissolve and can also penetrate into the structure. These calcium ions may replace the alkalis in the sol and continue to condense it. Eq. 2-4 illustrates this reaction.

$$2 \equiv Si - O \ldots M + Ca^{2+} \rightarrow \equiv Si - O \ldots Ca \ldots O - Si \equiv + 2M^+ \qquad \textbf{Eq.2-4}$$

On the other hand, Chatterji et al. (Chatterji et al., 1989) provided a different opinion on the diffusion of ions. Those authors used the size of ions to explain this reaction, where the effective size of calcium complex ions is larger than the alkali ions (Chatterji, 1987). Therefore, it is more difficult for calcium ions to penetrate into silica grains before dissolution. As mentioned above, the dissolution process loosens the structure, and this allows larger of ions

to enter and cause replacement. Wang & Gillott (Wang & Gillott, 1991) attribute diffusion to the concentration difference between the cement pore solution and aggregate grain.

In terms of the role of calcium ions, different ideas exist. Powers and Steinour (Powers & Steinour, 1955) stated that the different amount of calcium ions affect the types of products. If the calcium source is limiting in the raw material and dissolved calcium ions are restricted, some of them can penetrate into aggregate grains and form low-Ca ASR products. However, if the calcium ions are high enough in concentration around the aggregate, a phase more closely resembling the composition of calcium silicate hydrate (C-S-H) in Portland cement will form. The former is observed to transform to C-S-H in synthetic systems (Leemann et al., 2016). In recent years, different types of testing methods such as micro X-ray absorption spectroscopy (XAS), X-ray powder diffraction (XRD) and X-ray Absorption Near Edge Structure (XANES) showed that C-S-H and amorphous ASR products have certain similar structural features, and this will be explained in more detail in section 2.1.2. (Geng, Shi, Leemann, Borca, et al., 2020; Honorio et al., 2020; Leemann et al., 2020).

Swelling of the gel

The cracking of concrete caused by the swelling of ASR gel has been observed to take place when immersed in a high moisture environment, or in a position with less sunlight exposure (Duncan, 1973; Nixon et al., 1979). However, varying opinions are held by different researchers on this matter. For example, silica gel is considered as a porous structured product with large surface area which is surrounded by hydrophilic groups, as shown in Figure 2-3a, and it tends to dominate osmosis and swelling (Hench & Clark, 1978; Powers & Steinour, 1955). Conversely, Geng et al. (Geng et al., 2021) argued that some of the ASR products are crystalline and are limited in the ability to uptake water and cause swelling. From the perspective of the microstructure, Garcia-Diaz et al. (Garcia-Diaz et al., 2006) stated that the observed transformation from Q^4 to Q^3 tetrahedral silica caused by the presence of hydroxyl ions creates expansive ASR products, thus leading to an increase in the pore volume and further development of swelling. Figure 2-3b shows the theory of ion diffusion for the formation of cracking in the concrete (Ichikawa & Miura, 2007). Chatterji et al. (Chatterji et al., 1986) investigated this using X-ray diffraction associated with electron probe analysis, and thought that a differential diffusion rate between alkali ions and silicon ions leads to swelling. The rate

of penetration of alkali ions into the aggregate is higher than the rate of diffusion of silicon ions out of the aggregate. This idea has been supported by Ichikawa and Miura who thought that alkali silica gel formed around the aggregate can be treated as a semi-permeable membrane (Ichikawa & Miura, 2007). This membrane allows the penetration of the alkaline solution but not the alkali silicate gel, and therefore keeps the expansive pressure within the reacting aggregate. The accumulated pressure cracks the aggregate and surrounding cement.

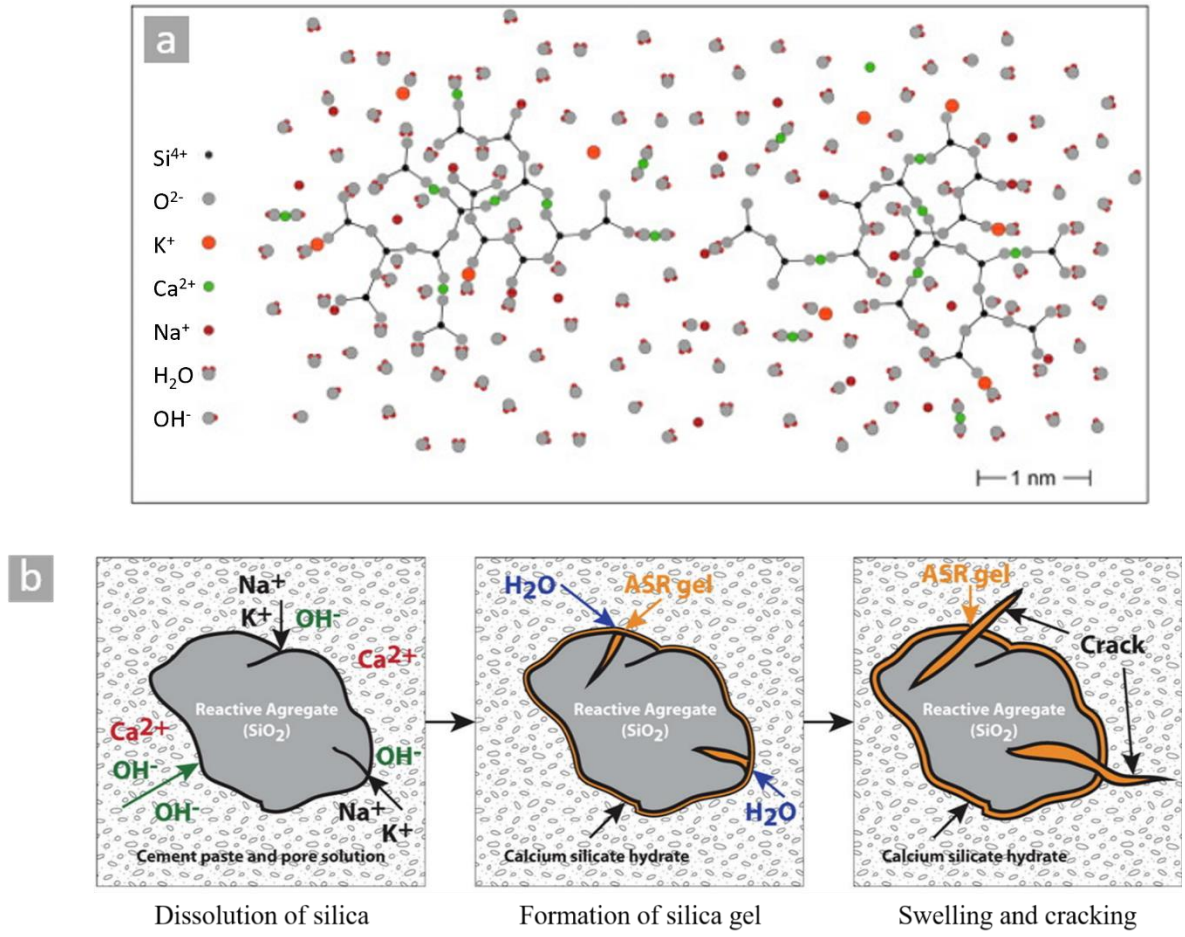

Figure 2-3 a: Representation of alkali silica gel formed in the pore solution with water and alkali ions from cement. b: Schematic representation of the process of cracking caused by ASR. Reaction rim generated from hydrated alkali silicate with the exchange of calcium ions around the aggregate eventually results in cracks inside the aggregate. Adapted from (Figueira et al., 2019)

2.1.1.2 Factors inducing ASR

According to the proposed mechanism of ASR damage, it is clear to summarise three main factors that induce the damage taking place. It is necessary to provide directions for how to prevent this reaction, and also to help researchers select non-damage-prone raw materials when producing concrete, to mitigate it from the beginning. Here three main reasons are listed, with explanations of their properties.

Reactive aggregate

Any aggregate grain containing silica has the potential reactive constituents for ASR to take place, based on the dissolution mechanism of the ASR reaction, but most of them will never react because the silica is in unreactive forms. However, there are some effects influencing the properties of aggregate which determine whether the reaction will be problematic (Rajabipour et al., 2015). The first one is the mineral constituents of aggregates. In early research studies, rock types instead of constituents were considered a determining factor for whether or not expansion happened (Poole, 1991). However, although the rock types may be the same, the reactive constituents can also show differences to some extent. This is mainly because the priority factor that needs to be considered is rock deformation. For example, natural or artificial aggregates can contain amorphous silica, often formed by rapid cooling or quenching from high temperature. This process leads to formation of lattice defects and/or residual strains (Maraghechi et al., 2012; Rajabipour et al., 2010). In addition, it is inevitable to form micro-cracks and microporosity when crushing aggregates in the concrete industry, and these acquired defects plus interior defects offer hydroxyl ions and alkali ions in the pore solution the natural paths to penetrate into aggregate grains (West, 2010). Here the types of aggregates that are prone to react are as follows:

Glassy silicates

Silicates having short-range order but long-range disorder are considered to be glassy. This is attributed partially to connection of non-bridging oxygen atoms with cations such as Ca, Na, and K, and is also due to various angles of Si-O-Si bonding between Si tetrahedra (Brauer & Möncke, 2016). The acidic character of some volcanic silicates such as rhyolitic, andesitic, and basaltic glasses leads to the reactivity of this type of aggregate. Additionally, a weak internal

structure in the presence of water molecules may be another reason for silicates to be reactive (Diamond, 1976).

Siliceous limestone

Limestone is a sedimentary carbonate rock, but in the siliceous type, amorphous silica partially replaces calcite in its structure. A petrographic report from Monnin et al. shows that reactive contents in siliceous limestone are xenomorph silica, chalcedony, and microcrystalline quartz (Monnin et al., 2006). Garcia-Diaz also found that there is some potential reactive free silica in the form of anhedral quartz in the siliceous limestone, which can cause ASR expansion (Garcia-Diaz et al., 2010).

Cryptocrystalline quartz

Quartz with a well-defined structure is always considered to be inert in ASR expansion testing, and is called macrocrystalline quartz. However, cryptocrystalline quartz has poorly crystalline silica, and chalcedony is a typical example of this type of quartz (Min et al., 1996). Its structure determines the reactivity of these aggregates.

Opaline silica

According to Jones and Segnit's work, natural hydrous silica can be divided into five parts: opal, opal-A, -C, and -CT, and opaline silica (Jones & Segnit, 1971). Opaline silica is representative of poorly crystalline silica, combining with hydroxyl groups in the silica surface (Gillott, 1975). As mentioned in Eq. 2-2, silanol groups at the surface of silica interact with solution and provide more spaces that allow hydroxyl ions in the pore solution of cement to attack the interior silica tetrahedra.

The second factor affecting the reactive properties of aggregate is the size. It is generally accepted that the particle size of reactive aggregate has a correlation with the expansion produced: there is a ‘pessimum size’, and expansion decreases when the size of reactive aggregate increases or decreases from this. It is worthwhile to note that the prerequisite should

be ensured that aggregates have at least similar mineral constituents when comparing their size effect. Multon et al. believed that the time of diffusion of hydroxyl and alkali ions depends on the size of aggregate, which led them to observe that expansion with larger aggregates was seven times more than that with smaller grains, although further increasing the size of aggregate slows down the penetration of ions into aggregates, thus affecting the degree of expansion. (Multon et al., 2008, 2010). Bazant and Steffens (Bazant & Steffens, 2000) proposed that larger size particles of aggregate easily cause larger swelling pressure and then affect nearby cement paste to form cracks, which is consistent with the results obtained by Dunant (Dunant & Scrivener, 2012). Gao et al. (Gao et al., 2013) also considered the relationship between aggregate size and specimen size, and found another effect called the scale effect: a larger ratio between the aggregate and specimen sizes causes greater stress intensity and cracks inside and around the aggregate.

Further reducing the size of artificial aggregates to a cement particle size range is also considered, and reactive silicates are used as supplementary cementitious materials (SCMs) when producing mortar or concrete. This has been studied for many years, and it has been proven that it may help mitigate expansion caused by ASR. One hypothesis to explain this is the pozzolanic reaction. Poyet et al. presented a chemical model and investigated expansions for different ranges of particle size from fine group (0.08-0.16 mm) to coarse group (2.5-3.15 mm) (Poyet et al., 2007). They believed that the fine aggregate group has no significant expansion. Ichikawa (Ichikawa, 2009) stated that reactive aggregates with a grain size lower than 50 μm undergo the pozzolanic reaction instead of ASR, where alkali ions and portlandite are consumed to form calcium silicate hydrate before completing the process of ASR .

In terms of the reactive content of aggregate as the third reason for triggering ASR, it also has a ‘pessimum’ effect: that is, when the reactive content reaches some level, a maximum expansion can be obtained, while the trend of expansion shows a decrease in both situations where reactive content decreases or surpasses the maximum level (Hobbs, 1988). Some researchers believed that the ‘pessimum’ effect depended on a corresponding pessimum size effect (Dent Glasser & Kataoka, 1981). However, when reducing the size of aggregate, the reactive content in aggregate does not change.

Alkali content

Alkali ions in conventional concretes mainly come from the Portland cement, which determines the pH level (connected to the hydroxyl ions concentration) of pore fluid. In addition, aggregates themselves, and external sources such as de-icing salts and SCMs, also contribute to the overall level of alkali ions. Therefore, in this section different sources of alkali will be introduced.

As cement producers focus on environmental protection and economic efficiency, alkalis from clay and other siliceous raw materials are left in kilns due to less vented equipment, and reuse of alkali-rich kiln dust leads to producing more alkali-rich cement and concrete, which aggravates the problem of ASR (Diamond, 1975). In general, the alkali content in cement is described based on Eq. 2-5, where 0.658 is the molecular weight ratio between Na_2O and K_2O (Hobbs, 1988).

$$Na_2O_{eq} = Na_2O + 0.658K_2O \qquad \textbf{Eq.2-5}$$

Supplementary cementitious materials are another source of alkalis, especially for fly ash, metakaolin, and silica fume which sometimes exceed that present in the Portland cement. For low to moderate alkali SCMs, the amount of alkalis in the cement matrix decreases due to the dilution effect (Kawabata & Yamada, 2017). Also, the lower Ca/Si ratio of the C-S-H formed gives a greater capability to bind alkalis, which causes the reduction of alkalis in the pore solution (Duchesne & Bérubé, 2001). However, when it comes to high alkali SCMs, for those alkalis that are present in crystalline structures, they may be non-reactive and safe considering reaction with aggregates (Glosser et al., 2021). While glassy phases in the SCMs contain more alkalis, they are available for long-term reaction due to relatively slow dissolution which may cause expansion. Figure 2-4 shows the relationship among alkalis, calcium content and expansion at 2 years for a set of concrete prisms with fly ash blended binders and reactive aggregates. Considering similar alkali contents, higher calcium causes higher expansion. However, compared with fly ash with intermediate Ca shown in the middle area of Figure 2-4, the expansion increases with increasing alkali contents (Boddy et al., 2003; Lorenzo et al., 1996; Shehata & Thomas, 2002, 2006).

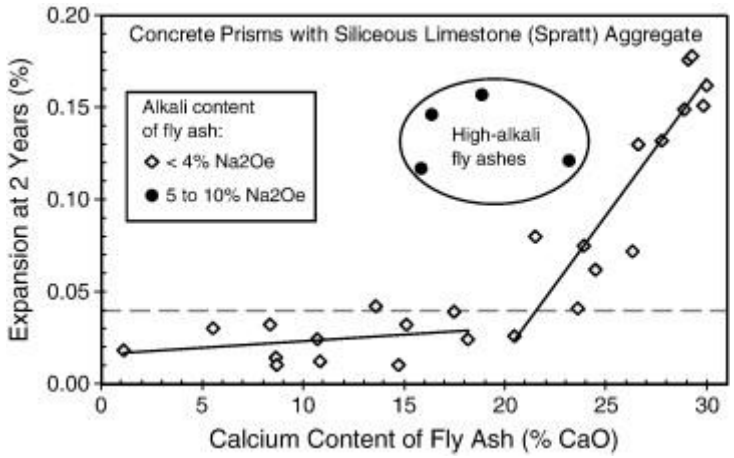

Figure 2-4 The relationship among alkalis, calcium content, and 2-year expansion in concretes made using fly ash blended cement. From (Thomas, 2011)

Alkalis in aggregates can be contributed by crystalline structured minerals or glassy phases. Once hydroxyl ions attack the aggregate structure, these alkalis are released into the pore solution. This factor also influences the whole level of alkalis that needs to be considered when assessing ASR risk. The typical examples with silicate crystalline structures are feldspar, basalts mica, and zeolites. In BRE Digest 330, the alkalis contributed by salts in aggregates are calculated from the measured chloride ion concentration in the aggregate and expressed as equivalent sodium oxide, shown in Eq. 2-6, although the soluble alkali content of UK aggregates is relatively small (BRE, 2004). In order to confirm the quantity of alkalis released from aggregates, many works have been done using solution-based leaching tests (Bérubé et al., 2002; Lindgård, Sellevold, et al., 2013; Menéndez et al., 2021; Multon & Sellier, 2016). While the aggregate is soaking in alkaline solution at different times, the solution is tested by titration or inductively coupled plasma (ICP) mass spectrometry methods. However, different alkaline solutions are used in different papers, which means that it is not always possible to compare results with each other, therefore, more standardised testing methods shown in Menéndez's work (Menéndez et al., 2021) should be developed in the near future.

$$Na_2O_{eq} = 0.76Cl^- \qquad \textbf{Eq.2-6}$$

Important ASR damage was found in the pavement of roads covered by deicing salts in northern countries in early research (Bérubé et al., 2003). This problem was difficult to find in cold winters since lower temperature results in low rate of diffusion in terms of alkali ions (Chatterji, 1979). However, once temperature starts to recover, alkali ions stored in the surface of pavement or in the pore solution penetrate and attack the infrastructure, and accelerate ASR and expansion. External alkali sources can include NaCl, and alkali acetates, especially potassium acetate, which have to be used carefully.

Moisture

Water controls two significant effects on ASR process. The role of water firstly is as a vehicle to transport hydroxyl and alkali ions into aggregate grain and induce further attack reaction (Lindgård, Sellevold, et al., 2013). Also, a moist environment leads to the swelling of the amorphous type of ASR gel. Duncan found that the gel itself can be seen as non-expansive and just remaining in the aggregate, without water (Duncan, 1973). Only when it is exposed to water, the expansion process takes place. Later results also confirmed that this problem would happen again if the sample is cured in a dry environment and re-stored in a moist environment (Multon & Toutlemonde, 2010). Bérubé and Fournier suggested that the relative humility (RH) should be higher than 80% for ASR to occur (Bérubé & Fournier, 1993). A similar phenomenon was found in constructed structures, where there was less ASR damage in dry and sunlight exposed areas, while more expansion occurred in the places that had accumulated water most of the year or were washed by rain (Plusquellec et al., 2018).

Another water source is contributed by the pore solution in the interior of the cement. However, different papers have different opinions on this issue. Wang and Gillott stated that concrete samples with reactive aggregates with low w/c shrunk at an early curing time (Wang & Gillott, 1991). There was then a certain level of expansion that covered the decrease of volume caused by shrinkage, which ultimately showed less expansion as a result. This idea was supported by Lindgård et al. (Lindgård, Thomas, et al., 2013). However, Smaoui et al. showed that concrete expansion increases with a decrease in w/c (Smaoui et al., 2005).

2.1.1.3 ASR in alkali activated cements

Alkali activated cement (AAC) has been paid significant attention as an alternative to traditional Portland cement (PC) in recent years, and is made by mixing aluminosilicate precursors and an alkaline activator (Provis, 2018; Provis et al., 2015). Apart from being considered as a eco-friendly binder to alleviate some of the environmental problems generated from cement and concrete industries, this cementitious material may have comparable or even superior performance compared with PC in terms of mechanical performance (Aydın & Baradan, 2012; Ding et al., 2016; Hassan et al., 2019), and chemical attack resistance (Bakharev et al., 2002, 2003; Chindaprasirt et al., 2013).

The effect of ASR on durability of AAC has been extensively investigated, but the results are contradictory. Talling and Brandstetr (Talling & Brandstetr, 1989) used different alkaline sources such as sodium or potassium hydroxide as activators to produce blast furnace slag based AAC, and their results showed that no expansion was observed during the hydration period. They attributed this to hydration products that absorbed most of the alkalis, although the pore solution of cement has more alkali ions than PC. This observation has agreement with Gifford and Gillott (Gifford & Gillott, 1996) to some extent. However, one-year expansion induced by ASR may still be problematic. Different results come from Bakharev et al. (Bakharev et al., 2001) who suggested that AAC concrete with reactive aggregates was more susceptible to ASR than conventional cement concrete, even in concrete prism testing (CPT). Recently ASR testing in AAC was conducted by the RILEM technical committee 247-DTA using both ASTM C1293 and RILEM AAR-3.1 (Winnefeld et al., 2020). Two testing methods show reliable identification of expansion: only known highly reactive aggregates displayed expansion, while there was no problem seen for non-reactive and potential expansive aggregates.

The reasons behind these contradictions may be multifactorial. Firstly, it is accepted that calcium ions have an important role in ASR expansion, and most of the precursors used in AAC contain less calcium in their composition than PC. García-Lodeiro et al. (García-Lodeiro et al., 2007) considered siliceous fly ash as a raw material to produce AAC mortar, and they found that the expansion of AAC is less than that of PC. This outcome is consistent with the findings of Wang et al. (Wang et al., 2022). The latter also used slag-based AAC as a control

group, but their results showed that fly ash based AAC has lower ASR expansion compared with slag based specimens due to the higher content of calcium in slag.

The second reason for these contradictions is the alkali activators. Shi et al. (Shi, Shi, Wan, et al., 2018) found that adding sodium silicate to produce AAC gave a higher expansion level than adding sodium hydroxide. In another study, Chen et al. (Chen et al., 2002) explored the expansion of slag-based AAC mortars that were activated with four types of activators. They used the mortar bar method to measure the expansion and found that the four systems expanded in a specific order, with waterglass showing the greatest expansion followed by Na_2CO_3, Na_2SO_4, and NaOH. From the perspective of the phases formed, less calcium hydroxide and more silicate form aluminium-substituted calcium silicate hydrate (C-A-S-H) with a low Ca/Si ratio, which binds more alkalis to prevent the ASR reaction process (Hong & Glasser, 2002; L'Hôpital et al., 2015; Myers et al., 2013). In addition, AACs with low calcium precursors precipitate another type of reaction product, called sodium or potassium aluminosilicate hydrate (N–A–S–H and K–A–S–H) gel, which consumes most of the alkali from the activator and thus mitigates the process of ASR (Provis & Bernal, 2014).

Some blended Portland cements with Al-rich SCMs such as fly ash and metakaolin were proven to have better resistance to ASR (Hay & Ostertag, 2021; Jones et al., 1992; Moser et al., 2010; Shehata & Thomas, 2002). For AACs that use these SCMs as a main mixture component, similar performance has been found in ASR research, which is supported by similar mechanisms. For example, similar to incorporating SCMs in Portland cement and forming low Ca/Si ratio of C-S-H by consuming $Ca(OH)_2$, AACs also form such phases that have greater capability of binding alkalis. In addition, Wang et al. (Wang et al., 2022) demonstrated that higher aluminium and lower calcium in fly ash based AACs are beneficial to form N-A-S-H gel, thus reducing available silica for the process of ASR.

2.1.2 Products of ASR

Although ASR is considered as 'cancer' in concretes, the lack of understanding and observation of the products of ASR restricts the understanding of this detrimental durability problem. The tiny amount of ASR products (as a fraction of the overall mass of concrete) that generally form,

and their location near the interfacial transition zone (ITZ) and inside aggregate particles, requires increasingly high resolution and spatially-resolved analytical instrumentation to properly observe and characterise these products (Boehm-Courjault et al., 2020). Additionally, when ASR products are investigated, they are sometimes difficult to distinguish from calcium silicate hydrates (C-S-H) due to their similar chemical compositions (Maraghechi et al., 2016). Recently, many advanced analytical techniques such as Raman microscopy (Balachandran et al., 2017; Leemann, 2017; Leemann et al., 2020), X-ray based measurement (Geng et al., 2021; Geng, Shi, Leemann, Borca, et al., 2020; Geng, Shi, Leemann, Glazyrin, et al., 2020), and transmission electron microscopy (Boehm-Courjault et al., 2020) have been used to observe the characteristics of ASR products, which brings better understanding about the composition and structure of ASR products.

The average atomic ratios of Ca/Si and (Na+K)/Si of ASR products have been measured to be 0.21-0.23 and 0.21-0.34, respectively, regardless of the amorphous or crystalline nature of the structures (Leemann et al., 2020; Leemann & Merz, 2013; Shi et al., 2015; Shi, Shi, Zhang, et al., 2018). However, the Na/K ratio is different between amorphous ASR products (0.46–0.76) and crystalline ones (0.10–0.27). In terms of amount of Ca in the products, the value decreases near the aggregate, while it increases when ASR products form in the cement paste (Thomas, 2001). Therefore, this is one of the reasons for difficulty of distinguishing ASR products and C-S-H inside the cracks in the cement paste based on the difference in Ca obtained via SEM-EDS mapping.

Most morphology investigations found that rosette crystalline products formed when ASR happens, shown in Figure 2-5 (Fernández-Jiménez & Puertas, 2002; García-Lodeiro et al., 2007; Leemann et al., 2020; Shi et al., 2015). The amorphous ASR products, as a plug, fill the crack formed in the interior of the aggregate and ITZ, with a thickness of a few micrometres to several hundred micrometres (shown in Figure 2-6, from Leemann et al., 2016). On the other hand, crystalline ASR products co-exist and are wrapped with amorphous ASR products. Some researchers believe that the crystalline material is considered to be a result of the aging process of an amorphous product (Peterson et al., 2006; Šachlová et al., 2010). However, the higher temperature required in the ASR testing may also result in accelerating the formation of crystalline products, which suggests that attention in explaining formation mechanisms should be paid more to the crystalline one.

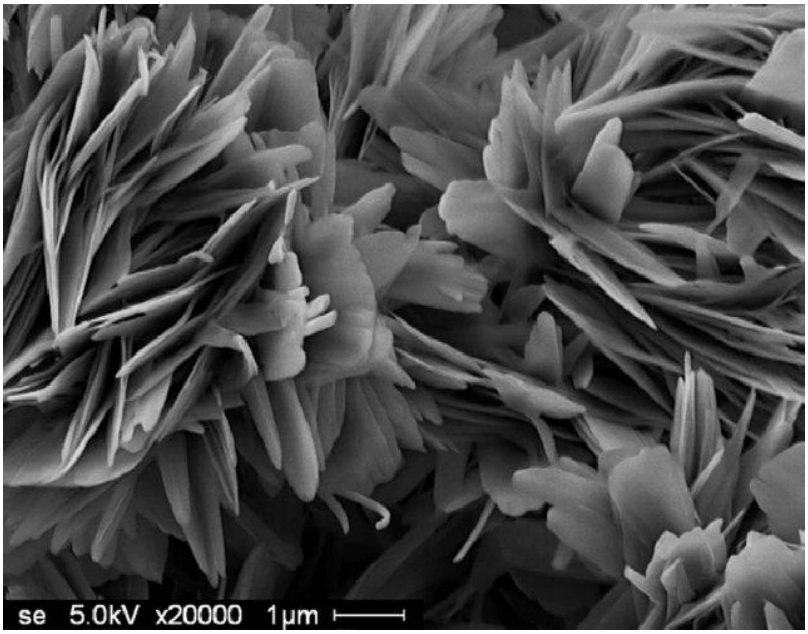

Figure 2-5 SEM image of rosette crystalline ASR products formed. Adapted from (Leemann et al., 2016)

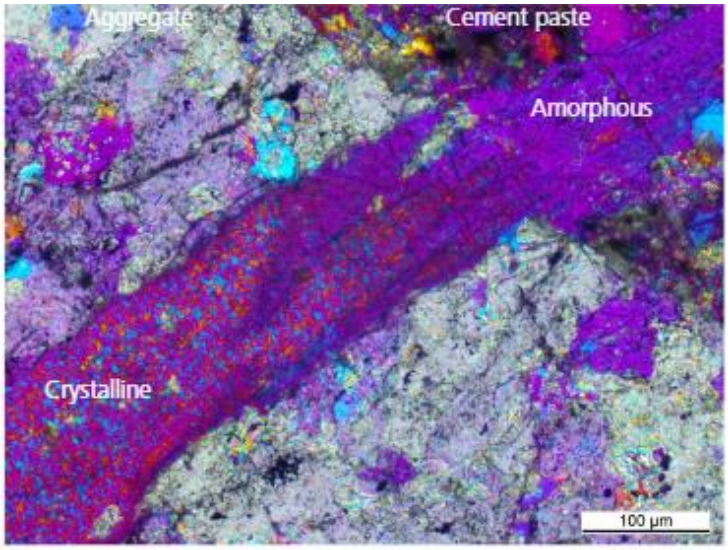

Figure 2-6 SEM image of amorphous (isotropic) and crystalline ASR products (refractive) found in a field concrete. Adapted from (Leemann et al., 2016)

To better understand crystalline ASR product structures, measurements by Raman microscopic and synchrotron micro-XRD Rietveld refinement were used, and showed that the ASR products have a layered silicate framework with cations such as sodium and potassium, and small molecules such as water, filling in the interlayer (Geng et al., 2021; Geng, Shi, Leemann, Borca, et al., 2020; Leemann, 2017; Leemann et al., 2016). Natural minerals such as cryptophyllite

($K_2CaSi_4O_{10}·5H_2O$) (Zubkova et al., 2010), mountainite ($KNa_2Ca_2[Si_8O_{19}(OH)]·6H_2O$) (Kawabata & Yamada, 2017) and rhodesite ($KHCa_2[Si_8O_{19}]·5H_2O$) (De Ceukelaire, 1991) are often used as natural analogues to compare with crystalline ASR products, and their crystal structures are shown in Figure 2-7a, c and d. Kanemite ($NaHSi_2O_5·3H_2O$) was also used to represent crystalline ASR products (Hou et al., 2005) but it seems to differ significantly from the real structures as it lacks Ca in its chemical composition. It is worthwhile to note that Shi *et al.* (Shi et al., 2019) considered that shlykovite-group minerals (see Figure 2-7b) have closer microstructure and chemistry to field-observed ASR products, and they have successfully synthesized two as types of ASR products ($KCaSi_4O_8(OH)_3·2H_2O$ and $NaCaSi_4O_8(OH)_3·2.3H_2O$) in the laboratory, where sodium substitutes for potassium in the layered structure and with slightly different interlayer water contents, as shown in Table 2-1.

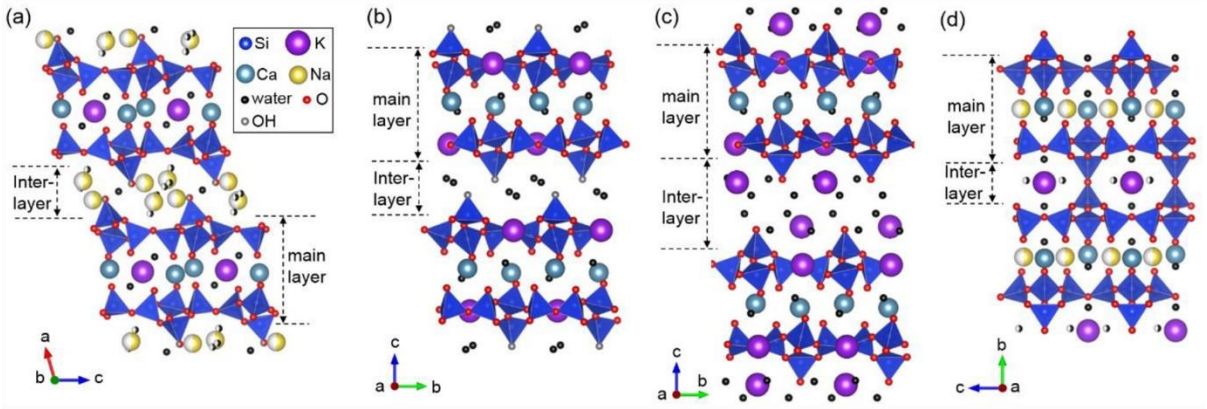

Figure 2-7 Illustrative crystal structures of (a) mountainite, (b) shlykovite, (c) cryptophyllite and (d) rhodesite. Adapted from (Geng, Shi, Leemann, Borca, et al., 2020)

Table 2-1 The crystallographic parameters of K-shlykovite and Na-shlykovite according to the analysis of natural mineral specimens (Pekov et al., 2010), and from molecular simulation results (Honorio et al., 2020)

ASR products	K-shlykovite	Na-shlykovite
Chemical composition	$KCaSi_4O_8(OH)_3 \cdot 2H_2O$	$NaCaSi_4O_8(OH)_3 \cdot 2.3H_2O$
Crystal system	Monoclinic	
a [Å]	6.4897	6.35
b [Å]	6.9969	6.92
c [Å]	26.714	24.89
β [°]	94.597	89.9
V [$Å^3$]	1209.12	1089

2.2 Different testing methods for ASR

In order to avoid degradation by ASR happening during the service life of concrete, it is necessary to have an assessment to evaluate the potential risk (Lindgård, Thomas, et al., 2013). This process includes aggregate reactivity classification and ASR expansion testing. In this part, different testing methods will be outlined, including the criteria for measurement of ASR in each, and comparison among them.

2.2.1 Aggregate reactivity classification

Knowing the reactivity of aggregates is an efficient and direct way to predict whether ASR will take place after mixing concrete. RILEM recommendations suggest that petrographic examination is a reliable method and can classify aggregates, based on reactive content obtained from XRD and XRF testing techniques and accumulated field knowledge (Nixon & Sims, 2016). If aggregates are classified as Class I (non-reactive) or Class III (high reactive), no further testing is performed, while Class II (potentially reactive) cannot give conclusive outcomes and expansion testing is necessary. Therefore, the precise technique for investigating unknown aggregates plays an important role in this assessment, which includes identifying composition, types of minerals, and concentrations of reactive contents. BRE Digest 330 defined the reactivity of certain aggregates as low/normal/high reactivity aggregates by the threshold alkali level in association with expansion behaviour (BRE, 2004).

2.2.2 ASR expansion testing

Preselection of aggregate is beneficial when comprehensively understanding an unknown aggregate. However, if there is lack of knowledge of certain reactive content, or if aggregates are classified into Class II mentioned above, expansion testing is recommended to assess potential damage. There are some testing methods used all around the world, and they can be divided into quick tests and concrete prism tests (CPT). An example of a quick test is ASTM C1260 (ASTM, 2007). Mortar samples are stored in 1 N NaOH solution at 80 ℃ and expansion is measured at 14 days. If the expansion is lower than 0.1% at 14 days, this type of aggregate is considered safe to use. The criteria here is relatively loose but acceptable because high temperature may accelerate the process of ASR and corresponding expansion. However, for those aggregates that dissolve slowly, this accelerated test may be misleading.

ASTM C1293 can be used as a CPT to assess fine and coarse aggregate in the concrete mixture (ASTM International, 2020). Then samples should be immersed for at least one year in the alkali solution with 1.25% Na_2Oeq at 38 °C, defining reactive aggregate as giving higher than 0.03% of expansion in concrete at one year. A similar method has been standardised in the UK as BS 812-123 (BSI, 1999).

ASTM C1293 is one of the most frequently tests used for various reasons. For one, there is no need to crush coarse aggregate, which is suitable for testing most of unknown aggregate reactivity. In addition, the one year testing duration allows this method to give good predictions for not only highly reactive aggregate, but also for slower types. However, because of the long time required, it is incompatible with the needs of the construction industry. Therefore, an accelerated CPT, RILEM AAR-4.1, has been developed by increasing the temperature from 38 °C to 60 ℃ (Nixon & Sims, 2015). The duration of the test can be reduced to 6 months. It should be noticed that the faster diffusion of alkalis caused by increasing temperature in accelerated testing may result in the alkali leaching in the long-term, which may affect expansion outcomes. Also, acceleration caused by higher temperature may have an influence on the degree of expansion (Bagheri et al., 2022). Therefore, more studies should be carried out to verify the effect of acceleration.

Generally, each different testing method has its own advantages and disadvantages. Figueira et al. (Figueira et al., 2019) suggested that determining the reactivity of certain unknown aggregates should not rely on only one testing outcome. However, this takes more time in waiting for more than one results. A short but efficient testing method and common criteria for most aggregates (and aggregate-cement combinations) are required. The prerequisite is to understand the conditions of the formation of expansive products, and build up a relationship between triggering factors and ASR products.

2.3 Mitigation methods for ASR

Alkali-silica reaction seems to be overcome in many cases by limiting the factors mentioned in section 2.1.1.2. Depending on the factors that are predicted to lead to ASR expansion in any given case, corresponding mitigation methods can be adopted. These potentially include methods of controlling the reactive contents in the aggregate, controlling the curing environment but they are relatively non-economic and inefficient when preparing mortars or concretes. Practical measures such as adding lithium compounds or supplementary cementitious materials (SCMs) will be discussed in terms of mitigation methods and their mechanism in this part.

2.3.1 The use of supplementary cementitious materials (SCMs)

In the last few decades, using SCMs to prevent ASR damage has been considered as the most effective and economic method (Thomas, 2011). SCMs such as ground granulated blast furnace slag, fly ash, silica fume and metakaolin are used to add when producing concrete (De Souza & Sanchez, 2023; Tapas et al., 2021). Not only increasing the long-term compressive strength, these mineral additives also improve the durability of concrete. In this part, the mechanism of different SCMs in mitigation of ASR expansion will be discussed.

2.3.1.1 Ground granulated blast furnace slag

Ground granulated blast furnace slag is the by-product of process of iron making in the majority of iron refineries. This non-crystalline glassy substance is mainly composed of calcium

aluminosilicate, which gives its potential hydration properties. Most research studies showed that incorporating slag into concrete reduces the expansion induced by ASR. The main mechanism of role of slag is to increase the consumption of $Ca(OH)_2$ and further decrease the OH^- mobility (Chatterji & Clausson-Kaas, 1984; Duchesne & Bérubé, 1994a). Consumption of $Ca(OH)_2$ by slag was supported by thermodynamic modelling (Lothenbach et al., 2011). Another hypothesis to explain the role of slag is alkali dilution if the slag has a lower alkali content than the cement (Arano & Kawamura, 2000; Hester et al., 2005). Even in high-alkali cement systems the expansion does not surpass the testing limitation with 20% slag addition. In terms of dosage, the degree of reduction of expansion by adding slag increased with the increase of replacement of slag. Most results suggested that 50% replacement of slag has a better impact on reducing expansion compared with low replacement (Hobbs, 1986; Lane & Ozyildirim, 1999; Rasheeduzzafar & Hussain, 1991; Tapas et al., 2021).

2.3.1.2 Silica fume

Silica fume contains a large amount of very fine amorphous silica, and its role in inhibiting the ASR expansion is controversial. One the one hand, fine silica can act as reactive silica which resembles that dissolved from aggregate and may enhance the detrimental reaction if the blending content and distribution is not controlled (Juenger & Ostertag, 2004; Marusin & Shotwell, 2000). On the other hand, the opposite results have also been obtained when adding SF. Concrete in Iceland tends to be prone to problems with ASR due to the relatively high alkalis the in raw materials available for cement production. SF, as a by-product of ferrosilicon plants, has been proved as an effective pozzolanic material used to inhibit ASR in Iceland since the 1970s (Gudmundsson & Olafsson, 1999). Incorporating SF into cement results in forming more C-S-H with a lower Ca/Si ratio, which can adsorb and further restrict the level of alkali metal ions (Duchesne & Bérubé, 1994a, 2001). However, it has been proposed that the replacement of SF should be higher than 10%, otherwise limiting its impact (Boddy et al., 2000; Davies & Oberholster, 1988; Duchesne & Bérubé, 2001).

2.3.1.3 Metakaolin and fly ash

FA and MK are considered as Al-rich SCMs, and they may have better performance in the mitigation of ASR expansion compared with the previous two materials discussed above. The potential roles of Al in influencing ASR have been explained by different authors:

(1) Alkali ions are stated to be bound into C-A-S-H gels in the presence of Al, which reduces the formation of ASR products. Hong and Glasser proposed that the formation of C-A-S-H gel led to higher capacity to retain alkalis by a simple acid-base reaction between alkali ions and Si-OH (Hong & Glasser, 2002). However, Chappex and Scrivener found that there was no significant increase in the alkali binding capability of C-S-H in the presence of Al, and the work of L'Hôpital in the same group was also consistent with these findngs (Chappex & Scrivener, 2012a, 2012b, 2013; L'Hôpital, Lothenbach, Scrivener, et al., 2016). The available data disagree with each other and more work is needed.
(2) The second mechanism attributes the effect of Al to formation of zeolite-like hydrates before forming alkali-silicate gel (Hay & Ostertag, 2019). Nevertheless, it should be noticed that zeolite-like products take more time to precipitate and thus are difficult to observe under realistic field conditions (only at 80 °C or in 1M NaOH solution (Hünger, 2007; Shi, Shi, Zhang, et al., 2018)). Therefore, more experiments and investigations should be performed to examine this theory.
(3) The dissolution of amorphous silica can be affected by Al (Bickmore et al., 2006). Al sorbs on the surface of silica, which enhances at lower pH and higher temperature (Bagheri et al., 2021). Shi et al. (Shi et al., 2021) also indirectly proved this idea: they synthesised ASR products and observed the formation and structure change in the presence of Al. Their results showed that concentrations of Al lower than 0.1 mM have no significant effect on ASR products at 40 °C. Blending FA and MK into cement also increases the amount of Al in the pore solution to this range (Vollpracht et al., 2016), which could feasibly result in slowing down the dissolution of silica.

Research on the mechanism of mitigating ASR using SCMs has been extensively reported, whereas the qualitative analysis to show the degree of decrease in ASR products formed is limited. This might be a straightforward way to express the expansion reduction, although it is also affected by other factors such as porosity. In addition, based on experimental results, the

effect of adding SCMs on inhibiting ASR seems to strongly depend on the composition of SCMs, which motivates researchers to consider another way or a simulation method to eliminate this variation, as will be done in this thesis. Lastly, the role of Al in SCMs still remains ambiguous. Thermodynamic modelling seems to be a good way to explain this from the perspective of solubility.

2.3.2 Other methods

2.3.2.1 Control the reactants in concrete

The potential reactants for ASR in concrete include alkali sources from cement or aggregates, and the reactive content of the aggregate. For the former, based on the effects of the quantity of alkalis in concrete on ASR expansion, using low alkali cement is beneficial for concrete durability (Duchesne & Bérubé, 2001; Goguel, 1995; Min & Mingshu, 1993). It is accepted that the content of alkalis in concrete should be controlled to less than 0.6% Na_2Oeq by mass of cement (Thomas, 2011). However, due to environmental and economic considerations, producing low-alkali cement becomes more difficult. This is mainly because high quality raw materials are limited, and cement kiln dust (which contains alkalis) is captured and reused in the production of clinker (Habert et al., 2020).

The corresponding solution that addresses the latter problem is to use non-reactive aggregates, in locations where these are available. Therefore, the petrographic measurement mentioned above is quite important before using aggregate that is unclear regarding its reactive content. Because the reactive content in aggregate depends on a range of factors such as crystalline structure, chemical composition and rock formation, it is advisable to select non-reactive aggregates using previous experience. According to RILEM recommendations (Sims & Nixon, 2003), Class I as mentioned in section 2.2.1 should be the best choice. In terms of petrographic assessment, general criteria have been developed, ASTM C1778 as an example, and will be suitable for different countries.

2.3.2.2 Control moisture

It was mentioned in section 2.1.1.2 that stopping the absorption of water by the ASR gel is important, and that water may come both from the interior of concrete and by exchange from the external environment. Therefore, controlling the water to cement ratio (w/c) could reduce the absorption of both internal and external water (Bérubé & Fournier, 1993). With respect to the environment, Deschenes et al. (Deschenes Jr et al., 2017) controlled moisture in the air to mitigate ASR expansion. However, this is cost-consuming and difficult to achieve for all projects, because the potential expansion still takes place once humidity changes. Bérubé et al. (Bérubé et al., 2002) tried to use silane, oligosiloxane and polysiloxane as sealant materials to prevent water transport, which obtained effective results. In general, trying to impede the interaction with water, either added or from the environment, seems to be a feasible but inefficient and expensive approach.

2.3.2.3 Using porous aggregate

In some locations it is inevitable that some aggregates containing reactive content will be used to some extent, as no alternative is available, and this encourages researchers to think about how to accommodate expansion. Vivian firstly proposed an insight to use porous aggregate (Vivian, 1947). Their results showed that no expansion happened in any samples. Collins (Collins, 1989) used carboniferous sandstones as aggregate to prevent ASR expansion. This method was effective and the reason for this is that alkali metal ions were diluted by the absorption of porous aggregate, and gel can be accommodated in these loose structures. Thereafter, Chatterji et al. (Chatterji et al., 1988) proposed a method of inhibiting ASR expansion by using air entrainment. An air bubble system is theoretically used to attach and isolate the reactive aggregates, thus reduce ASR expansion. However, fewer studies associated with these methods were carried out in recent years, mainly due to economic considerations.

2.3.2.4 Lithium compounds

McCoy and Caldwell (McCoy & Caldwell, 1951) first tried to use lithium compounds to mitigate ASR expansion in 1951. Thereafter, many works have focused on the role of lithium salts in controlling ASR damage. However, debates still exist in different papers. There are some mechanisms proposed:

(1) adding lithium compounds influences the silica dissolution and/or repolymerisation of silicate after dissolution (Collins et al., 2004).

(2) lithium could reduce repulsive forces between colloidal ASR gel particles. (Chatterji et al., 1989).

(3) lithium compounds mitigate expansion by forming a lithium silicate reaction product which acts as a protective barrier around the aggregate grain (Feng et al., 2010; Tremblay et al., 2010).

(4) the chemical composition and structure of ASR gel changes when adding lithium salts (Mo, 2005). In the presence of lithium, the sites for Ca in ASR gel are occupied by Li and repolymerisation of silica and silicates is decreasing (Leemann et al., 2014).

It is accepted that $LiNO_3$ is the most effective lithium salt in terms of preventing ASR damage (Feng et al., 2005).

From these papers, it also can be concluded that a lot of factors affect the process of ASR damage, and how lithium can influence it. These should be controlled seriously when measuring the effect of certain compounds or factors. In addition, due to controversial opinions on the effect of lithium compounds on the mitigation of ASR, further research such as thermodynamic modelling is needed to make a conclusion in the future.

2.4 Thermodynamic modelling of ASR

The variety of raw materials and industrial wastes used in the production of cement and concrete lead to increasing its complexity in terms of composition and durability performance (Scrivener & Kirkpatrick, 2008). As a result, the availability of a robust and time-saving predictive method seems to become urgent. In this case, thermodynamic modelling is an essential tool to predict multicomposition-multiphase systems, based on the principle of minimisation of Gibbs free energy and laws of mass action (Lothenbach, 2010; Lothenbach & Zajac, 2019). By using thermodynamic modelling, solution chemistry and phase assemblages can easily be calculated when considering different compositions of systems inputted, and various curing conditions such as temperature and humidity can be considered, in different cement systems (Baquerizo et al., 2016; Ke et al., 2020; Lothenbach et al., 2008). The progressive development of the database for hydration products, for example C-S-H absorbing

different ions, and the database for zeolites, help researchers to better understand the chemical reactions taking place in such complex systems (Kulik et al., 2022; Lothenbach et al., 2019; Ma & Lothenbach, 2021; Myers et al., 2014).

2.4.1 Key concepts in thermodynamic modelling

When considering a chemical reaction process, thermodynamic modelling is used to consider the formation of possible phases when the system is at equilibrium, based on the minimisation of Gibbs free energy. For example, a chemical reaction is shown in Eq. 2-7:

$$aA + bB \leftrightarrow cC + dD \qquad \textbf{Eq.2-7}$$

where uppercase letters mean reactants and products, and lowercase letters are the stoichiometric coefficients of each substance. The reaction no longer progresses, either forwards or backwards, when the Gibbs free energy reaches a minimal level. Until then, the reaction keeps changing toward whichever side minimises Gibbs free energy. This can also be related to the equilibrium constant K, which is represented as the ratio of the product concentrations to the reactant concentrations. However, in cement science there are also significant electrostatic interactions between solute-solvent and solute-solute molecules. Consequently, the behaviour of an electrolyte solution can deviate considerably from that an ideal solution. The equilibrium constant considering ions activity is shown in Eq. 2-8.

$$K = \frac{\{C\}^c\{D\}^d}{\{A\}^a\{D\}^b} \qquad \textbf{Eq.2-8}$$

where curly brackets denote the activity. If K>1, then equilibrium favours products, while at K<1 the equilibrium favours the reactants. Gibbs free energy of reaction is related to the solubility products:

$$\Delta_r G^\circ = \sum_i v_i \Delta_f G^\circ = -RT \ln K \qquad \textbf{Eq.2-9}$$

Where $\Delta_r G°$ is the Gibbs free energy of reaction, which is equal to the sum of Gibbs free energy of formation ($\Delta_f G°$) of each species multiplied by their corresponding stoichiometric coefficients (ν_i, defined to be negative for reactants and positive for products). R is the universal gas constant which is equal to 8.31451 J/mol·K, and T is the temperature in Kelvin. The activity of species *i* is calculated by Eq. 2-10:

$$a_i = \gamma_i * m_i \qquad \textbf{Eq.2-10}$$

where *a* is the activity of species *i*, γ denotes the activity coefficient and *m* is the concentration of species *i* at equilibrium. The activity coefficients of aqueous species are calculated by different relationships, but in cement science one that is commonly applied is the Truesdell-Jones form of the extended Debye-Hückel equation (Helgeson et al., 1981):

$$\log_{10} \gamma_i = \frac{-A_\gamma z_i^2 \sqrt{I}}{1 + aB_\gamma \sqrt{I}} + b_\gamma I \qquad \textbf{Eq.2-11}$$

where the coefficients A_γ and B_γ are related to the temperature and pressure of the system, z_i is the charge of species i, and *I* is the effective molal ionic strength, which is calculated by Eq. 2-12:

$$I = \frac{1}{2} \sum_{i=1}^{n} c_i \, z_i^2 \qquad \textbf{Eq.2-12}$$

where c_i is the concentration of the i^{th} ionic species. In Eq.2-11, a and b_γ are solution-dependent parameters. When NaOH solution is the main aqueous phase, a and b_γ are equal to 3.31 Å and 0.098 kg/mol; these become 3.67 Å and 0.123 kg/mol respectively in KOH-dominated solutions (Lothenbach et al., 2019).

Another important parameter that defines the formation of cement hydrates for the reference dissolution or precipitation reaction is saturation index (SI). By comparing the actual ion activity product (IAP) at any time (equilibrium or non-equilibrium) with equilibrium constants, especially solubility products, it can be determined whether the aqueous phase is undersaturated or supersaturated with respect to a particular solid phase, as shown in Eq. 2-13.

$$SI = \log_{10} \frac{IAP}{K} \qquad \textbf{Eq.2-13}$$

If SI=0, it means IAP is equal to K, the system is in equilibrium and hydrates are no longer formed or dissolved. If IAP>K (SI>0), this represents being supersaturated which favours precipitation. Otherwise, if IAP<K (SI<0), aqueous phases are preferred, and solids can dissolve.

2.4.2 The possibility and challenges of using thermodynamic modelling in studying ASR

Most previous computational studies have focused on simulating ASR according to its chemical sequence from the perspective of kinetics. For example, Dron and Brivot (Dron & Brivot, 1992, 1993) listed the chemical reactions of silica dissolved in the solution and reacting with alkalis to form ASR products. They also designed experiments to compare with calculation results. However, C-S-H gel binding K replacing ASR gel was used in the prediction process. Kim and Olek (Kim & Olek, 2014) selected $K_2Ca_4Si_6O_{17}{\cdot}10.5H_2O$ and $Na_2Ca_4Si_6O_{17}{\cdot}10.5H_2O$ as two ASR products to develop thermodynamic parameters and used them to simulate equilibrium states between $Ca(OH)_2$, α-cristobalite and alkali ions. The effects of pH value and reaction time were also considered based on kinetic rate laws. A kinetic-based model describes clearly the characteristics of ASR gel: gel is easy to form surrounding the aggregate, and the Ca/M ratio (M refers to Na or K ions) decreases with an increase in the distance within the aggregate.

Guthrie and Carey (Guthrie & Carey, 2015) established a new method to simulate ASR across the cement-aggregate interface. Ions related to ASR and the amount of silica dissolved in the solution, saturation indexes of ASR products were calculated near the ITZ, as shown in Figure

2-8. In their study, magadiite [$Na_2Si_7O_3(OH)\cdot 3H_2O$] and okenite [$CaSi_2O_5\cdot 2H_2O$] were used in the simulation as surrogates of ASR products. Those authors believed that pH is a determining factor in silica dissolution, which promotes the formation of ASR gel. Nevertheless, as discussed in section 2.1.2, the difficulty of finding representative ASR products prevents the development of thermodynamic modelling used in the ASR area. Magadiite and okenite, as used in the previous study, are no longer considered fully suitable as representatives of ASR products due to the lack of essential elements within their structures (Geng, Shi, Leemann, Borca, et al., 2020; Shi et al., 2019). Zhou (Zhou, Chen, Zheng, et al., 2022, 2022; Zhou et al., 2019) also used thermodynamic modelling to discuss the role of Al in mitigating ASR. However, they did not consider hydration results in the presence of ASR products, which leaves scope for future improvements.

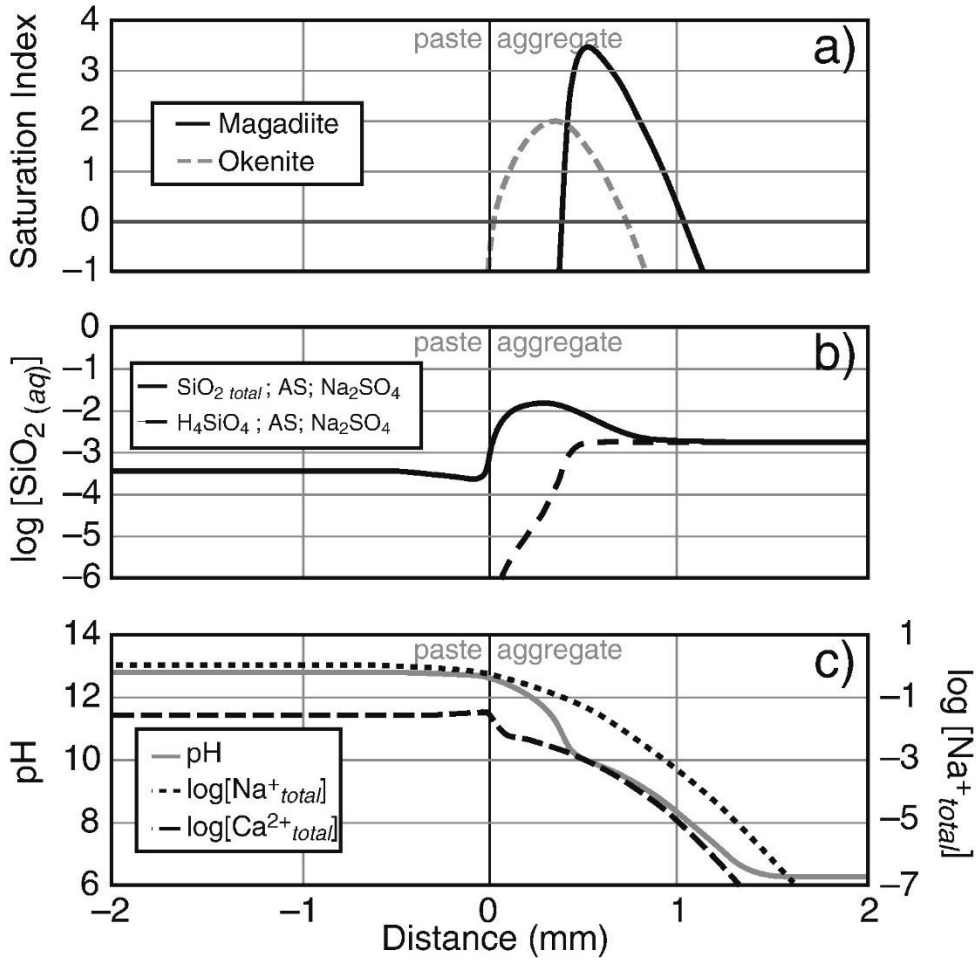

Figure 2-8 Investigation of saturation index of representative ASR products (magadiite and okenite), silica dissolved, and ionic concentration change with pH value near the ITZ, with the alkali source of Na_2SO_4. Adapted from (Guthrie & Carey, 2015)

The main challenge in applying thermodynamic modelling into ASR research is the lack of understanding of expansive products and their thermodynamic database. Previous studies used the calculated saturation index to determine whether ASR gel forms or not. However, this parameter is not precise because of the use of inappropriate representations of the ASR. The successful synthesis of shlykovite-type products may result in the establishment of new thermodynamic database entries. Also, the application of a volume-based method to calculate entropy and heat capacity allow the modelling to be performed at different temperatures, which can be used to compare with experimental results gained in different testing methods at higher temperature.

2.5 The gaps existing in the literature

Based on the literature, some gaps exist, some for the requirement of advanced measurement and some for the variation of material used. This section summarises the key gaps identified, as follows:

- The current studies have primarily focused on the investigation of ASR using potentially reactive aggregate and the methods to mitigate this, using different testing methods with different conditions and durations. However, the experimental results strongly depend on the testing methods and the composition of material used. Thermodynamic modelling may be a good choice as a way to generate comparison with experiment.
- The understanding of ASR products is limited. Therefore, there is a lack of thermodynamic database entries for them, if simulation is applied in ASR research. In addition, no modelling approach can yet assess the results of testing at higher temperature.
- There are few studies presenting a relationship between solution chemistry and the formation of ASR products. In other words, there is not yet an evaluation method to predict the possibility of ASR taking place in certain types of cement and the efficacy of certain SCMs. It takes a long time to experimentally investigate the effects of certain SCMs on ASR and the reactivity of unknown aggregates.

- The reason for less ASR expansion in AAC remains unknown. Given the variations mentioned above, it is urgent to use other methods of assessing phase formation instead of only relying on experiments.

2.6 Conclusions

ASR is the sequential reaction between alkalis, mainly from Portland cement, and reactive silica from reactive aggregates, which causes expansion when exposed to moisture. Many studies have been done to deepen understanding about the mechanism of ASR, which shows that the process of ASR depends on the alkali source, types of reactive aggregates, and curing environments. Advancement in analytical equipment allows researchers to investigate ASR products in more detail. Different types of ASR products, both amorphous and crystalline, have been found, with similar average atomic ratios Ca/Si and (Na+K)/Si of 0.21-0.23 and 0.21-0.34, respectively. The amount of Ca in the products decreases near the aggregate, while it increases when ASR products form in the cement paste. Raman microscopic and synchrotron micro-XRD Rietveld refinement showed that the crystalline ASR products have a layered silicate framework with cations such as sodium and potassium and small molecules such as water filled in the interlayer. Shi et al. (Shi et al., 2019) have successfully synthesised two shlykovite-type ASR products ($KCaSi_4O_8(OH)_3 \cdot 2H_2O$ and $NaCaSi_4O_8(OH)_3 \cdot 2.3H_2O$) in the laboratory, which is beneficial to bring better knowledge of ASR mechanisms.

Alkali-silica reaction seems to be overcome by limiting the factors mentioned in section 2.1.1.2. Depending on the factors that are predicted to lead to alkali-silica reaction expansion in any given case, corresponding mitigation methods can be adopted. These potentially include methods of controlling the reactive contents in the aggregate, or controlling the curing environment, but some of these are relatively non-economic and inefficient when preparing mortars or concretes. Practical and preventative measures such as adding lithium compounds or supplementary cementitious materials (SCMs) are also applied. Therefore, in this thesis, methods will be discussed in terms of mitigation methods and their mechanisms, viewed using thermodynamic modelling.

In the last few decades, using SCMs to prevent ASR damage has been considered as the most effective and economic method. SCMs such as ground granulated blast furnace slag, fly ash, silica fume and metakaolin are added to cement or when producing concrete. Incorporating SCMs can greatly reduce the amount of portlandite left in the cement matrix, which plays a significant role in forming expansive products. Also, the available alkalis in the pore solution decrease in the presence of SCMs, either due to the formation of low Ca/Si ratio C-S-H which may have increased capacity for binding alkalis, or just due to the dilution effect caused by low alkali SCMs. Al-rich SCMs can enhance the mitigation by slowing down the dissolution of reactive aggregates.

Thermodynamic modelling is a robust and time-saving predictive method to predict multicomposition-multiphase systems, based on the principle of minimisation of Gibbs free energy and laws of mass action. Most previous computational studies have focused on simulating ASR according to its chemical sequence from the perspective of kinetics. A kinetic-based model can describe clearly the characteristics of ASR gel: gel is easy to form surrounding the aggregate, and the Ca/M ratio (M refers to Na or K ion) decreasing with an increase in the distance within the aggregate. However, the difficulty of finding proper ASR products has restricted the development of thermodynamic modelling used in the ASR area. Also, there is no study developing a product-oriented method to discuss the role of SCMs in ASR and to guide practice without necessarily using very time-consuming testing, which leaves scope for future improvements. Given that these reasons, building up thermodynamic parameters of proper ASR products and applying them into new modelling work will be presented in the next chapters.

Chapter 3 . ASSESSMENT OF THE THERMODYNAMICS OF Na,K-SHLYKOVITE AS POTENTIAL ALKALI-SILICA REACTION PRODUCTS IN THE $(Na,K)_2O$-CaO–SiO_2-H_2O SYSTEM

Note: This chapter is based primarily on the paper "*Assessment of the thermodynamics of Na, K-shlykovite as potential alkali-silica reaction products in the $(Na,K)_2O$-CaO–SiO_2-H_2O system*", by H. Jin, S. Ghazizadeh, J. L. Provis, published in *Cement and Concrete Research*, 2023, 172, 107253.

Abstract

The thermodynamic description of the alkali-silica reaction (ASR) is incomplete, due to the lack of thermodynamic data for the alkali-silica reaction products. Here, the temperature-dependent thermodynamic properties of Na- or K-shlykovite are estimated; these phases are found to form during alkali-silica reaction in concrete. The thermodynamic properties are then used to produce a series of binary phase diagrams considering different concentrations of alkalis. The results show that these two products start to form at 0.01 mol/kg of alkalis in the CaO–SiO_2 binary phase diagrams. Both Na- and K-shlykovite can co-exist with C-S-H at an increased concentration of CaO, consistent with findings that these ASR products may form in real cement systems. However, there is a maximum alkali concentration in the binary phase diagram beyond which shlykovite cannot form, due to limited calcium solubility. This work can help understand and improve alkali-silica testing protocols proposed in standards.

3.1 Introduction

One of the most important factors that restricts the development of research into alkali-silica reaction (ASR) in concretes is the lack of understanding and observation of the products of ASR. The tiny amount of ASR products (as a fraction of the overall mass of concrete) that generally form, and their location near the interfacial transition zone (ITZ) and inside aggregate particles, requires increasingly high resolution and spatially-resolved analytical instrumentation to properly observe and characterise these products (Boehm-Courjault et al., 2020). Additionally, when ASR products are investigated, they are sometimes difficult to distinguish from calcium silicate hydrates (C-S-H) due to their similar chemical compositions (Maraghechi et al., 2016). Recently, many advanced analytical techniques such as Raman microscopy (Balachandran et al., 2017; Leemann, 2017; Leemann et al., 2020), in-situ synchrotron-based micro-X-ray diffraction (Geng et al., 2021), and micro X-ray absorption spectroscopy (XAS) (Geng, Shi, Leemann, Borca, et al., 2020) have been used to observe the characteristics of ASR products, and have shown that amorphous products were formed in cracks within aggregate particles in the early reaction period, and then later transform into crystalline forms as the reaction proceeds (Leemann et al., 2020).

ASR products are formed by reaction between alkali (sourced largely but not solely from cement paste), and silicate from reactive aggregates. Calcium ions from the cement also take part in the reaction, alongside the alkali ions, as ASR proceeds. The average atomic ratios of Ca/Si and (Na+K)/Si of ASR products have been measured to be 0.21-0.23 and 0.21-0.34, respectively, regardless of the amorphous or crystalline nature of the structures (Fernández-Jiménez & Puertas, 2002; Leemann et al., 2020; Shi et al., 2015, 2018). Raman microscopic results showed that the ASR products have a layered silicate framework with cations such as sodium and potassium and small molecules such as water filled in the interlayer (Leemann et al., 2016). To better understanding ASR product structures and the mechanism of expansion, natural minerals such as okenite ($CaSi_2O_5 \cdot 2H_2O$) (Peterson et al., 2006), mountainite ($KNa_2Ca_2[Si_8O_{19}(OH)] \cdot 6H_2O$) (Kawabata & Yamada, 2017) and rhodesite ($KHCa_2[Si_8O_{19}] \cdot 5H_2O$) are often used as natural analogues to compare with crystalline ASR products. It is also worthwhile to note that Shi et al. (Shi et al., 2019) have successfully synthesized two shlykovite-group minerals as types of ASR products ($KCaSi_4O_8(OH)_3 \cdot 2H_2O$ and $NaCaSi_4O_8(OH)_3 \cdot 2.3H_2O$) in the laboratory where sodium substitutes for potassium in the

layered structure and with slightly different interlayer water contents (see Section 2.1.2, Table 2-1). These are considered to have closer microstructure and chemistry to field-observed ASR products (Pekov et al., 2010). The detailed information for these was shown in the section 2.1.2 in Chapter 2.

Thermodynamic modelling is a mature way to predict phase assemblages in cement research, based on the principle of Gibbs energy minimisation with mass balance constraints. The increasing completeness of the databases of minerals and other phases relevant to cement and concrete science are now allowing this approach to be considered as an efficient method to predict durability-oriented performance within different external environments, and to complement the established experimental approaches. This is particularly important for slow degradation phenomena such as ASR, for which standard testing lasts at least 12 months for analysis of cement-aggregate combinations in concrete prisms under representative conditions.

The modelling that has previously been published for ASR processes has focused mainly on investigating the dissolution of silica and conducting some theoretical calculations (Dron & Brivot, 1992, 1993). As more natural minerals that are similar to ASR products are identified and the database further constructed, the modelling results can better reflect and explain the formation of ASR products. For example, Kim and Olek (Kim & Olek, 2014) considered the role of OH^- in the pore solution in the process of the dissolution of reactive silica, using kanemite ($KHSi_2O_5 \cdot 3H_2O$ or $NaHSi_2O_5 \cdot 3H_2O$) as model ASR products. Guthrie and Carey (Guthrie & Carey, 2015) provided a model to investigate the effect of pH gradients on the dissolution of silica and ASR precipitation. In their modelling, magadiite [$Na_2Si_7O_3(OH) \cdot 3H_2O$], and okenite [$CaSi_2O_5 \cdot 2H_2O$] were used to simulate low-calcium and high-calcium crystalline ASR products respectively. It is also valuable to enrich the understanding that can be gained from experimental data by using thermodynamic modelling where the consumption of $Ca(OH)_2$ controls the ASR process (Hou et al., 2004).

However, the fact that some key structural aspects of these minerals do not correspond fully to the best available understanding of ASR products leads to the suggestion that kanemite- and okenite-type gels may no longer be the most suitable comparators for modelling of field-

observed ASR products (Boehm-Courjault et al., 2020; Leemann, 2017; Shi & Lothenbach, 2019). Shi et al. (Shi et al., 2019) did model the formation of synthetic shlykovite-type products at 80°C and compared them with their experimental data, which proved the efficacy of thermodynamic modelling for these particular ASR product analogues. Nevertheless, one issue that needs to be noted is that average logK values were applied in their thermodynamic calculation and the potential errors caused by pH estimation seem to be omitted, which may affect the accuracy of modelling results. Also, a key challenge of applying this method to ASR research is the incomplete thermodynamic database for shlykovite-type ASR products at 25°C, which is required to underpin accurate modelling for ASR without thermal acceleration.

The aim of this chapter is therefore to build up information regarding the thermodynamic parameters of two shlykovite-type ASR products at ambient temperature. Binary phase diagrams with different concentration of alkalis are established to verify the reliability of the calculated parameters in conjunction with the established Cemdata database, by comparison with published experimental data. The results can provide a fundamental method to build up thermodynamic parameters for ASR products, with possible application also for other potential ASR products. The phase diagrams show a foundation for further predicting phase assemblages for certain combinations of ion concentrations at ambient and higher temperature. The modelling results can also provide some constructive suggestions for standardising ASR testing.

3.2 Methods

3.2.1 Software and database

Modelling in this study is performed using the Gibbs energy minimisation software GEM-Selektor v.3 (http://gems.web.psi.ch/GEMS3/). The Cemdata18.1 cement thermodynamic database (Lothenbach et al., 2019) is used in this paper; see Appendix, Table A2. The reason for using this latest database is that a complete and accurate thermodynamic database improves the quality of simulations, and this database is specialised and developed for simulation of cements. At ambient temperature the formation of quartz is quite slow, and thus this phase is excluded from the modelling calculations. The CSHQ solid solution model included in Cemdata18.1 is used to represent C-S-H with varying Ca/Si ratios. Here this type of model rather than other C-S-H model such as ECSH-1 and CSH3T is used because the Ca/Si ratio of

the CSHQ model is closer to the C-S-H in the real cement. Also, other end-members such as Sr-bearing phases are not considered in this simulation. The activity coefficients of aqueous species are calculated by the Truesdell-Jones form of the extended Debye-Hückel equation, described in Eq. 2-11 in section 2.4.1.

3.2.2 Thermodynamic parameter estimation for ASR products

In this study, K-shlykovite ($KCaSi_4O_8(OH)_3 \cdot 2H_2O$) and Na-type ($NaCaSi_4O_8(OH)_3 \cdot 2.3H_2O$) are considered as representative potential ASR products and used to build up thermodynamic parameters, although there are some variations mentioned in the literature regarding the precise nature of the ASR products that form in real cements (Leemann et al., 2020; Shi et al., 2020; Shi & Lothenbach, 2019). The factors controlling the structures and the formation of different types of ASR products (in terms of their relationship to different model minerals) are poorly understood and may involve both kinetic and thermodynamic issues. These factors are very difficult to probe experimentally, involving long experiment durations, and further work in this area is ongoing in many laboratories.

For solid hydrates (Ghazizadeh et al., 2020), standard molar entropy and molar heat capacity (where these have not been determined experimentally) are correlated with formula unit volume V_m, and can be calculated by Eq. 3-3 and Eq. 3-4 (Glasser & Jenkins, 2011) respectively:

$$S^\circ = 1579 \cdot V_m + 6 \qquad \textbf{Eq.3-3}$$

$$Cp^\circ = 1388.1 \cdot V_m + 4.58 \qquad \textbf{Eq.3-4}$$

There do exist other methods to calculate entropy and heat capacity, such as direct experimental measurement, and additivity methods that set a material characteristic equal to the sum of the standard molar properties of constituent oxides and hydroxides. However, one prerequisite is that pure phase of interest is easy to prepare in the laboratory while ASR products are not in this range, not to mention knowing constituent oxides or hydroxides. Ghazizadeh et al. stated that there are about 7.4% of errors associated with this estimation (Ghazizadeh et al., 2020),

which is acceptable for the simulation. Gibbs free energies of formation for different ASR products are obtained according to Eq. 3-5,

$$\Delta_r G^\circ = -RT \ln K \qquad \textbf{Eq.3-5}$$

where $\Delta_r G°$ is the Gibbs free energy of reaction, which is equal to the sum of Gibbs free energy of formation ($\Delta_f G°$) of each species multiplied by their corresponding stoichiometric coefficients (v_i, defined to be negative for reactants and positive for products). R is the universal gas constant which is equal to 8.31451 J/mol·K, T is the temperature in Kelvin, and K is the solubility product constant associated with the reference reaction. In this case, the solubility products of the two ASR products are based on Eq. 3-6 and Eq. 3-7, respectively (Shi & Lothenbach, 2019).

K-shlykovite: $KCaSi_4O_8(OH)_3{\cdot}2H_2O = K^+ + Ca^{2+} + 4SiO_2 + 3OH^- + 2H_2O \quad K_{s1}$ **Eq.3-6**

Na-shlykovite: $NaCaSi_4O_8(OH)_3{\cdot}2.3H_2O = Na^+ + Ca^{2+} + 4SiO_2 + 3OH^- + 2.3H_2O \quad K_{s2}$ **Eq.3-7**

In the work of Shi and Lothenbach (Shi & Lothenbach, 2019), the available solubility products are obtained at 80 °C.K_{s1} and K_{s2} are the solubility products of two ASR products as obtained from Shi's paper ($\log_{10} K_{s1}$ = -25.8 ± 2, $\log_{10} K_{s2}$ = -26.5 ± 2) (Shi & Lothenbach, 2019). However, all parameters need to be converted to a reference temperature of 25 °C for use in standard Gibbs free energy calculations. Therefore, Eq. 3-8, with parameters defined by Eqs. 3-9 to 3-11, is used to obtain a temperature-dependent log K_T:

$$\log K_T = A_0 + A_2 T^{-1} + A_3 \ln T \qquad \textbf{Eq.3-8}$$

$$A_0 = \frac{0.4343}{R} \cdot \left[\Delta_r S^0_{T_0} - \Delta_r Cp^0_{T_0}(1 + \ln T_0)\right] \qquad \textbf{Eq.3-9}$$

$$A_2 = \frac{0.4343}{R} \cdot \left(\Delta_r H^0_{T_0} - \Delta_r Cp^0_{T_0} T_0\right) \qquad \textbf{Eq.3-10}$$

$$A_3 = \frac{0.4343}{R} \cdot \Delta_r Cp^0_{T_0} \qquad \textbf{Eq.3-11}$$

Where A_0, A_2, A_3 are empirical coefficients, T_0 is 298.15 K (25 °C), and T is the calculation temperature of interest. The quantities $\Delta_r S^0_{T_0}$, $\Delta_r Cp^0_{T_0}$ and $\Delta_r H^0_{T_0}$ are molar entropy, heat capacity, and enthalpy of reaction at T_0, which are calculated from an equation taking the form of Eq. 3-12 for each quantity; Eq. (12) is defined in terms of a dummy quantity Φ to maintain generality.

$$\Phi_r = \sum_j \nu_j \Phi_{f_j} - \sum_i \nu_i \Phi_{f_i} \qquad \textbf{Eq.3-12}$$

Where Φ_r is either molar entropy, heat capacity, or enthalpy of reaction, while Φ_f is the corresponding parameter of formation; *i* and *j* denote reactants and products respectively, and the ν values are the stoichiometric coefficients according to the reference reaction. However, for molar enthalpy of reaction calculations, the standard molar enthalpy of formation for each ASR product is unknown. Therefore, this value may be estimated and fitted iteratively; log K_T can be obtained by keeping changing T in Eq. 3-8 from 298.15 K to 353.15K, terminating when the calculated solubility product at 80 °C matches the experimental data from Shi and Lothenbach (Shi & Lothenbach, 2019).

The data composing the phase diagram is only calculated from the simulation instead of experiments. In terms of the effect of alkalis on the formation of ASR product, the determination of the range of alkalis used does not depend on real cement system because here a relationship between the alkalis and ASR products will be established. The alkali distribution will be considered in the Chapter 4 and 5.

3.3 Results and discussion

3.3.1. Discussion and refinement of errors associated with the solubility products of two ASR products

The term “solubility product” is used to refer to the product of the activities (or often, but less precisely, the concentrations) of dissolved ions at equilibrium with the solid phase of interest, at a certain temperature. In past calculation of the solubility product of shlykovite-type phases

(Shi & Lothenbach, 2019), the hydroxyl ion activity was obtained from pH measurement at about 23°C, while the concentrations of other ions were gained from ion chromatography (IC) analysis for solutions equilibrated at 80°C. The pH value was simply corrected by 1.47 units to represent the decrease of pH value from 23°C to 80°C. In fact, this decrease becomes more complex when involving more ions in the solution, which introduces added uncertainty in the calculation method used, and merits further assessment. Here, experimental pH values by simulation using GEMS were refined, and used to estimate the solubility product at 80°C and fit it to 25°C, as shown in Figure 3-1. The black line represents experimental data (Shi & Lothenbach, 2019) while the red line is the recalculation of results in this study. The pH values show a smaller decrease when increasing temperature from 25°C to 80°C, compared with the estimates from Shi and Lothenbach (Shi & Lothenbach, 2019), which means that the solubility products obtained using the new pH value become smaller. In the process of calculating solubility products, the concentrations of other elements were kept as the same as in Shi's paper (Shi & Lothenbach, 2019). New solubility product data for these two ASR products can improve the quality of thermodynamic modelling, for example, accurately assessing solubility boundaries in the phase diagrams in this chapter, and predicting the volume of the phases formed as mentioned in the next two chapters. In addition, the error bars associated with the solubility products become smaller (±0.4 for Na-shlykovite and ±1.2 for K-shlykovite) in comparison with those provided by Shi and Lothenbach (Shi & Lothenbach, 2019) (±2 units). Nonetheless, further experimental studies are still necessary to validate the estimated/calculated parameters. The intention here is to build up a systematic method to develop thermodynamic parameters of potential ASR products, and to use these to achieve improved thermodynamic modelling of ASR processes. In this case, Table 3-1 summarises the resulting thermodynamic parameters for the two potential ASR products at 25 °C.

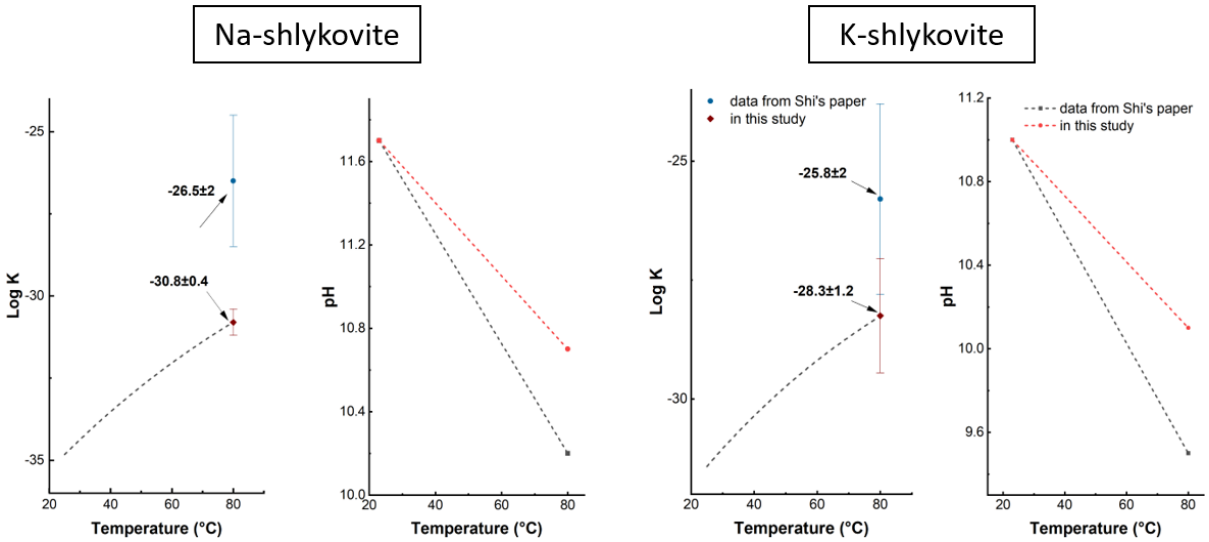

Figure 3-1 Refinement and estimation of solubility products of two ASR products at 25 °C by recalculating pH value

Table 3-1 Thermodynamic properties for ASR products at 25°C

Products	V° (cm^3/mol)	$\Delta_f H°$ (kJ/mol)	$\Delta_f G°$ (kJ/mol)	S° (J/mol·K)	Cp° (J/mol·K)	$Log_{10}K$ at 25°C
K-shlykovite: $KCaSi_4O_8(OH)_3 \cdot 2H_2O$	183	-5163.6±8	-5293.1±3	485.8±48	426.8±42	-31.2±1.2
Na-shlykovite: $NaCaSi_4O_8(OH)_3 \cdot 2.3H_2O$	164	-5267.5±9	-5364.4±2	435.9±43	382.9±38	-34.8±0.4

3.3.2 Thermodynamic modelling results

In this section, thermodynamic parameters of ASR products will be used to predict phase assemblages in the CaO–SiO_2-H_2O system with or without added alkali oxides, coupled with other potential hydration products. Table 2-2 summarizes the concentration of oxides used in all phase diagrams in this section. It is worth noting that although error does exist, as mentioned in section 3.1, the effect of error on each phase diagram will also be discussed in this section.

Table 2-2 The concentration of oxides used in this section

Section X *	CaO (mol/kg H_2O) **	SiO_2 (mol/kg H_2O) **	Na_2O/K_2O (mol/kg H_2O) **	H_2O (g)	Temperature (°C)
3.3.2.1	$1x10^{-6}$ to $1x10^{-1}$	$1x10^{-6}$ to 1	0	1000	25
3.3.2.2	$1x10^{-7}$ to $1x10^{-1}$	$1x10^{-6}$ to 1	0.01	1000	25
3.3.2.3	0.01	$1x10^{-6}$ to 1	0.01 to 2	1000	25
3.3.2.4	0.01	$1x10^{-6}$ to 1	0.01 to 2	1000	38/60/80

* X represents the number of section.

** Each step for CaO is an order of magnitude greater than the previous, starting at 1×10^{-6} in section 3.3.2.1 and 1×10^{-7} in section 3.3.2.1 and increasing to 1×10^{-1}, the same step is applied for SiO_2, but ending at 1. For alkalis, the step is fixed at 0.01 throughout the simulation.

3.3.2.1 Binary phase diagram without alkali ions

The $CaO\text{-}SiO_2$ binary phase diagram obtained by thermodynamic modelling is shown in Figure 3-2a, which is similar to Figure 3-2b, plotted from experimental data and reproduced from (Brown, 1990). The lines represent the solubility curves of each phase. There are many similarities between the two phase diagrams, including three phases formed, a clear solubility boundary between solution and phases, and phase formation regions. Other phases that are not included in the Cemdata 18.1 are not considered in the simulation because this result lays a foundation for the next chapter covering ASR modelling in cement systems. Cemdata 18.1 covers enough phases to predict the relevant behaviour. It is important to note that amorphous silica was used instead of quartz in the modelling, thus the solubility product of amorphous silica should correspond to point B in Figure 3-2b. However, there still exist some differences here. The main difference is the solubility boundary between C-S-H, and the region with amorphous silica plus C-S-H (dashed line), which is a straight vertical line in Figure 3-2a, but sloping in Figure 3-2b. This is indicating that the Ca^{2+} concentration at which C-S-H is predicted to form in the presence of excess silica is relatively insensitive to the silica concentration, and this may be related to challenges in describing the speciation of polynuclear silicate species in this thermodynamic database (Shi & Lothenbach, 2019). Obviously, without alkali ions there is no ASR product found in the $CaO\text{-}SiO_2$ binary phase diagram, but it is useful

to simulate this system to validate the underlying model and to provide a point of comparison for the alkali-containing systems.

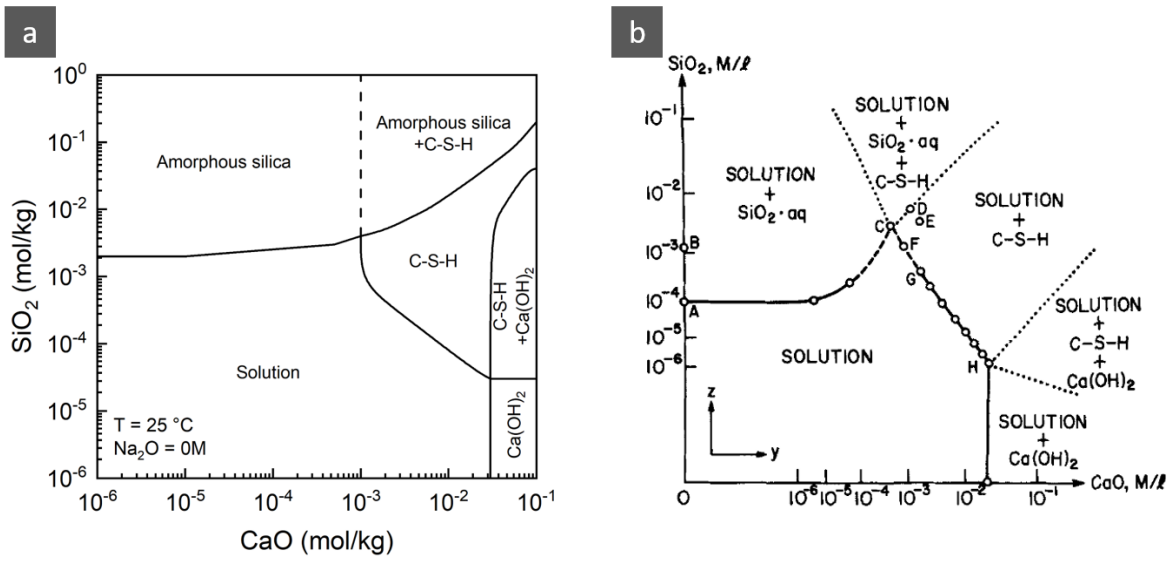

Figure 3-2 The CaO-SiO_2 binary phase diagram, (a): obtained by modelling in this study using the GEMS software; (b): experimental data, reproduced by permission from Brown (Brown, 1990), copyright John Wiley & Sons. Note the difference in axis scaling; (a) uses a logarithmic scale for molal concentrations, while (b) is scaled to the 10^{th} root of molar concentrations.

3.3.2.2 Binary phase diagram with addition of a low content of alkalis

The CaO-SiO_2 binary phase diagram with 0.01 mol Na_2O/kg H_2O is shown in Figure 3-3a. Note that the units used throughout the paper are molal; "mol/kg" henceforth refers to moles of solute per kg of water. Compared with the unmodified CaO-SiO_2 binary phase diagram, there exist many differences although the basic layout is similar. Firstly, Na-shlykovite is found in all ranges of concentration of SiO_2 because of the presence of Na; regions that form this ASR product occupy partly areas that was solution or formed C-S-H, and the area that corresponded to amorphous silica in the absence of Na has disappeared. This indicates that amorphous silica reacts with Na^+ and CaO to form ASR products instead of C-S-H; the ASR product forms at slightly lower concentrations of SiO_2 and CaO compared with Figure 3-2a. It can also be seen that the ASR product can co-exist with C-S-H, which indicates that with an increased concentration of CaO, Na has been partially consumed via the formation of ASR

product, while the rest of the Ca continues to react with amorphous silica to form C-S-H. The influence of ASR product and C-S-H formation on aqueous chemistry in these simulations will be explored in more detail in section 3.3.4 below.

Another significant difference, when comparing Figure 3-3a to Figure 3-2a (i.e. with and without added Na), can be seen in the position of the solubility boundaries. For example, the solubility of $Ca(OH)_2$ (defined here as the concentration of aqueous Ca^{2+} that exists at the phase boundary where $Ca(OH)_2$ begins to precipitate) also changes from about 0.03 mol/kg (Figure 3-2a) to 0.02 mol/kg (Figure 3-3a) when Na is added.

Replacing K_2O by Na_2O in the thermodynamic modelling, to reflect the importance of potassium in some Portland cements, yields the phase diagram with 0.01 mol/kg of K_2O as shown in Figure 3-3b. This phase diagram is evidently similar to the phase diagram with 0.01 mol/kg of Na_2O in the Figure 3-3a; the most notable difference is the area at which the ASR product alone forms. It can be seen from Figure 3-3b that the area representing the formation of K-shlykovite is smaller than for Na-shlykovite. In other words, K-shlykovite formation commences at a higher concentration of SiO_2, consistent with its less negative solubility product as presented in section 3.2.2. In addition, forming K-shlykovite at higher concentrations of SiO_2 leads to a raising of the boundary between the C-S-H single-phase region and the region in which C-S-H coexists with K-shlykovite, compared with that shown in Figure 3-3a for the Na-bearing case.

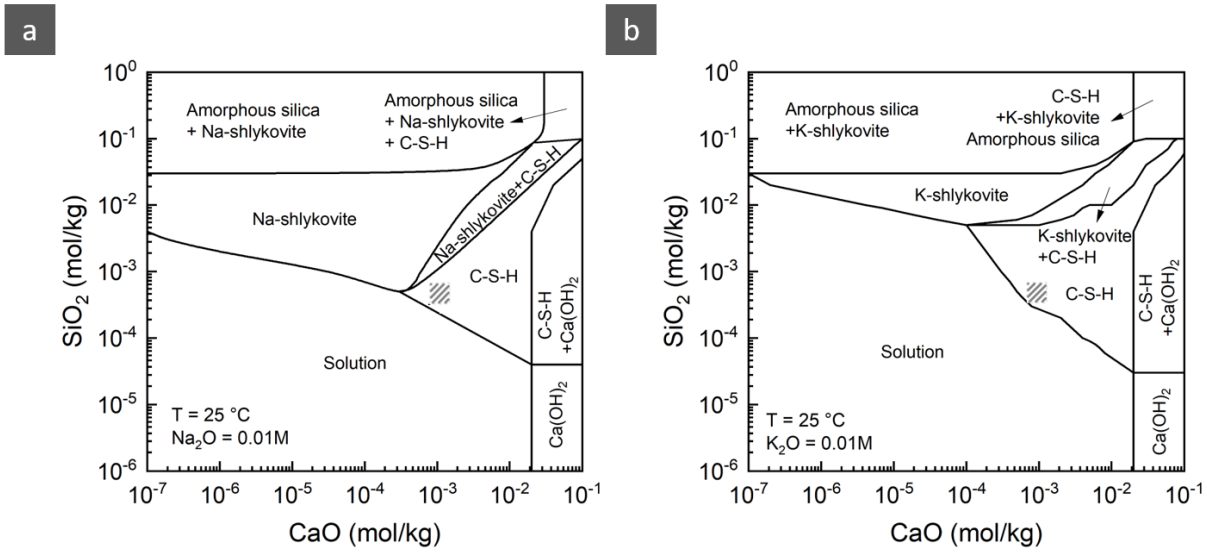

Figure 3-3 The CaO-SiO_2 binary phase diagram with 0.01 mol alkalis/kg H_2O: a: Na_2O, b: K_2O. The shaded region represents the approximate dissolved Ca and Si concentrations in the pore fluid of hydrated Portland cement, showing that the simulation accurately predicts this pore fluid to be saturated or slightly supersaturated with respect to C-S-H formation.

In terms of the effect of error on the phase diagram, phase formation does not change with the change of solubility product. The only difference is the area representing the formation of ASR products, regardless of whether Na or K is the dominant alkali. The ASR products area in the phase diagram becomes larger if a larger solubility product (within the known error bounds) is used in the model, and vice versa.

3.3.2.3 The effects of concentration of alkali ions

To present the effects of concentration of alkali ions on the formation of ASR products and other phases, Figure 3-4 shows the effect of varying the amount of alkalis in the simulation from 0.01 mol/kg to 2 mol/kg, at a fixed content of 0.01 mol/kg of CaO. The reason for selecting 0.01 mol/kg of CaO is that the majority of phases formed across system of interest may potentially be present at this CaO concentration (at different concentrations of alkalis and silica) as shown in Figure 3-3a. Figure 3-4a then highlights that when increasing the concentration of Na_2O from 0.01 mol/kg to 0.03 mol/kg, $Ca(OH)_2$ remains undersaturated, so the bottom left corner of Figure 3-4a only contains solution. After that, the addition of extra hydroxide along with the Na^+ moves the solubility curve of $Ca(OH)_2$ to lower concentrations

due to the common ion effect, thus $Ca(OH)_2$ starts to form when adding more Na_2O (Brown, 1990). In terms of C-S-H formation, as can be seen in both Figure 3-3a and Figure 3-4a, this phase is predicted to be formed even at low concentrations of CaO, and hence the solubility curve that represents the formation of C-S-H begins at the x-axis in Figure 3-4a.

Na-shlykovite also forms in Figure 3-4a, from 0.01 mol/kg addition of Na_2O and upwards. The areas containing this ASR product are divided into three parts: one where this phase co-exists with C-S-H, while in the other it is present along with amorphous silica due to the depletion of calcium. Between them is the Na-shlykovite single-phase region. The former of these regions is more likely to be achieved in Portland cement-based materials as there is likely to be enough portlandite in the hydrated cement to prevent full calcium depletion. These results are in accordance with the trends shown in Figure 3-3a, and the aqueous chemistry will be further discussed in section 3.3.4. With a rise in the concentration of SiO_2, more Na is likely to react with the dissolved silica to form ASR products. However, it does not necessarily mean that adding more Na will lead to the formation of more Na-shlykovite; rather, there is a maximum concentration of Na_2O for the formation of Na-shlykovite. Below 1.48 mol/kg of Na_2O, the existence of shlykovite-type ASR products shows the possibility of alkali-silica reactions resulting in this phase. However, above 1.48 mol/kg of Na_2O, this type of ASR product is no longer predicted to form, due to the suppression of calcium solubility. This finding is potentially of interest in the discussion of higher-alkalinity cementitious binders such as alkali-activated cements, for which further insight into the mechanisms of ASR reaction processes is very much needed (Winnefeld et al., 2020). Although the temperature of the modelling conducted in this work is different from that used by Shi and Lothenbach (Shi & Lothenbach, 2020), the results are consistent in showing that at higher Ca/Si ratio and higher alkali contents, C-S-H instead of the ASR product is more stable.

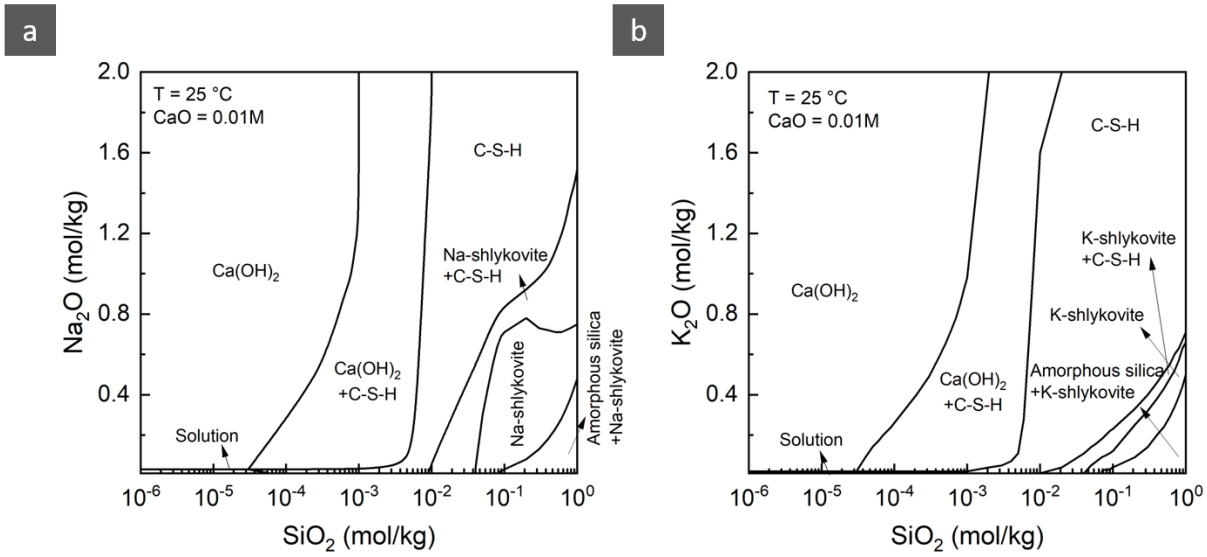

Figure 3-4 The alkali-SiO_2 binary phase diagram with fixed 0.01 mol/kg of CaO: a: Na_2O, b: K_2O.

Likewise, the K_2O-SiO_2 binary phase diagram with 0.01 mol/kg of CaO is shown in Figure 3-4b. In general, it shows similar trends to the Na_2O-SiO_2 phase diagram, other than a slight difference in the ASR product area. In the presence of K, the threshold for the formation of K-shlykovite reduces to 0.71 mol/kg of K_2O compared with the Na-bearing case. This seems to be consistent with the logK value calculation. The smaller area representing K-shlykovite indicates that it is less favourable to form this product than Na-shlykovite under comparable conditions.

The findings here are not strongly influenced by the uncertainty in solubility products; there exists a threshold for the formation of ASR products. The areas representing the rest of the phases remain unchanged.

3.3.3 The effect of temperature on the phase diagram

The Na_2O-SiO_2 phase diagrams with 0.01 mol/kg of CaO, at three different temperatures, are shown in Figure 3-5; the three temperatures shown are selected because these are commonly used in different testing methods that are applied in the laboratory for prediction of ASR. Compared with each other, they have similar areas containing each of the combinations of

reaction products, and there are no changes in the phases identified overall. One key difference is that the solution region at very low Na_2O content disappeared at the higher temperatures, instead becoming a $Ca(OH)_2$ area. This is consistent with the well-known retrograde solubility of $Ca(OH)_2$, which means that it forms more readily at higher temperature. There is also some temperature dependence in the Na_2O concentration above which the ASR product disappears. From 38 °C to 80 °C, this phase boundary (at 1 mol/kg of SiO_2) reduced from 1.16 mol/kg to 0.62 mol/kg, and correspondingly also decreased at lower SiO_2 contents. This information might indicate that it is worthwhile to consider modifying ASR testing to use lower concentrations of alkali at higher temperature, to avoid false-negative results caused by suppression of ASR product formation at very high alkalinity, especially for quick testing at higher temperatures.

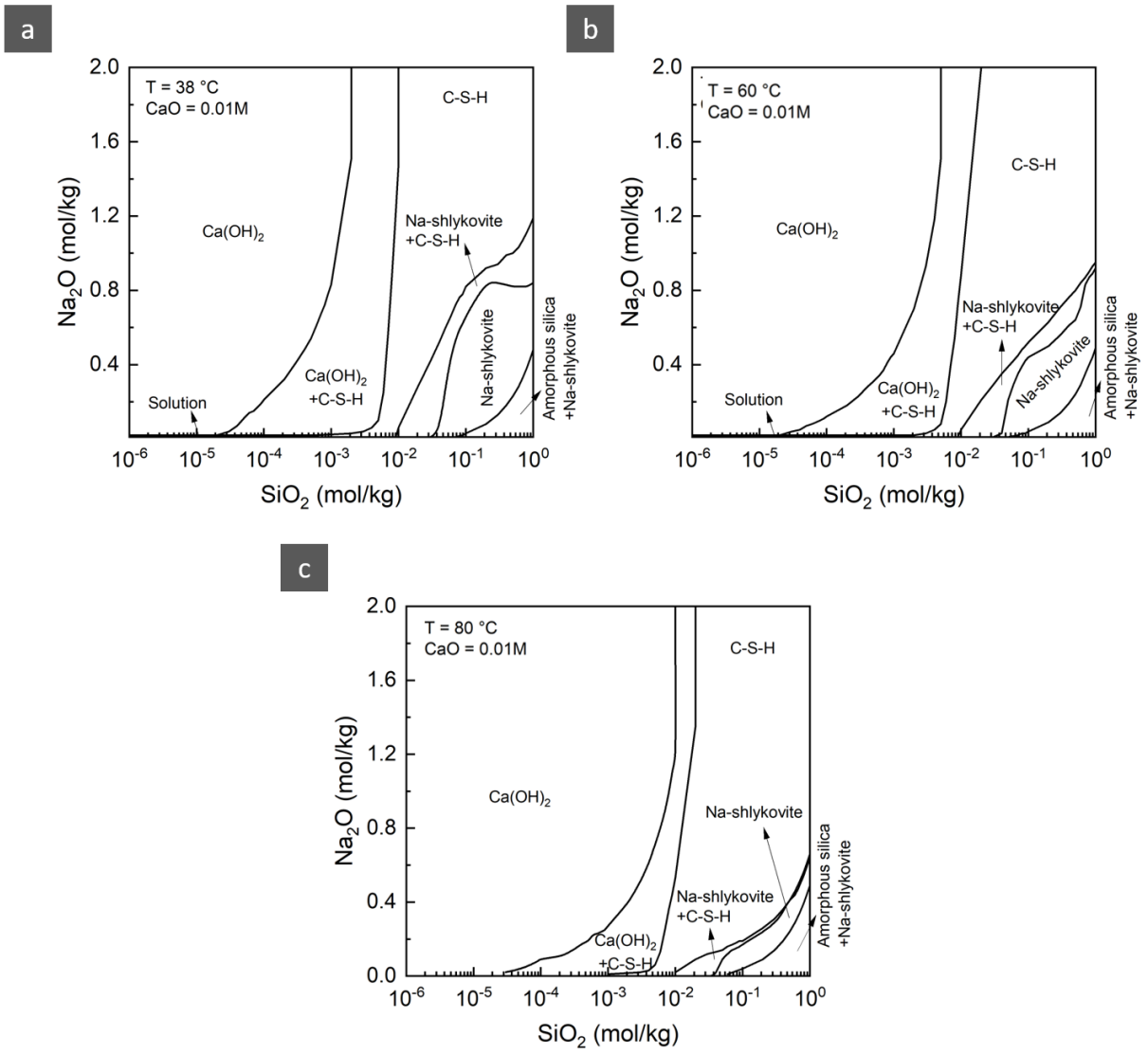

Figure 3-5 a: The Na_2O-SiO_2 binary phase diagram with fixed 0.01 mol/kg of CaO at 38 °C; b: the Na_2O-SiO_2 binary phase diagram with fixed 0.01 mol/kg of CaO at 60 °C; c: the Na_2O-SiO_2 binary phase diagram with fixed 0.01 mol/kg of CaO at 80 °C

3.3.4. Solution chemistry

In order to check and further explain the modelling results, selected regions of the phase diagrams were also analysed in more detail with regard to aqueous chemistry, to calculate the amounts of Na, Ca, Si, and OH^- in the aqueous phase in each case. Because the results presented above for K_2O and Na_2O systems are similar, this analysis is focused solely on the Na_2O-SiO_2 system.

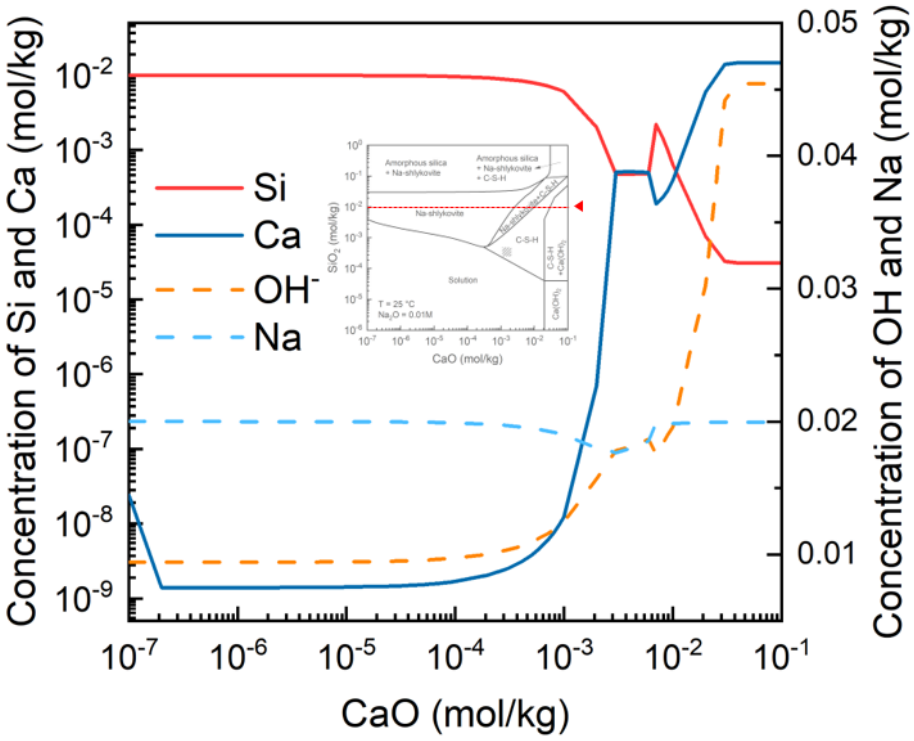

Figure 3-6 The concentrations of Si, Ca, Na, and OH^- in the aqueous solution with increasing addition of CaO, with fixed 0.01 mol/kg of SiO_2 and 0.01 mol/kg of Na_2O (indicated on the inset as a line sketched across a copy of Figure 3-3a, for context).

Figure 3-6 shows the concentrations of the main components in the solution phase when adding different concentrations of CaO with fixed 0.01 mol/kg of SiO_2, and 0.01 mol/kg of Na_2O. It

is worth noting that the concentration of dissolved Ca reduces at $2x10^{-7}$ mol/kg of CaO, which is due to the formation of more Na-shlykovite with increasing concentration of CaO, as shown in Figure 3-3a. After that, the concentration of Ca remains constant due to the formation of this ASR product until 10^{-3} mol/kg of CaO is added, where the rest of Ca stays in the solution because of depletion of the Na_2O added, which leads to an increase in the amount of Ca required to retain saturation with respect to Na-shlykovite. This trend changes at 2 $x10^{-3}$ mol/kg of CaO where C-S-H begins to co-exist with the ASR product, as no further Na-shlykovite can form. Then, dissolved Ca tends to decrease in the C-S-H single-phase region. The trend increases again until $Ca(OH)_2$ forms, as shown in Figure 3-3a. The concentration of OH^- is directly interrelated with the amount of Ca staying in the solution, thus shows a similar trend.

In order to investigate the difference of solution chemistries at different concentrations of SiO_2 with the increase of the concentration of Na_2O, three concentrations of SiO_2 are chosen for further analysis of the aqueous phases, and marked as red dashed lines on the inset phase diagrams in Figure 3-7 and Figure 3-8.

At the lower concentration of SiO_2 selected (10^{-6} mol/kg, Figure 3-7a), the red line falls across two compositional regions, and the calculated component molalities are in good agreement with the phase diagram. The concentration of Ca reaches a plateau before the concentration of Na_2O reaches 0.02 mol/kg because there is no solid phase formed, meaning that all dissolved ions are in the solution. With an increase in Na_2O, $Ca(OH)_2$ starts to form, which leads to the decrease of the concentration of Ca to maintain saturation in the aqueous phase. Since no Na-containing phase is formed at 10^{-6} mol/kg of SiO_2, the concentration of dissolved Na ions gradually increases.

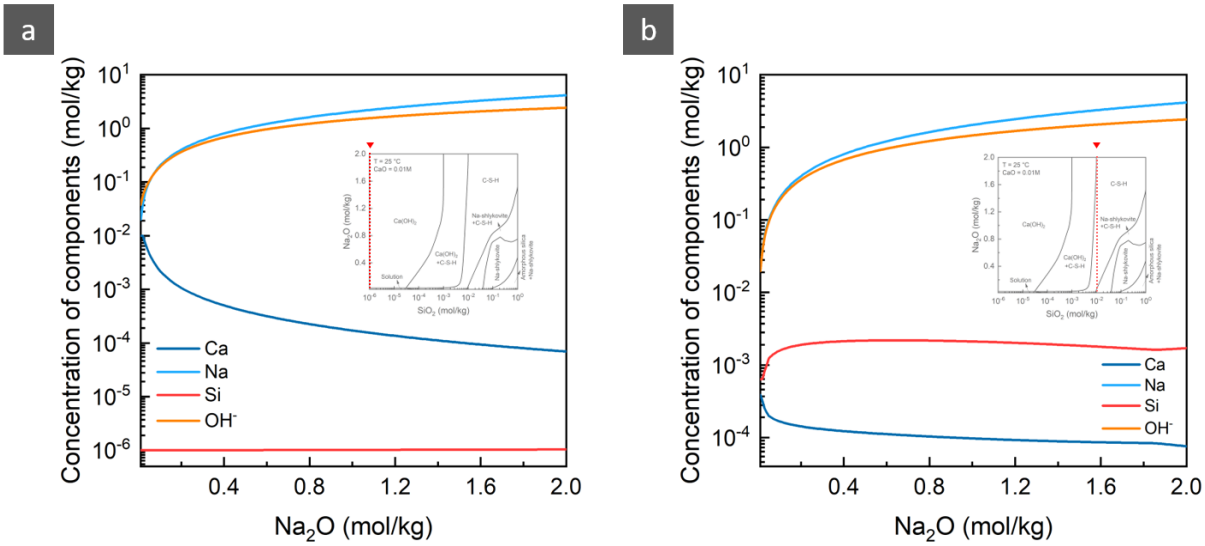

Figure 3-7 The concentrations of Si, Ca, Na, and OH^- in the solution with increased addition of Na_2O. a: 10^{-6} mol/kg of SiO_2, b: 0.01 mol/kg of SiO_2. The inset diagram in each case places this calculation with respect to the phase diagram by reproducing Figure 3-4a, with a dashed line to indicate the compositions depicted.

When the concentration of SiO_2 reaches 0.01 mol/kg (Figure 3-7b), C-S-H is the only solid phase identified in the whole range of Na_2O addition levels. Therefore, the concentrations of Ca are at very low and constant. Due to the low concentration of CaO, the rest of the Si remains in the solution when the amount of formation of C-S-H reaches the maximum possible level. Also, Na-shlykovite is not found across most of this compositional range, meaning that there is no incorporation of Na into solid phases, and thus the trend in Na concentration is similar to that at low concentration of SiO_2.

Moving to higher Si concentration, Na-shlykovite appears at 2 mol/kg of SiO_2 (Figure 3-8), and the trends for the four components are different compared with the two lower concentrations that were discussed above. Due to the formation of Na-shlykovite, the amount of Ca reduces in the very low Na_2O concentration range. In addition, the increment in dissolved Na concentration becomes very slight because of the formation of the ASR product. The concentration of SiO_2 is sufficient to form the ASR product by consuming Na and Ca, and amorphous silica can also form. However, the amount of amorphous silica declines with an increased concentration of Na_2O added, as the rising pH also increases SiO_2 solubility.

Therefore, the molarities of Si in the solution become large. When the concentration of Na_2O reaches 0.47 mol/kg, C-S-H and Na-shlykovite co-exist in the phase diagram and the concentration of Si in the solution stays constant then reduces above this addition level, as the supplied Si starts to react with Na_2O and CaO to form various constituents of the C-S-H solid solution. Also, less Ca is consumed by the reaction, thus causing an increase in the amount of Ca in the solution.

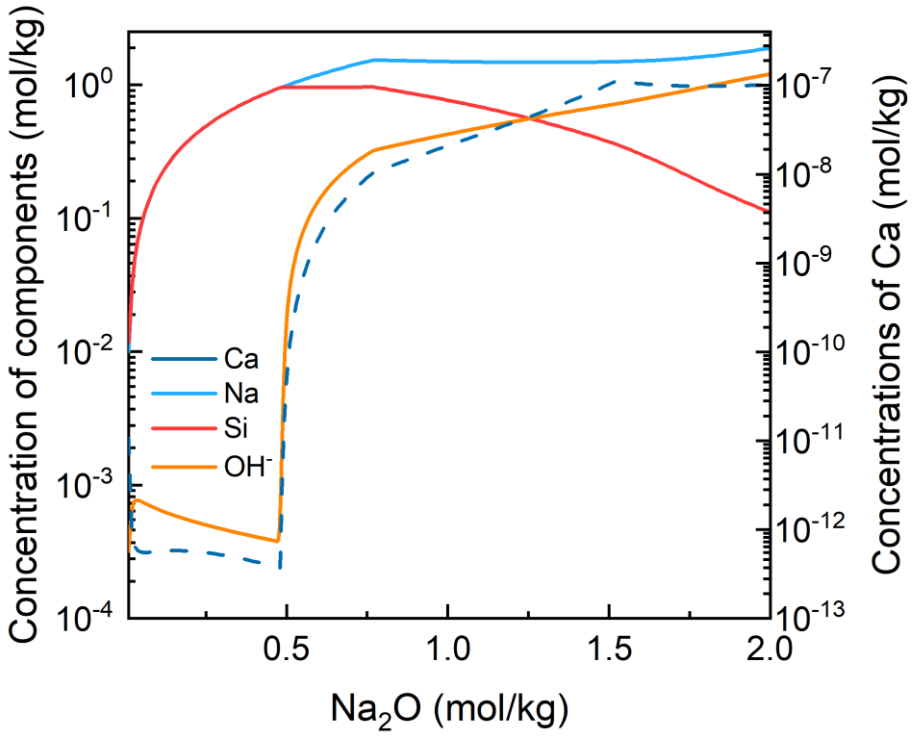

Figure 3-8 The concentrations of Si, Na, and OH^- (left-hand axis, solid lines), and Ca (right-hand axis, dashed line) present in the solution as a function of the concentration of Na_2O added, with 1 mol/kg of SiO_2. The inset diagram places this calculation with respect to the phase diagram by reproducing Figure 3-4a, with a dashed line to indicate the compositions depicted.

Shi and co-workers (Shi et al., 2021b; Shi & Lothenbach, 2019, 2020) have presented some thermodynamic modelling to check their experimental data for ASR processes at 80 °C. In this work, their results have been refined and extended this to the analysis of reaction at 25 °C. The results have some similarities. For example, ASR products are stable at certain concentrations of alkali ions, where they convert to C-S-H when increasing the concentration of dissolved

alkalis and Ca (Shi & Lothenbach, 2020). However, the specific point of conversion of ASR products to C-S-H (or vice versa) is unclear in those previous studies. This work provides more comprehensive modelling data that might guide experiments, and aid in more accurately defining and understanding the existence of a 'pessimum' content of alkalis. More importantly, the modelling presented in this paper is extended to ambient temperature. It means that these results have the possibility to be used in predicting alkali-silica reaction under realistic field conditions. Finally, this work may indicate the need to carefully consider the choice of alkali content in the standard tests for ASR, to gain optimised experimental data and avoid the possibility of false negative test results.

3.4 Conclusions

The aim of this study has been to develop the thermodynamic parameters estimation of Na- and K-shlykovite, phases that are found to form in concrete during alkali-silica reaction (ASR) at ambient temperature. Solubility products of two ASR products by recalculating pH values in the GEM-Selektor v.3 software were refined. Thermodynamic modelling is used to predict the formation of these two ASR products in the (Na, $K)_2O$-CaO–SiO_2-H_2O system, using GEMS with the Cemdata18 database and new thermodynamic parameters obtained from the current study. Binary phase diagrams with different concentration of alkalis are established to verify the reliability of database and compare with experimental data that has been published. The conclusions are summarised as follows:

(1) Without alkali ions there is no ASR product found in the binary phase diagram. When adding 0.01 mol/kg of Na_2O, Na-shlykovite is found, and regions that form this ASR product occupy areas that formed C-S-H and amorphous silica in the absence of Na. The ASR product can co-exist with C-S-H, which indicates that with an increased concentration of CaO, Na has been partially consumed via the formation of ASR products, while the rest of the Ca continues to react with amorphous silica to form C-S-H.

(2) Adding more Na does not always mean the formation of more Na-shlykovite. There is a maximum concentration of Na_2O that enables the formation of Na-shlykovite. Below 1.48 mol/kg of Na_2O, the existence of ASR product proves the possibility of alkali-silica reaction happening. However, beyond that concentration, this type of ASR products is no longer predicted to form, due to the suppression of calcium solubility.

(3) Solubility chemistry results show that adding more Na_2O increases the pH of solution, thus increasing the dissolution of Si and further forming more Na-shlykovite. The formation of Na-shlykovite consumes Ca and Na in the solution, which leads to the decrease in the concentration of Ca and Na. Less Ca is used to take part in the reaction due to the suppression of calcium solubility, and the Si source starts to react with Na_2O and CaO to form C-S-H instead of shlykovite-group minerals.

Chapter 4 . THERMODYNAMIC MODELLING OF ALKALI-SILICA REACTIONS IN BLENDED CEMENTS

Note: This chapter is based primarily on the manuscript "*Thermodynamic modelling of alkali-silica reactions in blended cements*", by H. Jin, S. Ghazizadeh, J. L. Provis, *Cement and Concrete Research*, 2024, 181, 107543.

Abstract

Experiments and field observations have shown that supplementary cementitious materials (SCMs) mitigate the risk of alkali-silica reaction (ASR) in Portland cement blends, but this is difficult to describe thermodynamically due to the lack of appropriate thermodynamic database and challenges in defining the kinetic factors. This paper examines how four well-known SCMs (namely ground granulated blast furnace slag, silica fume, metakaolin, and fly ash) mitigate ASR, by using a multi-stage simulation and a newly extended thermodynamic database. Calcium hydroxide consumption by SCMs hydration, dilution of available alkalis, and alkali binding in calcium-alkali-aluminosilicate hydrate solid solutions, play pivotal roles in understanding the SCMs influence in ASRs. Blending aluminium-rich SCMs in ASR-prone systems appears to act by preventing the dissolution of reactive silica in aggregates rather than suppressing the formation of ASR products. This paper provides new thermodynamic insights into the mechanism by which SCMs enhance concrete durability against ASR.

4.1 Introduction

Using Portland cement blends with supplementary cementitious materials (SCMs), is widely known to control expansion caused by alkali-silica reaction (ASR) in concretes with reactive aggregates. The roles of different types of SCMs are documented in many studies investigating different aspects of ASR (e.g., SCM dosage (Duchesne & Bérubé, 2001; Kandasamy & Shehata,

2014; Moser et al., 2010), composition (Boddy et al., 2003; Shehata & Thomas, 2000), or alkali content (Shehata & Thomas, 2006)). While much remains to be understood about ASR, there is general consensus that SCMs, such as ground granulated blast furnace slag (GGBFS) and silica fume (SF), control ASR by increasing the consumption of $Ca(OH)_2$ from cement hydration (Thomas, 2011). This process reduces the pH of the pore solution and generates calcium silicate hydrate (C-S-H) with a relatively lower Ca/Si ratio. The lower alkalinity slows down the silica dissolution in reactive aggregates, but the C-S-H with lower Ca/Si also binds more alkalis from the pore solution, reducing their availability for ASR (Canham et al., 1987).

SCMs rich in Al, such as metakaolin (MK) from calcined clays or fly ash (FA), are found to be particularly effective in mitigating ASR. One explanation for this is based on the kinetics of aggregate dissolution, where dissolution of reactive silica is suppressed by the sorption of $Al(OH)_4^-$ on its surface (Bickmore et al., 2006). This phenomenon is especially favoured at pH values lower than 13 (Bagheri et al., 2021). The second reason is that it is possible to incorporate Al to replace part of the Si in C-S-H to form calcium aluminium silicate hydrate (C-A-S-H) in the presence of Al-rich SCMs, which leads to an increase in both the basal spacing and the net negative charge on the silicate chains in the C-S-H structure (L'Hôpital, Lothenbach, Kulik, et al., 2016; Yan et al., 2022). Cations from the concrete pore solution may then be expected to compensate this negative charge (Hong & Glasser, 2002; Sun et al., 2006). However, Chappex and Scrivener (Chappex & Scrivener, 2012a, 2012b) suggested that the reduction of alkali ion concentrations in the pore solution when replacing cement by Al-rich SCMs is because of dilution effect. This viewpoint was supported by L'Hôpital et al. (L'Hôpital, Lothenbach, Scrivener, et al., 2016) who showed that there is no remarkable increase in the alkalis uptake in synthetic C-A-S-H compared with C-S-H.

Another school of thought in the literature states that Al could suppress the formation of ASR products by forming some zeolite-like phases with alkalis (Hünger, 2007; Shi et al., 2021), especially in alkali-activated cements where the "N-A-S-H" type binding gel shares important nanostructural features with some common zeolites. However, it is well known that it is difficult to form crystalline zeolites at ambient temperature due to kinetic limitations (Lothenba et al., 2017), meaning that any such alkali-aluminosilicate phases that do form in reality would be more likely to be disordered. Krüger et al. (Krüger et al., 2023) investigated the structure of

ASR gel with and without Al by ^{29}Si and ^{27}Al nuclear magnetic resonance (NMR) and Fourier-transform infrared (FTIR) spectroscopy, and found that changes in the structure of swelling gel, instead of precipitation of discrete zeolites, were the main reason for differences in observed performance when incorporating aluminium.

Thermodynamic modelling is a robust method to predict phase assemblages and solution chemistry in cementitious systems. Various studies have applied thermodynamics to ASR. For example, Zhou et al. (Zhou, Chen, Liu, et al., 2022; Zhou, Chen, Zheng, et al., 2022; Zhou et al., 2019) investigated the role of metakaolin and γ-Al_2O_3 in inhibiting the damage caused by ASR, and used modelling to verify the results obtained from experiments, but the thermodynamic database they used in their model, did not include several important potential ASR products such as shlykovite-type phases. Guthrie and Carey (Guthrie & Carey, 2015) developed a model to predict the formation of magadiite and okenite, which are two possible ASR products, and Shi et al. (Shi et al., 2019) have successfully synthesised and characterised two shlykovite-type ASR products which they identified as being more similar to phases found in field concretes. Jin et al. (Jin et al., 2023) built upon this work to further refine the thermodynamic properties of shlykovite-type phases, and modelled their formation at 25°C in a series of alkali-CaO-SiO_2 systems, providing a foundation for further predictions of ASR products in cementitious systems.

Additionally, while hydration prediction for cements with different SCMs has been comprehensively developed, as described by Lothenbach et al. (Lothenbach et al., 2011), there is a lack of literature covering thermodynamic models to predict ASR in blended cements. The aim of this paper is to model ASR products in blended cements at ambient temperature, using the thermodynamic data from the earlier study [27]. A two-step approach is used to model ASR in Portland cement blends with four SCMs: GGBFS, FA, MK or SF. The first step models cement hydration whereas the second step models ASR (a much slower process) using the result of the first step. The modelling is particularly focused on the influence of Al from SCMs on ASR. This can help select the most useful SCMs for ASR resistance, to predict ASR in cement blends and to complement or better understand the ASR durability test results.

4.2 Methods and model description

4.2.1 Software and database

The GEM-Selektor software (http://gems.web.psi.ch/GEMS3/) (Kulik et al., 2013; Wagner et al., 2012) was used to calculate ion interactions and phase predictions based on minimization of Gibbs free energy with mass balance constraints. The activity coefficients of aqueous species are calculated by the Truesdell-Jones form of the extended Debye-Hückel equation, which is shown in the Eq. 2-11 in section 2.4,1.Assuming that the aqueous phase in a cement or blended system is dominated by KOH solution, a and b_γ are 3.67 Å and 0.123 kg/mol respectively (Helgeson et al., 1981).

The Cemdata18 database (Lothenbach et al., 2019) covers the majority of phases used in this study, complemented by the ASR product parameters (for Na- and K-shlykovite) obtained from the previous research (Jin et al., 2023).

4.2.2 Model description

4.2.2.1. Input parameters

The study considers the effect of four main SCMs (GGBFS, SF, MK, FA) blended with Portland cement. Two types of fly ash are used in the modelling work: Fly ash S (FA S) is a siliceous fly ash (also described as “class F” under the ASTM C618 standard), while fly ash C (FA C) is calcareous (corresponding approximately to ASTM C618 class C). The compositions of SCMs and Portland cement are variable between sources, and so a set of representative compositions were selected for use here, based on published data: (Moser et al., 2010) for FAC; (Duchesne & Bérubé, 2001) for PC, SF, FAS; (Tapas et al., 2021) for GGBFS; and (Ramlochan et al., 2004) for MK. Table 4-1 summarizes the chemical compositions of these materials, along with the SCM replacement ratios simulated. When inputting the composition of a cement or SCM in the GEMS software, selecting the constituent oxides or cementitious phases gains the same results, and the oxide approach was used here. The water to cementitious solids ratio (w/s) is selected as 0.47 in all cases. This w/s ratio is chosen to match the ASTM C1567 alkali-silica reactivity testing requirement. The temperature here was chosen to be 25°C.

Table 4-1 The chemical compositions of the SCMs and Portland cement used in the modelling, expressed as wt% of oxides and with replacement percentages calculated on a mass basis.

	SiO_2	CaO	Al_2O_3	Fe_2O_3	MgO	Na_2O	K_2O	SO_3[a]	Replacement levels
Portland cement	20.5	63.1	5.5	2.5	2.8	0.3	1.2	2.6	0
GGBFS	34.1	41.6	14.4	0.3	5.3	0.4	0.3	2.8	20/30/40/50%
SF	94.2	0.5	0.2	0.3	0.5	0	1.2	0.1	5/10/15%
MK	52.1	0.1	45.3	0.6	0	0.2	0.2	0	5/10/15%
FA S	42.2	1.9	21.6	27.6	0.9	0.7	2.6	1.1	20/40%
FA C	36.9	24.8	18.1	6.1	5.9	1.9	0.5	1.7	20/40%

[a] Sulfur is represented in oxide form in tabulating the compositions here.

4.2.2.2 Model assumptions

If not carefully designed, thermodynamic models are not able to directly describe kinetic aspects of a process. This is important for ASR modelling, as ASR impacts concrete after most of the cement and/or SCMs hydration is complete. The formation of ASR products takes much longer than cement hydration. If ASR is modelled, by assuming that the cement, SCMs, and silica from the reactive aggregates react simultaneously with water, this would only show that silica undergoes a pozzolanic reaction and ASR products would not form. To be able to describe ASR, cement hydration modelling therefore must be separated from ASR, as shown in Figure 4-1.

The author separates the timescales of cement hydration and ASR entirely and assumes that cement hydration (with or without SCMs) is essentially completed before ASR happens. Cement hydration occurs mainly within a period of weeks, then decelerates significantly to reach a rate that is effectively negligible when considering the multi-year timescales of ASR at

room temperature. The first step in the simulation models cement hydration, where the author allows for cement and/or SCMs to hydrate only up to a certain degree. In the second step, the silica from reactive aggregate, is added to the system to participate in reactions with the calcium hydroxide and pore solution contents derived from the first step.

The available body of evidence indicates that $Ca(OH)_2$ is the main hydration product that could affect or take part in ASR (Chatterji, 1979; Hou et al., 2004). Other hydrates have a minor effect and thus they are not considered in the second step of the simulation. Further indirect support for this approach is provided by the work of Tapas et al., (Tapas et al., 2021) who proposed a modified solution to simulate the pore solution of cement paste, and used this to replace traditional ASR testing solutions in their investigation of ASR.

Although ASR tests in standards add an artificially high amount of extra alkali – either in the mix water or by immersion – no boosted alkali level is applied in this study. The aim of this approach is to predict ASR in real cementitious systems without any external alkali source. In order to simulate the formation of ASR products via this modelling approach, the quantity of available silica from reactive aggregates is set to be 50 g per 100 g of total cementitious materials, as an oxide. This has been selected from preliminary simulation work. When the added silica content is too low, it reacts with portlandite to form other hydrates such as C-S-H due to the suppression of calcium solubility, instead of forming ASR products. However, beyond this level of added silica, the potentially reactive cementitious phases are depleted and so the formation of ASR products no longer increases; the remainder exists as amorphous silica. Therefore, 50 g of silica representing the dissolution of reactive silica from the aggregate is suitable for the simulation.

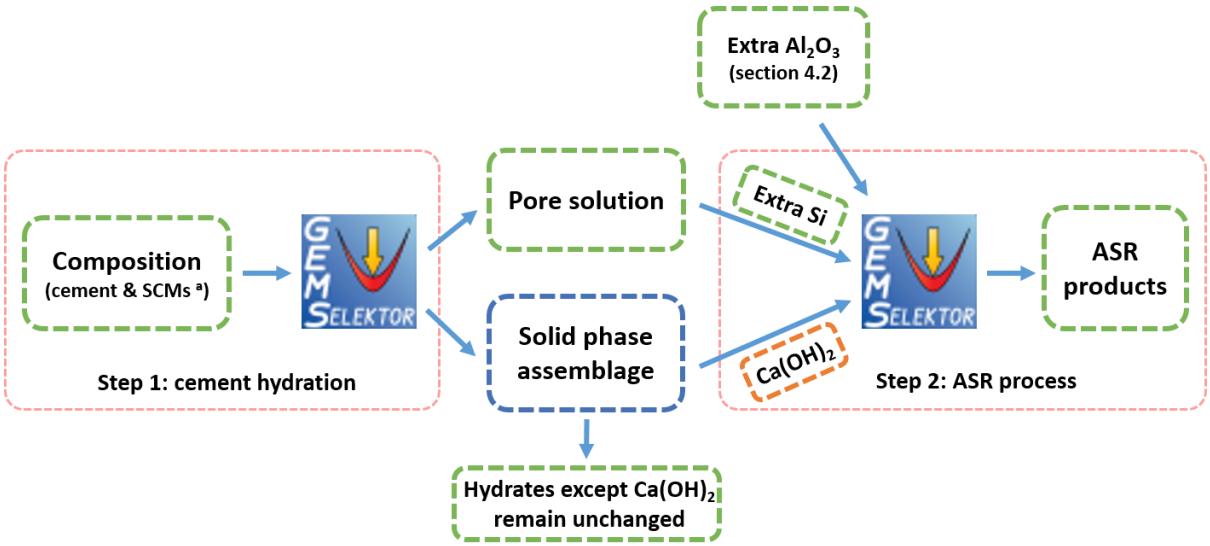

Figure 4-1 Illustration of the two-step method used to simulate the process of ASR.

[a] Cement and SCMs each have the specified degree of reaction applied in the simulation (see section 4.2.2.3)

Table 4-2 Simulations variants conducted in this study to investigate ASR processes (step 2 of Figure 4-1, all data are calculated from the GEMS software; information is shown in more detail in the Appendix A)

Simulation		Pore solution content (mol) [a]	Pore solution pH	Pore solution total $K^+ + Na^+$ concentration (mol/kg H_2O)	$Ca(OH)_2$ (g)	Reactive SiO_2 (g)
PC [b]		0.79	13.4	0.38	43.12	50
PC + GGBFS	20%	0.89	13.3	0.31	31.45	50
	30%	0.94	13.2	0.28	25.48	50
	40%	1.01	13.2	0.25	19.52	50
	50%	1.04	13.2	0.23	13.72	50
PC + SF	5%	0.81	13.3	0.30	33.31	50
	10%	0.83	13.2	0.25	23.51	50

	15%	0.85	13.1	0.21	13.69	50
PC + MK	5%	0.86	13.4	0.35	36.65	50
	10%	0.93	13.4	0.32	29.92	50
	15%	0.96	13.3	0.31	23.49	50
PC + FA	20% FAS	1.08	13.4	0.38	25.36	50
	40% FAS	1.37	13.4	0.38	7.32	50
	20% FAC	1.04	13.4	0.37	30.19	50
	40% FAC	1.29	13.4	0.37	16.99	50

[a] Defined as the amount of pore solution remaining after hydration of 100 g of each cementitious blend (to the degree of reaction as specified in section 4.2.2.3) by reaction with 47 g of water. Full compositions of the pore solutions in each case are given as Supporting Information

[b] This composition was also used for simulations where extra Al_2O_3 (1 – 10 g) was added directly into stage 2, see section 4.4.2.

4.2.2.3 Degree of reaction of cementitious materials

This study assumes that the Portland cement fully hydrates in the calculation of its portlandite content and pore fluid chemistry, for use in the ASR modelling step. The different types of SCMs will each have a different degree of hydration (DoH) in the blended cements – the assumptions for this are shown in Table 4-3. The hydration of GGBFS in blended cements is relatively extensive but not fully complete; in this study, the DoH of slag is set to 70% (Lothenbach et al., 2011). SF is extremely fine and amorphous, leading to high reactivity (Siddique, 2011), and so the DoH of silica fume in the cementitious blends is allowed to reach 100%. The MK used in the simulations is relatively pure without a significant quartz impurity according to its Si/Al ratio; MK reactivity depends on the crystallinity of the original kaolinite, the degree of dehydroxylation, and its particle size (Bich et al., 2009; Kakali et al., 2001). A 50% DoH of MK was applied in the modelling work presented in (Kunther et al., 2016; Ramanathan et al., 2019), and is also applied in this study.

For fly ash, many studies have reported DoH of this material in cement blends using different methods (Durdziński, Dunant, et al., 2015; Durdziński et al., 2017; Durdziński, Snellings, et al., 2015; Glosser et al., 2021), reaching results which tend to be rather scattered. There are several types of glass composition in the heterogeneous fly ash particles (e.g., silicate, calcium-silicate, aluminosilicate, and calcium-rich aluminosilicate) which may have different contributions to the hydration reaction, while stable crystalline minerals remain unreacted. Therefore, a truly precise description of fly ash in a thermodynamic model should extract the content of crystalline material from the chemical compositions obtained from X-ray fluorescence (XRF) analysis to enable simulation of the reactive fraction only. However, the aim of this study is mainly to provide a modelling method to simulate ASR in blended cements in general, rather than to focus on the characteristics of a specific ash, and so a 40% DoH (based on bulk XRF composition and neglecting differential reactivity between phases) is used for both types of fly ash. All DoH values used in this study are summarised in Table 4-3.

Table 4-3. Degree of hydration (DoH) for the supplementary cementitious materials used in this study

	Slag	Silica fume	Metakaolin	Fly ash (C or S)
DoH/%	70	100	50	40

Additional simulations were also conducted using the Portland cement pore fluid chemistry with the addition of small amounts of Al_2O_3 from 1 to 10 g (see Table 4-2), to isolate the direct Al chemical effects from the effects of SCM hydration on pore fluid chemistry – see section 4.4.2.

4.3 Results and discussion

4.3.1 Simulation of blended cement hydration

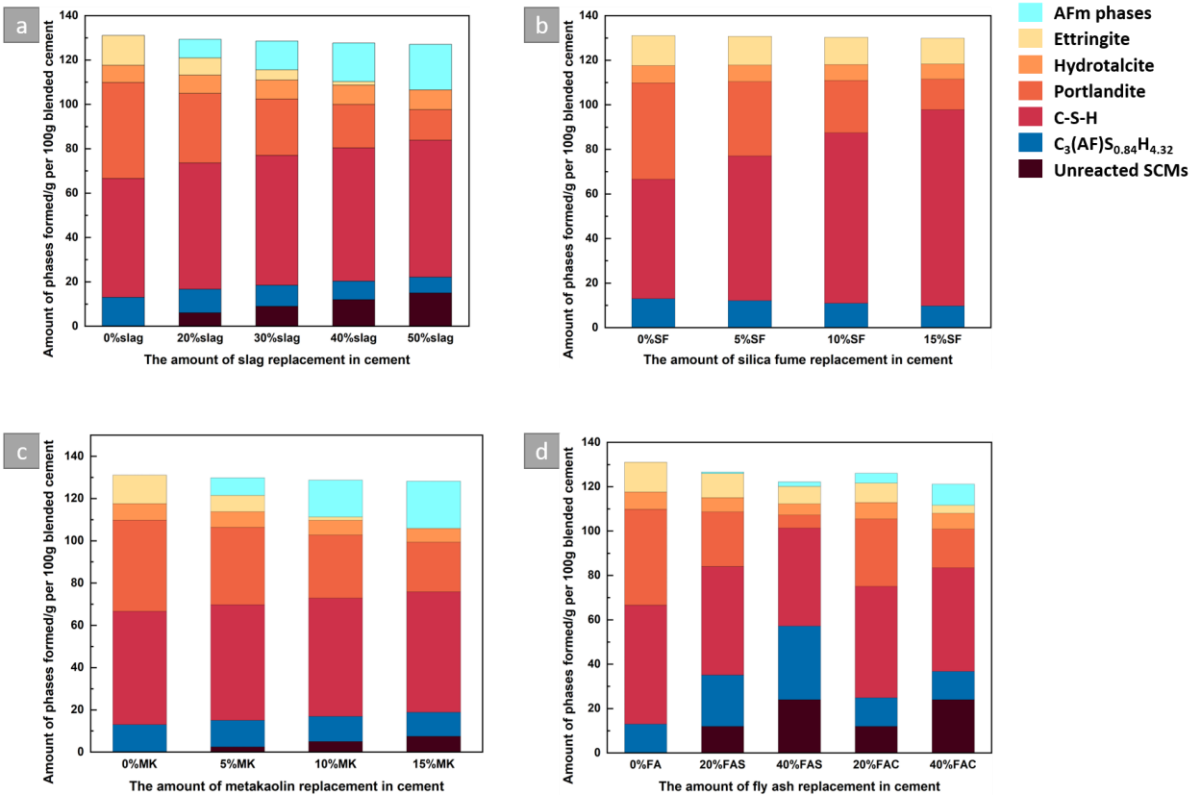

Figure 4-2 Phase assemblage after hydration in cement blended with different types of SCMs. a: ground granulated blast furnace slag, b: silica fume, c: metakaolin, d: fly ash

Incorporating each of the four types of SCMs into hydrating cement changes the phase assemblage formed after hydration, as shown in Figure 4-2. In the absence of SCMs, the predicted hydration products contain C-S-H, portlandite, ettringite, siliceous hydrogarnet, and hydrotalcite. Hydrotalcite is predicted in the simulations as the final destination of the small amount of Mg from the Portland cement clinker, as the models used here do not account for any minor uptake of Mg into the other hydrate phases. The formation of more AFm phases is found in the blended cements, except when SF is used as an SCM, due to the extra Al sources added without extra SO_3, meaning that ettringite is less favoured and sulfate-containing AFm phases instead form at increased SCM content (Matschei et al., 2007a). In addition, the amount of C-S-H formed increases in the presence of most of the SCMs, although it decreases when incorporating both fly ashes, due largely to the presence of the inert/unreacted fraction of the fly ash, which is in good agreement with previous modelling [28]. There is no monocarbonate

AFm formed in results; the SCM compositions defined here do not include carbonate. Strätlingite is also not observed.

The consumption of $Ca(OH)_2$ in SCM hydration is often discussed as a mechanism for the mitigation of ASR (Chatterji & Clausson-Kaas, 1984; De Souza & Sanchez, 2023; Duchesne & Bérubé, 1994b; Figueira et al., 2019), and the results here show that the reduction in Ca availability for shlykovite formation is potentially important. For example, blending more SF into the cement formulation increases the consumption of portlandite during hydration, with its content falling from 43.2 g from hydration of 100 g of the plain cement, to 13.7 g with 15% SF. The results here are in good agreement with the modelling conducted by Lothenbach et al. (Lothenbach et al., 2011), although there are a few differences due to the composition of SF. Compared with those results where they used pure SiO_2 in the SF-cement simulation, the level of consumption of portlandite is higher than is predicted here, and the increase in low Ca/Si C-S-H formed is also predicted (Lothenbach et al., 2011). Beyond about 17% of replacement, portlandite was fully consumed. Because most of research regarding the role of SF in mitigating ASR focused on its dosage below 20%, rather than the higher contents used to formulate low-pH cements in that previous study, the modelling is carried out within this lower range (Aquino et al., 2001; Bektas et al., 2005; Juenger & Ostertag, 2004; Maas et al., 2007; Zhang & Wang, 2008).

It can be also seen that the decrease in $Ca(OH)_2$ at 15% metakaolin is lower than that mentioned in the experimental study of Jones et al. (Jones et al., 1992), who stated that no $Ca(OH)_2$ was found in their samples at this composition. The difference between modelling and experiment might be related to the curing temperature; 38°C was adopted in their whole experimental process, and a higher temperature could lead to preferential acceleration of the reaction process of one blend constituent over the other if there is a difference in their apparent activation energies, which appears to be the case for metakaolin and Portland cement (Williams et al., 2016), thus consuming more $Ca(OH)_2$. Another explanation for this might be the degree of reaction of metakaolin. In this study, a 50% DoH of metakaolin was used in the modelling, which was assumed based on several literature studies (Kunther et al., 2016; Ramanathan et al., 2019). A higher DoH – which may also result from a higher hydration temperature – could also

result in a decrease in the formation of $Ca(OH)_2$ (Briki et al., 2021). The complete details of the mass of each phase formed during cement hydration can be seen in the Appendix A.

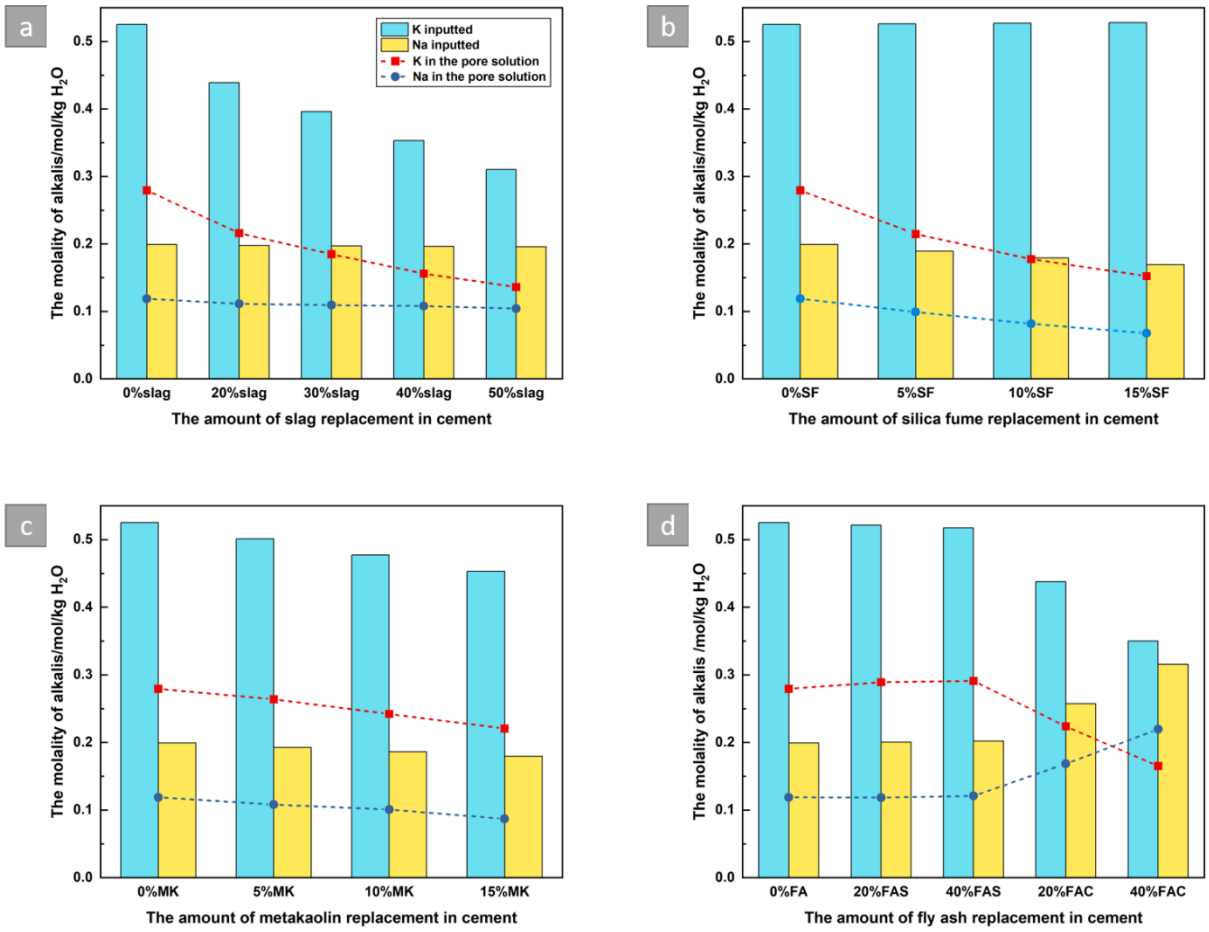

Figure 4-3 Alkalis inputted in step 1 (columns) and remaining in the pore solution after hydration (points), for cements blended with SCMs. a: ground granulated blast furnace slag, b: silica fume, c: metakaolin, d: fly ash

Another factor that may affect the formation of ASR products is the quantity of alkalis left in the pore solution (Kim et al., 2015; Multon et al., 2008; Plusquellec et al., 2018; Shi & Lothenbach, 2020). To investigate this, Figure 4-3 shows alkali sources in the cement with or without SCMs, and the quantities remaining in the pore solution after hydration. It is clear that the molality of K and Na inputted decrease to varying degrees when incorporating slag, metakaolin and calcareous fly ash. However, silica fume and siliceous fly ash have higher K_2O content, while calcareous fly ash has higher Na_2O content (see Table 4-1).

After hydration, the alkali concentrations left in the pore solution are determined at least by the SCM replacement level, which is partly attributed to the dilution effect (Arano & Kawamura, 2000). For example, as can be seen in Figure 4-3a, presenting the alkali contents and pore fluid alkali concentrations for cements blended with slag, the molality decreased from 0.28 mol/L for K and 0.118 mol/L for Na in cement to 0.13 mol/L for K and 0.104 mol/L for Na in cement blended with 50% slag, respectively. A similar trend is seen in the metakaolin and fly ash blended cements. In the presence of silica fume the quantity of K left in the pore solution after hydration behaves rather differently; with an increase in the replacement level of silica fume, the concentrations of K in the pore solution show a marked decreasing trend, similar to the trend observed for Na, although these cement formulations have the same K contents because both the SF and PC described here are defined to have 1.2 wt.% K_2O. This may be caused by chemical binding of alkalis taking place in the C-S-H phase, which here has a Ca/Si ratio lower than 1.6 (Bernard et al., 2021; Hong & Glasser, 1999), which compensates in part for the negative surface charge at lower Ca content. The mechanism of reduction in alkali availability for ASR product formation, and its effects, will be discussed in more detail in section 4.4.

4.3.2 The effect of SCMs on mitigating the formation of ASR products

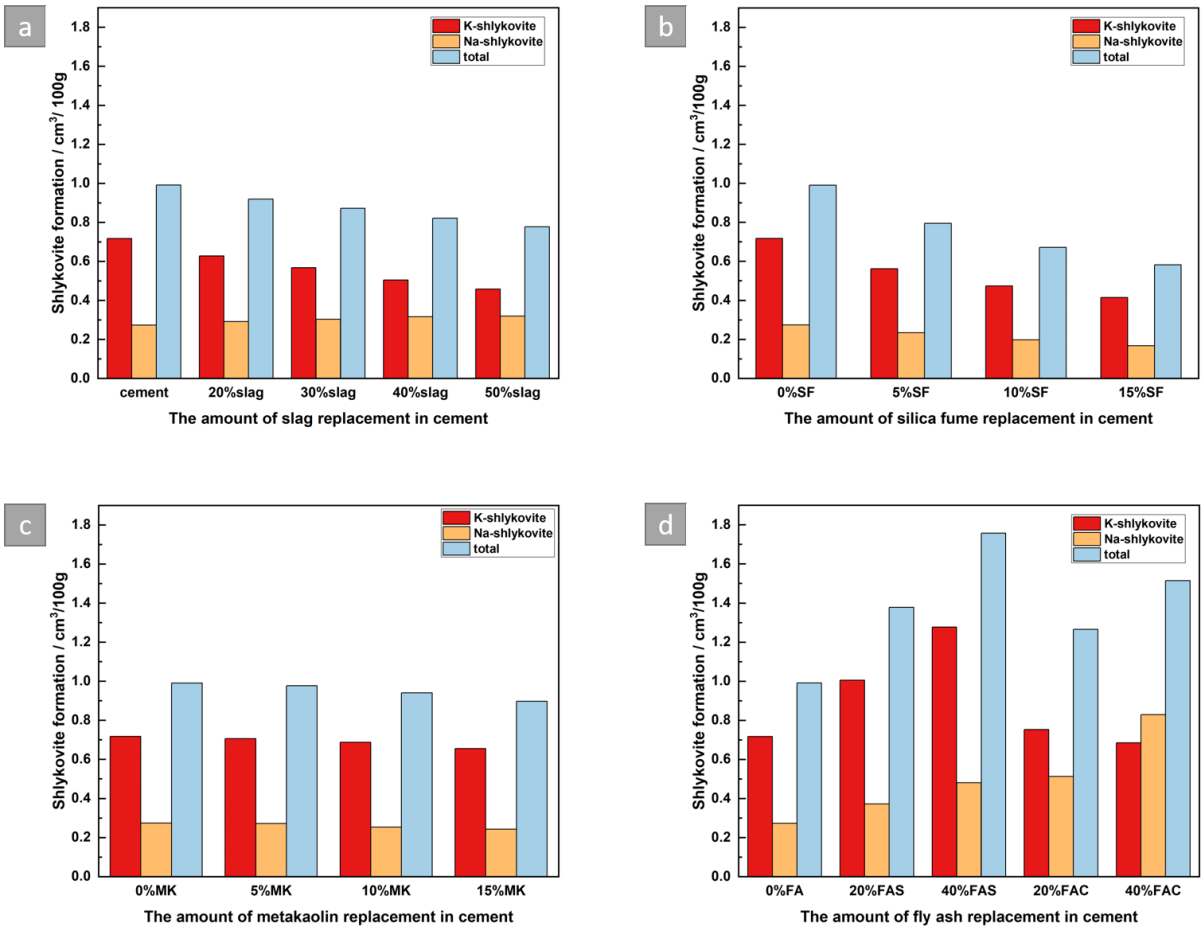

Figure 4-4 The volumes of ASR products predicted to form in the cements blended with different amounts of SCMs. a: ground granulated blast furnace slag, b: silica fume, c: metakaolin, d: fly ash

The volumes of the two ASR products precipitated, and the totals of their volumes, are shown in Figure 4-4 for the simulations of incorporation of different types of SCMs into the cements at different replacement levels. It can be seen that the total volume of ASR products formed reduced in the presence of slag, and the degree of reduction increased with increasing slag content, which is consistent with trends shown in the literature (Hobbs, 1986; Lane & Ozyildirim, 1999; Rasheeduzzafar & Ehtesham Hussain, 1991; Tapas et al., 2021). Although the ASR reaction process does proceed in the presence of slag according to these simulations, the decreased volume of ASR products supports observations of the effectiveness of slag in mitigating this durability problem. A 50% replacement level of slag is enough to have a

significant impact on reducing the volumetric expansion caused by ASR (Duchesne & Bérubé, 2001).

Boddy et al. (Boddy et al., 2003) stated that silica fume led to delaying instead of full mitigation of ASR when the replacement of silica fume is lower than 5%, which is in part consistent with the current results where the volumes of shlykovite-type products formed decrease. The simulation approach used here is not able to specifically address questions around the time-dependence of the onset of ASR. When increasing the replacement level of silica fume to 15%, the volumes of ASR products formed reduced dramatically, from almost 1 cm^3 per 100 g of plain cement, to 0.58 cm^3 per 100 g of SF blended cement. This trend is in good agreement with Bektas et al. (Bektas et al., 2005) who showed that 16% silica fume in a blend with PC has the strongest effect on expansion suppression (and limits expansion to below 0.1%).

Compared with cement blended with slag or silica fume, the effect of metakaolin seem to be weak in terms of the mitigation of the formation of ASR products, with only a small decrease in the total volume of shlykovite-type phase formation (from 0.99 to 0.89 cm^3 per 100 g cement) with metakaolin addition at up to 15%. These results seem to be incompatible with experimental data (Aquino et al., 2001; Duchesne & Bérubé, 2001) that show metakaolin to be highly effective in controlling ASR. However, it should once again be noted that this modelling work is based on thermodynamics, which means that reaction kinetics (for example suppression of silica dissolution by the Al that is rapidly released by metakaolin dissolution) may be another factor controlling the process that is not included in the current modelling.

Fly ash, as another Al-rich SCM, is also used to inhibit ASR in the field (Hay & Ostertag, 2021; Kawabata & Yamada, 2017), and its effect on the formation of ASR products is shown in Figure 4-4d for both low-calcium (FA S) and high-calcium (FA C) ashes. However, compared with the other three SCMs studied, both types of fly ashes simulated here seem to promote shlykovite precipitation, especially for FAS which is more alkali-rich than any other of the cementitious constituents studied. Both K- and Na-shlykovite show an increasing trend within the equilibrium phase assemblages as the replacement of cement by siliceous fly ash increases. Conversely, the volume of K-shlykovite decreases when calcareous fly ash is added, while Na-

shlykovite still increases. This is directly aligned with the bulk ash compositions. The overall ASR process is, of course, controlled by a combination of factors more complex than simply the volume of reaction products, including both the crystallisation pressure and the kinetics of reaction, but the simulations presented here do provide new insight into the thermodynamic aspects which influence (but do not always fully control) the trends in observed behaviour.

4.4 Discussion

4.4.1 The role of SCMs

Calcium plays an important role in the process of ASR. On one hand, calcium may replace alkalis in the ASR gel during the early stage of ASR to form expansive products, which otherwise is not detrimental in the absence of Ca, shown in Eq. 4-3 where M^+ indicates alkali metal ions and … indicates strong Van der Waals bonding (Leemann et al., 2011; Rajabipour et al., 2015). Alkalis recycled via this reaction can further participate in the precipitation of ASR gel. On the other hand, $Ca(OH)_2$ can be considered as a buffer for the pH value of the pore solution, which is the key driving force for the dissolution of reactive aggregates (Maraghechi et al., 2016; Wang & Gillott, 1991). In a Portland cement system, the calcium source for this process is mainly portlandite, and so decreasing its content in the hydrate phase assemblage thus becomes a key method to mitigate ASR damage.

$$2 \equiv Si - O \ldots M + \ Ca^{2+} \ \rightarrow \equiv Si - O \ldots Ca \ldots O - Si \equiv + 2M^+ \qquad \textbf{Eq.4-3}$$

Figure 4-5 presents the relationship between the formation of $Ca(OH)_2$ and the volume of two shlykovite-type ASR products formed when incorporating different types of SCMs. Combining the results presented in Figure 4-2, it can be concluded that the degree of consumption of $Ca(OH)_2$ is generally significant in the presence of SCMs, which results in reduced availability of OH^- ions and thus gives a decreased driving force for further dissolution of the reactive aggregates. The modelling results support the majority of studies which have experimentally investigated the role of SCMs.

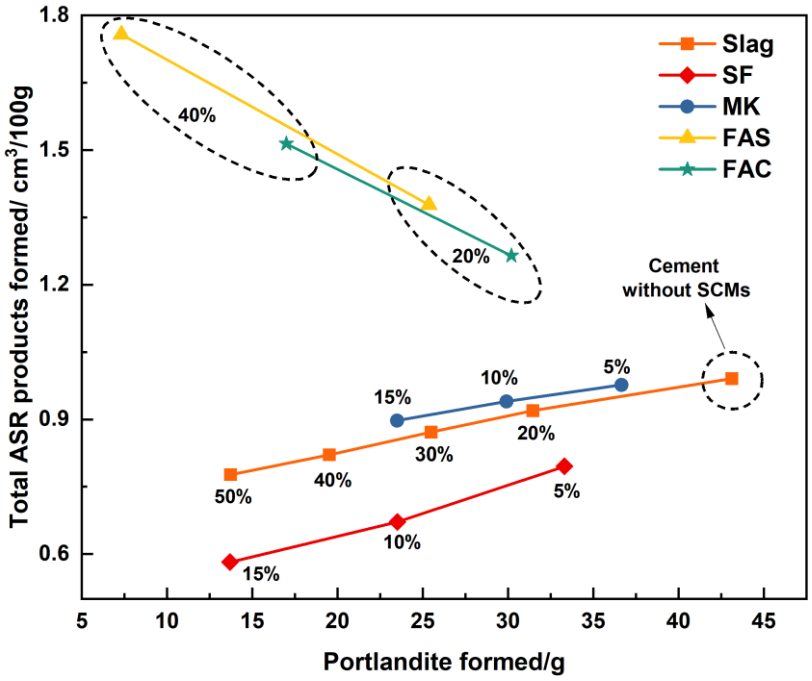

Figure 4-5 The relationship between the formation of portlandite and ASR products in cement blended with different types of SCMs

However, if solely emphasising the importance of reducing the amount of portlandite, some of the simulations do seem to be incompatible with the established understanding of the effectiveness of SCMs, especially when considering fly ash. Therefore, there must be another vital factor that influences the formation of ASR products. Incorporating slag, at least into a blend with a relatively high-alkali PC, leads to a reduction in the alkalis available to participate in the ASR process from the source (Figure 4-3a), thus reducing the amount of ASR products formed; this is a dilution effect. This effect can also be used to explain the decrease in the alkali content for MK-cement blends. Due to the relatively high K content in the silica fume used in the simulations here (although representing an average value compiled from various literature), being approximately the same as in the PC, the amount of K inputted into the cement hydration modelling remains constant at all SF contents simulated, as shown in Figure 4-3b. This indicates that unlike the roles of blast furnace slag and metakaolin that dilute the concentration of alkalis inputted, incorporating silica fume into cement in these simulations leads to binding of more alkalis and rendering them unavailable for ASR processes, thus reducing the formation of ASR products and consequent expansion in this way.

Increasing C-S-H content, as shown in Figure 4-2b, can be identified as a primary reason for binding of more alkalis to remove them from the pore solution. However, the simulations provide information at a deeper level than this, when considering the different end-members present in the solid solution model used to describe the C-S-H type hydrate phases (Kulik et al., 2022; Myers et al., 2014; Shi & Lothenbach, 2019), Figure 4-6.

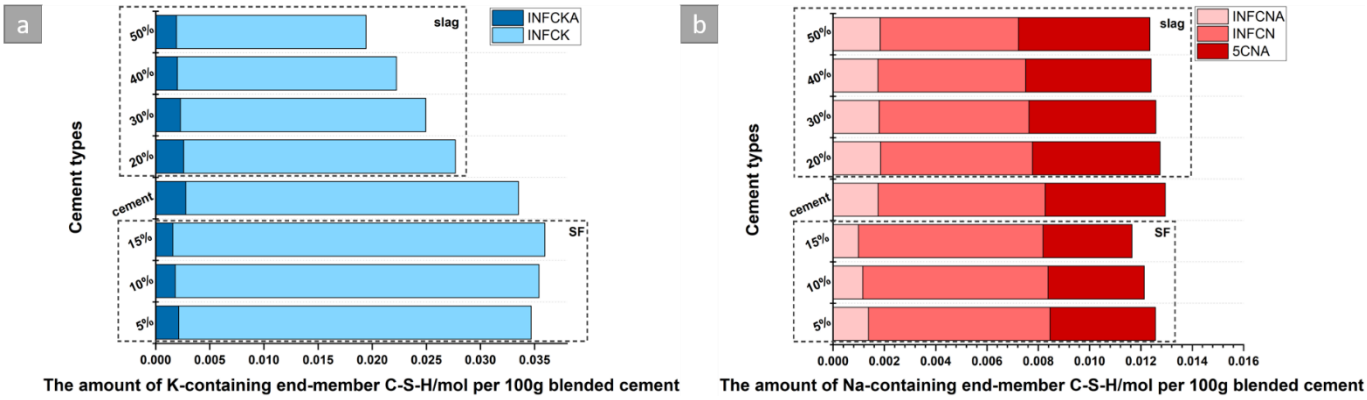

Figure 4-6 The amount of the alkali-containing C-S-H solid solution end-members formed in hydration of cements with different amounts of slag and silica fume: INFCK and INFCKA for K-containing end-members in (a); 5CNA, INFCN, and INFCNA for Na-containing end-members in (b); acronyms are defined in Table 4-4.

*Table 4-4 The composition of end-members of the C-A-(N,K)-S-H solid solution used in this study (**bold** means binding K or Na)*

End-member	Composition	With alkalis (K or Na)
5CA	$(CaO)_{1.25}(Al_2O_3)_{0.125}(SiO_2)_1(H_2O)_{1.625}$	
INFCA	$(CaO)_1(Al_2O_3)_{0.15625}(SiO_2)_{1.1875}(H_2O)_{1.65625}$	
5CNA	$\mathbf{(CaO)_{1.25}(Na_2O)_{0.25}(Al_2O_3)_{0.125}(SiO_2)_1(H_2O)_{1.375}}$	√
INFCNA	$\mathbf{(CaO)_1(Na_2O)_{0.34375}(Al_2O_3)_{0.15625}(SiO_2)_{1.1875}(H_2O)_{1.3125}}$	√
INFCN	$\mathbf{(CaO)_1(Na_2O)_{0.3125}(SiO_2)_{1.5}(H_2O)_{1.1875}}$	√

INFCKA	**$(CaO)_1(K_2O)_{0.34375}(Al_2O_3)_{0.15625}(SiO_2)_{1.1875}(H_2O)_{1.3125}$**	√
INFCK	**$(CaO)_1(K_2O)_{0.3125}(SiO_2)_{1.5}(H_2O)_{1.1875}$**	√
T2C	$(CaO)_{1.5}(SiO_2)_1(H_2O)_{2.5}$	
T5C	$(CaO)_{1.25}(SiO_2)_{1.25}(H_2O)_{2.5}$	
TobH	$(CaO)_1(SiO_2)_{1.5}(H_2O)_{2.5}$	

The high-chain-length alkalis-containing end-members of the C-S-H and C-A-S-H solid solution (INFCK and INFCKA as K-containing end-members, and 5CNA, INFCN, and INFCNA with Na) were described in (Myers et al., 2014; Shi & Lothenbach, 2019), and their presence among the simulated C-S-H type gel structure can be used to represent C-S-H binding some of the alkalis from the pore solution. The development of thermodynamic data of these end-members was based on alkali activated cements which pay more emphasis on Na-activators rather than potassium-types; the 5CKA type end member of C-S-H is thus incomplete and not included in this study. The compositions of these end-members can be seen in Table 4-4. Figure 4-6 shows the amount of alkali-binding end-members of C-S-H that are formed in the plain hydrated cement, and also for cements blended with different amounts of silica fume or slag. Incorporating silica fume into cement increases the formation of K-containing end-members, which is favoured by lower Ca/Si ratios that lead to higher chain lengths, and indicates that the ability to bind alkalis in C-S-H improves in the presence of silica fume. Conversely, C-S-H in the cements containing slag has less of this K-containing end-member due to the presence of less K in the formulations. In terms of Na-type end-members, blending slag or silica fume does not affect the formation very much. This is partially due to the lower content of Na in the blend. However, the sum of C-S-H binding of both alkalis still increases. This result supports the idea mentioned above, that the presence of silica fume aids alkali binding through the formation of more C-S-H. The potential role of Al in alkali binding will be discussed in the next section.

Overall, Figure 4-7 summarise the relationship between the available alkalis in the pore solution and the formation of ASR products when considering the role of each of the SCMs. There exists a linear relationship, that more alkalis in the pore solution result in precipitation

of more ASR phases. Combining this with the relationship shown in Figure 4-5, the data gained in simulations are sufficiently verified.

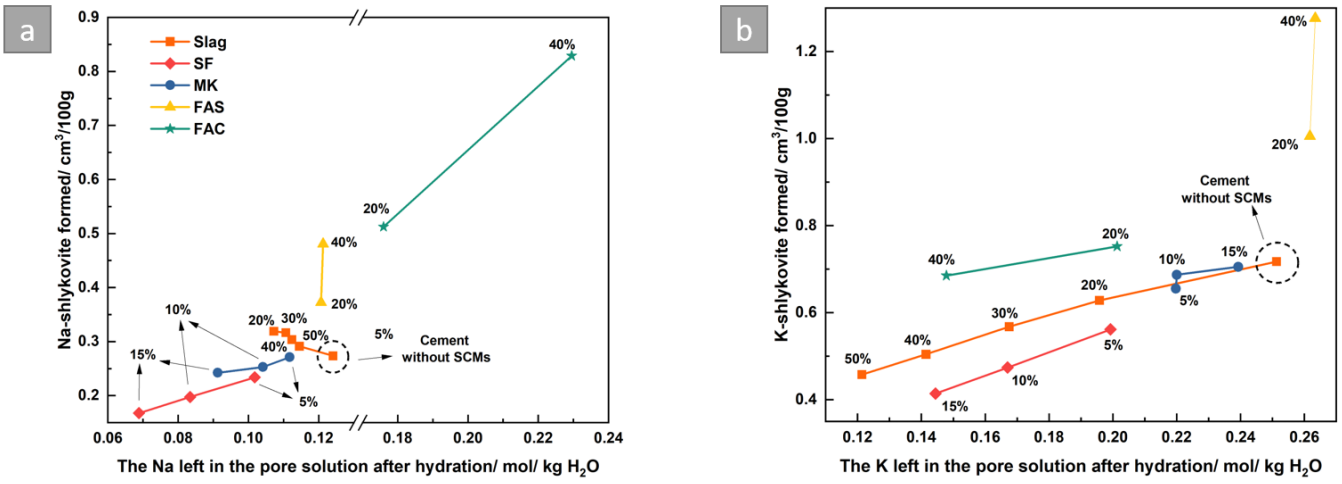

Figure 4-7 the relationship between the alkalis left in the pore solution and the formation of correspondingly shlykovite phases in blended cement

4.4.2 The role of Al

In terms of the role of Al supplied by Al-rich SCMs, Hong and Glasser (Hong & Glasser, 2002) emphasised the binding capability of alkali onto C-A-S-H. However, this was disputed by Chappex and Scrivener, who claimed instead that the effect of alumina on alkali fixation of synthesised C–S–H is insignificant (Chappex & Scrivener, 2012a, 2012b). For the simulations conducted here, Figure 4-8 shows the change in the amount of alkali-containing C-S-H end-members formed, with the change of Al/Si ratio in the C-A-S-H, as a function of metakaolin content. When increasing the replacement level of metakaolin, the Al/Si ratio in the C-A-S-H increases slightly, from 0.067 to 0.089. However, the amounts of C-S-H endmembers containing alkalis do not increase. In fact, instead of growing, the alkali-bearing C-S-H endmembers gradually reduce with metakaolin addition due to the dilution of alkalis caused by replacing the (relatively high-alkali) cement by the low-alkali metakaolin used in these simulations. In order to further assess the competition between dilution effects and alkali fixation in C-S-H, the degree of reduction of alkalis present, against those which are bound in the C-S-H and free in the pore solution, is shown in Figure 4-9. If the alkali binding capability of C-S-H increases when using Al-rich SCMs, the trend for the degree of alkali reduction in the C-S-H should stay steady or negative although the total quantity of alkalis present decreases. However, it can be seen that the slopes of lines in Figure 4-9a and b are similar. In addition,

for K in the pore solution the degrees of reduction become negative, which indicates that more K is left in the pore solution rather than being bound in the C-S-H. These data support the findings of Chappex and Scrivener (Chappex & Scrivener, 2012a, 2012b).

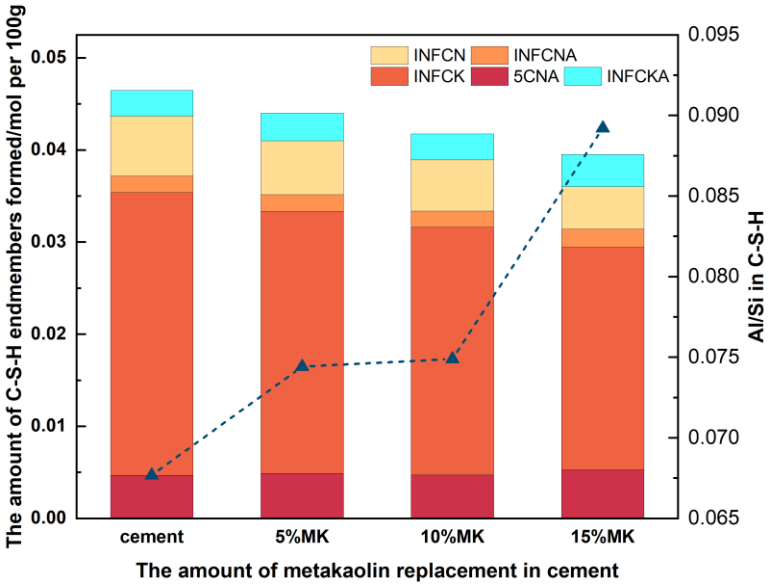

Figure 4-8. The amounts of C-S-H end-members containing alkalis that are predicted to be formed and Al/Si ratio in C-S-H.

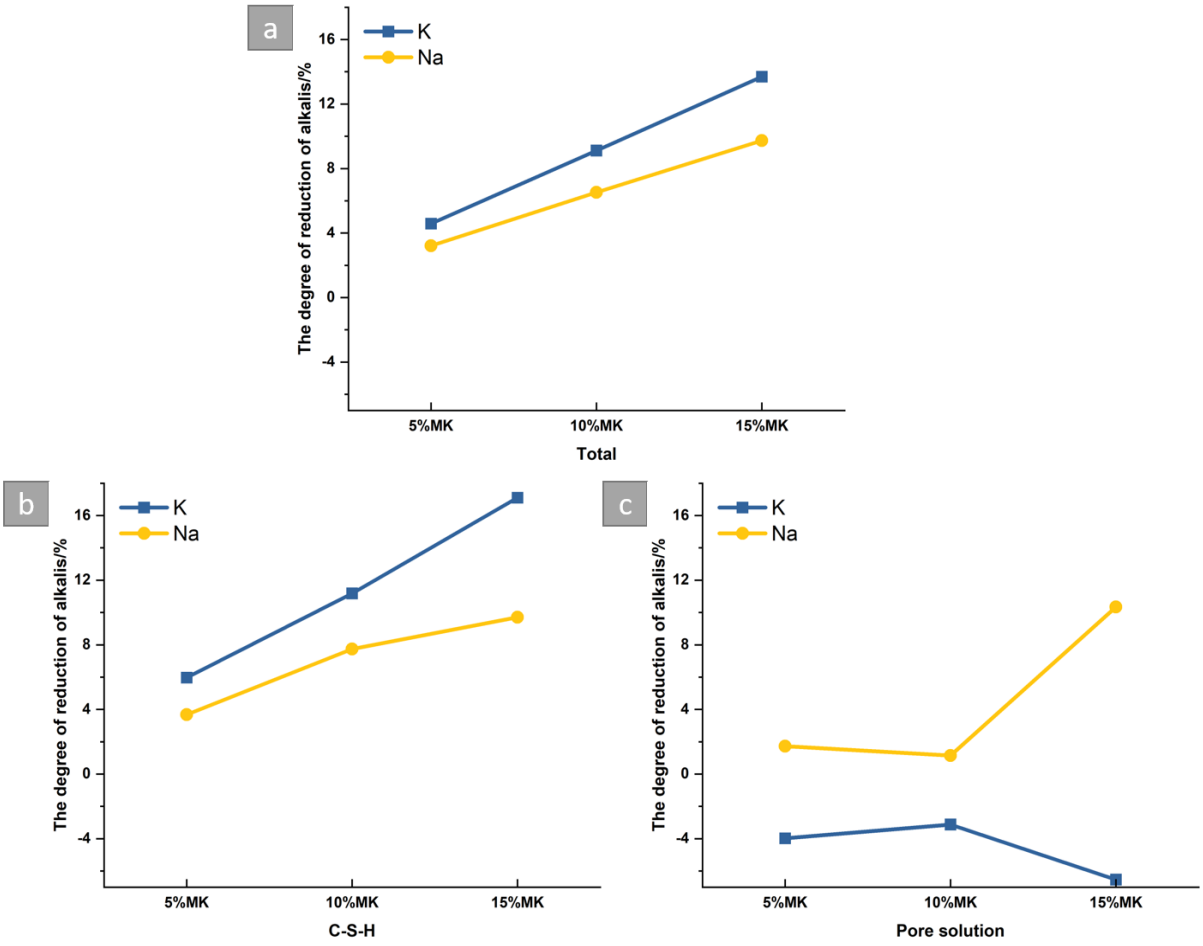

Figure 4-9 The degree of reduction of alkalis as a function of metakaolin replacement. a: total content in the cement plus SCM, b: in the C-S-H, c: in the pore solution.

Likewise, considering the role of fly ash, Figure 4-2 appears to indicate that, although $Ca(OH)_2$ plays an important role in the formation of ASR products, it cannot fully control the amount of ASR products formed unless it is removed to a greater degree than is the case here. Incorporating siliceous fly ash into cement does not change the total quantity of alkalis present, while the calcareous type dilutes the K but increases the Na. The trend for the alkali left in the pore solution is compatible with this, which triggers the formation of more ASR products. The alkali binding ability of the C-S-H formed is shown in Figure 4-10. Due to the moderate degree of reaction (40%) adopted in the modelling, less C-S-H precipitated at higher replacement levels of fly ash, especially for siliceous fly ash. In addition, the alkali-containing end-members in the FAS blended cement decrease with an increase in the SCM used, which is in good agreement with results in Figure 4-3d where more alkalis are left in the pore solution. The

modelling here supports again the conclusion of Chappex and Scrivener (Chappex & Scrivener, 2012a, 2012b) as discussed above.

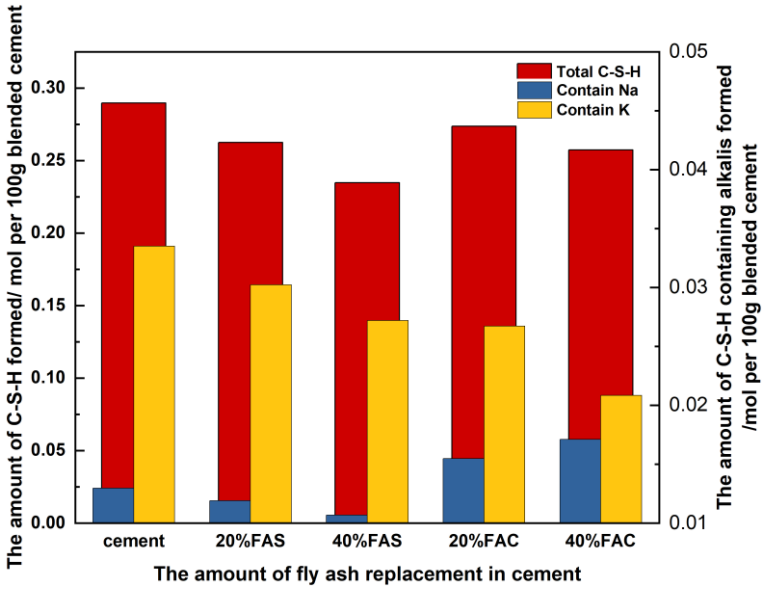

Figure 4-10 The total amount of C-S-H (left-hand vertical axis) and the amounts of end-members containing alkalis (right-hand vertical axis) formed in fly ash blended cements

Further reasons that could explain the role of Al-rich SCMs in inhibiting ASR damage include the contribution of alkalis and Al to the formation of non-expansive aluminosilicate (potentially zeolite-like) products, and reducing the rate of dissolution of the reactive silica (Bickmore et al., 2006; Hünger, 2007; Shi et al., 2021). In this study, the thermodynamic modelling approach that is used cannot directly address kinetic problems such as the influence of soluble species on aggregate dissolution rates, although it must be stated that it is highly likely that this is an important contributing factor (Hay & Ostertag, 2021).

In terms of precipitating zeolite-like phases, there is no prediction of any zeolite phase forming through the ASR process when using metakaolin and fly ash additions, which seem to indicate that this might not be relevant in these blended Portland cement-based binders. The author also modelled the effect of direct Al_2O_3 addition on phase formation in step two of the simulations of PC (shown schematically in Figure 4-1), and the results are shown in Figure 4-11. As can be seen, shlykovite-type ASR products are predicted to form without added Al_2O_3 in the system

(Jin et al., 2023; Shi et al., 2021). However, with low addition levels of Al_2O_3, ASR products start to transform to different types of zeolites. Specifically, the main Na-bearing phase becomes natrolite rather than Na-shlykovite with an increase in the amount of Al_2O_3 to 8 g, while instead of K-shlykovite, the K is hosted by clinoptilolite-type K-zeolites when adding up to 1 g of Al_2O_3. These modelling results indicate that in the presence of Al, alkali ions prefer to interact with it to form lower-solubility zeolite phases (or their disordered analogues K-A-S-H or N-A-S-H gels, which are comparable in nanostructure, and thus solubility, but lack long-range crystallographic order (Walkley et al., 2021)), which could become a possible (although almost certainly partial) explanation for the role of Al in mitigating ASR processes.

This finding is in general agreement with ref. (Shi et al., 2021), which also predicted phase assemblage in the CaO-SiO_2-Al_2O_3-K_2O system, and stated that K-zeolites precipitated in the presence of higher amounts of Al at 80 °C. However, the zeolites predicted to form in this study differ from the phillipsite mentioned by Shi et al. (Shi et al., 2021), although both zeolites are considered when modelling. The reasons for this may be as follows: firstly, Ma and Lothenbach (Ma & Lothenbach, 2021) have recently expanded the thermodynamic database used in this work with 14 types of K-zeolite, and the current modelling covers all of them, which indicates that phillipsite is no longer the best choice to precipitate in this cement formulation. Secondly, a lower temperature (25 °C) is used in this study compared with the work of Shi et al. (Shi et al., 2021) (80 °C); the results of Barrer and Mainwaring (Barrer & Mainwaring, 1972) also show that phillipsite tends to form at higher temperature in the KOH-metakaolin-silica system in the absence of calcium.

For cement hydration, the author assumes that all of the Portland cement is fully hydrated before the beginning of ASR. More AFm phases and ettringite are formed in the presence of Al-rich SCMs such as metakaolin and fly ash (Kunther et al., 2016; Lothenbach et al., 2011). Therefore, there is not a significant available Al source free to participate in the ASR process, because the Al in the pore solution – although it is present at a higher concentration than in plain Portland cement - is not enough to form zeolite phases. The fundamental assumption used to set up the ASR simulations here – which is that the timescales of hydration and ASR process can be wholly separated – means that the Al remaining in the unreacted SCMs, and also the Al incorporated into hydrate products, do not become available later in time to alter the progress

of the ASR process. This is obviously an approximation inherent in the thermodynamic simulation setup used here, which may differ from the reality of long-term cementitious material evolution in service, but the fact that this approach is not able to reproduce the effects of Al in mitigating ASR does provide useful support for the theory that Al acts through mainly kinetic, rather than equilibrium-derived, mechanisms in ASR suppression.

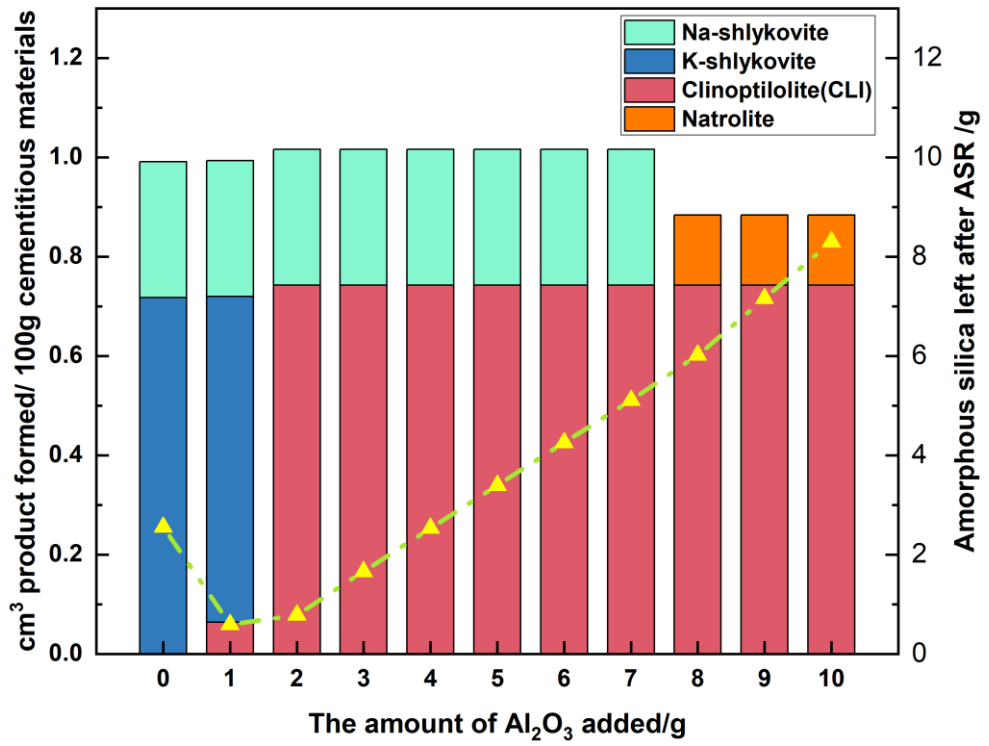

Figure 4-11 ASR phases and zeolites formed, and the remaining quantity of amorphous silica, when adding different amount of Al_2O_3 to the pore fluid and portlandite generated by hydration of Portland cement to model the ASR process

Another finding in this modelling is that the fraction of the amorphous silica remaining unreacted after the ASR process is simulated (stage two) increases when increasing the amount of Al added. Although the modelling setup makes available the same amount of amorphous silica to react in the second stage in each simulation, this result seems to indicate that there is a thermodynamic constraint, in addition to the well-known kinetic effect, that restricts the reaction of silica with cementitious pore fluid in the long-term in the presence of Al. Combined with the results presented in section 4.3.1, as long as it is possible to ensure the presence of an extra Al source in the system, ASR mitigation may be possible. Therefore, addition of some

less reactive Al-containing waste materials seems to be another possible economical way to inhibit ASR in the long term due to the possible formation of non-expansive aluminosilicate phases instead of expansive silicates. To be effective under this hypothesis, the Al source does not particularly need to participate in initial cement hydration as a reactive SCM, but it needs to be sufficiently soluble to provide Al when needed in the longer term. Meanwhile, although largely by a process of eliminating other possibilities rather than by giving direct kinetic information, the results presented here seem to indirectly support the theory that the main ASR-suppression mechanism of the Al provided by SCMs is in reducing the rate of dissolution of reactive silica from aggregates.

4.5 Conclusions

The aim of this study has been to apply thermodynamic modelling in simulating the alkali-silica reaction, considering cementitious blends including four types of supplementary cementitious materials: ground granulated blast furnace slag, silica fume, metakaolin and fly ash. A two-step modelling method was used to investigate the volumes of ASR products formed in cements with or without SCMs, by separating the cement hydration process and the ASR process in time and allowing only the pore solution and Ca(OH)2 resulting from cement (or blended cement) hydration to react with silica in ASR processes. This research provides new insight regarding investigation of the role of SCMs in mitigating ASR from the perspective of thermodynamic equilibrium. The conclusions are summarised as follows:

(1) By investigating the phase assemblages of cement blended with various SCMs, the consumption of $Ca(OH)_2$ in SCM hydration (latent hydraulic or pozzolanic) is considered to be the main reason explaining the role of SCMs in reducing the volume of K- and Na-shlykovite products formed. However, precipitation of ASR products also depends on the content of alkalis available in the pore solution after cement hydration. This study establishes for the first time the relationship between available alkalis remaining in the pore solution after hydration, and the formation of ASR phases.

(2) The reduction of alkali content in the pore solution by incorporating GGBFS and MK is responsible for diluting ASR product formation, especially at increased replacement levels of these two SCMs. The key identified role of silica fume, however, is to form more of the alkali-bearing endmember of the C-S-H solid solution, thus binding alkalis and reducing the amount left in the pore solution.

(3) Considering the role of Al, there is a tendency toward zeolite precipitation in preference to ASR products when considering a situation where Al is added alone, and after the cement hydration simulation has been completed. However, this does not take place in the cements incorporating Al-rich SCMs. These thermodynamic modelling results seem to indirectly support the kinetic hypothesis that the main role of Al is to reduce the rate of dissolution of reactive aggregate, rather than forming Al-bearing phases in the process of ASR.

Chapter 5 . INVESTIGATION OF ALKALI-SILICA REACTION IN ALKALI ACTIVATED CEMENTS USING THERMODYNAMIC MODELLING

Abstract

The possibility of the alkali-silica reaction (ASR) taking place in alkali-activated concretes is still under discussion, due largely to the characteristically high alkali levels of this class of cements. In this study, the author uses thermodynamic modelling with a newly extended database and a two-stage (time-separated) reaction simulation approach, to probe questions related to the potential formation of ASR products in slag-based alkali-activated materials (AAMs). The effects of different activators (NaOH, Na_2SO_4, Na_2CO_3, Na_2SiO_3) with different dosages, and the influence of the modulus of waterglass, are considered in calculating the volume of shlykovite-type ASR products predicted to be formed in AAMs, compared with results obtained for Portland cement. The solution chemistry and phase assemblage after hydration provide further information to aid in explaining the observed trends. In comparison with Portland cement, ASR is less susceptible to AAM: there is much less Na-shlykovite formed in AAMs although Na-bearing activators were used, while K-shlykovite is not predicted in any of the simulations due to the low level of K present. The volume of Na-shlykovite formed decreases with an increase in the dosage of activators (for all activators tested), and with a decrease in the modulus of waterglass when this is the activator used. The modelling results prove that instead of the concentration of alkalis in the pore solution, the ASR process can be triggered by a high concentration of Ca after hydration. The type of comprehensive simulation approach used here can provide robust theoretical support to aid analysis of experimental evidence, and to guide research in this area.

5.1 Introduction

The alkali-silica reaction (ASR) is an important mechanism of degradation in some concretes; opinions regarding whether this is a major problem in alkali-activated materials (AAMs) are divided, and this topic requires further attention. Alkali sources (mainly, but not solely, from the paste) and reactive silicates in the aggregates are the essential factors triggering the process of ASR in the presence of available calcium and moisture, forming expansive ASR gels. Because of the very high content of alkalis present in AAMs, which can be an order of magnitude higher than the levels conventionally considered "safe" in Portland cement, some researchers have proposed on this basis that AAMs may be expected to be more susceptible to ASR than Portland cement (Bakharev et al., 2001; Krivenko et al., 2014; Tänzer et al., 2017). On the other hand, experimental evidence tends not to fulfil those predictions. In an early study, Gifford and Gillott (Gifford & Gillott, 1996) stated that there is less expansion caused by ASR in AAMs than in conventional mortars. This observation was supported by the work of García-Lodeiro et al. (García-Lodeiro et al., 2007), and also by the early European work summarised in the review of Talling and Brandstetr (Talling & Brandstetr, 1989). Those authors attributed the ASR resistance of AAMs to the hydration products containing and binding more of the alkalis. More recently, Wang et al. (Wang et al., 2022) investigated ASR in alkali-activated binders produced from a blend of slag and fly ash, and gave the conclusion that dissolved reactive silicates were consumed to form hydration products, which combined with autogenous shrinkage during hydration, was proposed to inhibit the process of ASR. The factors that affect ASR in AAMs have been reviewed in detail in (Shi et al., 2015; Wang & Noguchi, 2020) and in several other studies, leading to an understanding that low-calcium AAMs tend to show less ASR than their higher-calcium counterparts (Rodrigue et al., 2020), and that further development of testing methods is needed to ensure that representative results are obtained in any comparison between AAM binder types, or against a Portland cement baseline (Winnefeld et al., 2020).

The conclusion of this assessment is that, due to the variation in the composition of precursors, activators, and testing methods used in the experiments that have been provided in the literature, and the lack of clarity about fundamental mechanisms at a physicochemical level, more comprehensive research studies should be designed to gain a deeper understanding of the mechanism and implications of ASR in AAMs. The intention of the current study is to provide

theoretical insight in support of the experimental campaigns that are ongoing, by assessing the thermodynamic basis for ASR processes in AAMs.

The extensive development of the cementitious hydrate phase database for thermodynamic modelling in recent years has enabled researchers to computationally predict the formation and composition of both solid and liquid phase assemblages, for both Portland-based cements and alkali-activated cements. For example, Lothenbach and co-workers reviewed the applications of thermodynamic modelling in the cement science and pointed out some potential examples that can be solved using this method (Lothenbach, 2010; Lothenbach & Zajac, 2019). Importantly for the modelling of AAMs, Myers et al. (Myers et al., 2014) proposed a new solid solution model to establish the database for sodium/aluminium-substituted calcium silicate hydrate (C-N-A-S-H). Kulik et al. (Kulik et al., 2022; L'Hôpital, Lothenbach, Scrivener, et al., 2016) have also contributed very important insight into the thermodynamics of calcium silicate hydrate phases when incorporating aluminium, and alkalis such as sodium and potassium. These updated models allow improved prediction of phase formation and stability in the AAM system. In terms of modelling ASR, the limited thermochemical or solubility data available for some relevant potential ASR products, as well as the ongoing discussion of what exactly is the structure of the ASR gel formed under different circumstances, has been an obstacle in the development of thermodynamic modelling applications in this area, for both Portland and AAM cements. However, in an important recent advance, Shi et al. (Shi et al., 2019) successfully synthesised shlykovite-type ASR products at 80 °C and thereafter their thermodynamic parameters were calculated by Jin et al. (Jin et al., 2023) (Chapter 3 of this thesis). This type of advancement in material characterisation and database development, supported by modelling approaches allowing the separation of timescales between successive reaction processes (hydration and ASR), has made thermodynamic modelling more soundly-based as a tool for ASR prediction, as demonstrated in (Jin et al., 2024) (Chapter 4 of this thesis) for the case of Portland blended cements.

The aim of this chapter is to investigate ASR processes in AAMs using thermodynamic modelling, focusing on phase evolution at ambient temperature to simulate field exposure conditions. AAMs based on ground granulated blast furnace slag (GGBFS) with different activators (NaOH, Na_2SO_4, $Na_2O{\cdot}nSiO_2$, Na_2CO_3) with different dosage and modulus will be

considered in terms of the volume of ASR products formed, compared with Portland cement as a baseline case. Information about pore solution chemistry and phase assemblages before the process of ASR is also used to explain the effects of these factors on the formation of ASR products. These modelling results can be used as a baseline when studying ASR in AAMs, in support of (and to aid design of) long-term or accelerated experiments in the future.

5.2 Materials and methods

5.2.1 Materials

The chemical composition of GGBFS used in the study is shown in Table 5-1, and is reproduced from the work of Mundra (Mundra et al., 2020) who also used this slag composition to model AAMs for chloride transport prediction. A 60% degree of reaction of the GGBFS has been adopted in the model, to represent the long-term characteristics of a relatively mature binder. To investigate the difference between AAM and Portland cement (PC) under ASR-generating conditions, the latter (with an assumed 100% degree of hydration) is also considered as a control system in the analysis, and the composition simulated is listed in Table 5-1, consistent with the previous work on blended cements (Jin et al., 2024) where the author selected a cement composition from (Duchesne & Bérubé, 2001).

The four activators (NaOH, Na_2SO_4, $Na_2O{\cdot}nSiO_2$, Na_2CO_3) are used with dosages that are set to achieve equivalent Na_2O contents of 2, 4, 6, and 8 g Na_2O per 100 g BBGFS – abbreviated for conciseness as 2, 4, 6, and 8% Na_2O for discussion in the text and graphics. The different modulus values of waterglass (n = 0.5, 1, 1.5, and 2 in the formula $Na_2O{\cdot}nSiO_2$, defined on a molar basis) are considered to evaluate its effect on ASR in waterglass-activated AAM. The water to solids mass ratio is 0.40 for all AAMs, and 0.47 for cement. The mix design information is summarised in Table 5-2.

Table 5-1. The composition of GGBFS and Portland cement used in the simulations in this study, expressed as wt% of oxides

	CaO	*SiO_2*	*Al_2O_3*	*Fe_2O_3*	*MgO*	*Na_2O*	*K_2O*	*SO_3*
GGBFS	42.3	32.3	13.3	0.6	5.2	0	0.3	2.9

PC	63.12	20.47	5.51	2.45	2.82	0.29	1.16	2.6

Table 5-2. The activator dosages and modulus values of waterglass considered in this study, expressed as equivalent Na_2O% (g Na_2O per 100 g GGBFS). w/s is the water to solids mass ratio.

Activators	*NaOH*	*Na_2SO_4*	*$Na_2O{\cdot}nSiO_2$*	*Na_2CO_3*
Dosage	2,4,6,8%	2,4,6,8%	2,4,6,8%	2,4,6,8%
Modulus (value of n)	0.5, 1.0, 1.5, 2.0			
w/s	0.40			

5.2.2 Methods and modelling description

The simulation methodology and software details used in this paper were based on the authors' previous work (Jin et al., 2024), where a two-step approach to modelling ASR in blended cements was developed and validated. Detailed information is given below.

5.2.2.1 Software and database

To simulate ion interactions and phase assemblages involved in the process of ASR, the GEM-Selektor software, based on minimization of Gibbs free energy with mass balance constraints, was used. The activity coefficients of aqueous species are calculated by the Truesdell-Jones form of the extended Debye-Hückel equation, which is shown in Eq. 2.11 in section 2.4.1.

The thermodynamic data for the solid phases considered in the simulation are listed in Appendix A and Appendix B, along with the data for shlykovite-type phases as obtained in Chapter 3.

2.2.2. Model description

The two-part reaction sequence used to represent the successive processes of AAM hydration and ASR has been validated in Chapter 4 (Jin et al., 2024), and the author is also applying that approach in the current simulation: the author assumes that the process of AAM hydration has reached effective completion (i.e. achieved the specified degree of reaction) before the formation of ASR products commences. This is based on the understanding that ASR is a slow process at room temperature. Therefore, precursor hydration is the main task in the first part of simulation. Ions in the pore solution, and portlandite in Portland cement, have been reported to take significant roles in affecting the process of ASR (Chatterji, 1979; Hou et al., 2004), and so these are used as the potentially reactive mix constituents in the second stage of the simulations. These alkaline components react with an additional silica source (50 g per 100 g GGBFS hydrated) representing the dissolution of silica from the aggregate, to simulate the process of ASR, considering the rest of the hydrates to be inert in this process.

Although the high alkalinity of AAM systems may enhance the dissolution of reactive aggregates, it is assumed that there is no silica dissolved from the aggregates in the initial (fast) stage of the hydration reaction process; the aggregate is only allowed to participate in the second (longer-term) stage of the reaction process once the hydration or alkali-activation simulation is completed.

5.3 Results and Discussion

5.3.1 Phase assemblage

The phase assemblages formed through alkali-activation, i.e. before AAMs are subjected to the simulated ASR process, are shown in Figure 5-1. The simulated phases and their volumes are broadly consistent with those obtained from the work of Mundra et al. (Mundra et al., 2020). The slight differences mainly come from the volumes of certain products that form, for example C_3AH_6 in the NaOH-activated GGBFS and ettringite in the Na_2SO_4-activated GGBFS. The reason for this is due to the updated Cemdata18 database used in the study (Lothenbach et al., 2019), while Mundra et al. (Mundra et al., 2020) used Cemdata14, where changes in the relative stabilities of hydrogarnet phases with respect to other aluminates were a particularly important update that was made between these two database versions (Dilnesa et al., 2014; Lothenbach et al., 2019; Matschei et al., 2007b). It can be seen clearly from Figure 5-1 that C-(K,N)-A-S-

H is the main Ca-bearing product, along with some other phases containing Ca such as C_3AH_6, C_4AcH_{11}, C_4AsH_{12}, and calcite. Although there is a decrease in the formation of C-(K, N)-A-S-H for Na_2SO_4-activated and Na_2CO_3-activated GGBFS when increasing the activator dosage, more secondary hydration products precipitate, and this results in more Ca being consumed from the pore solution. Thus, increasing the dosage of the activator enhances the combination of ions in the pore solution and the formation of solid phases.

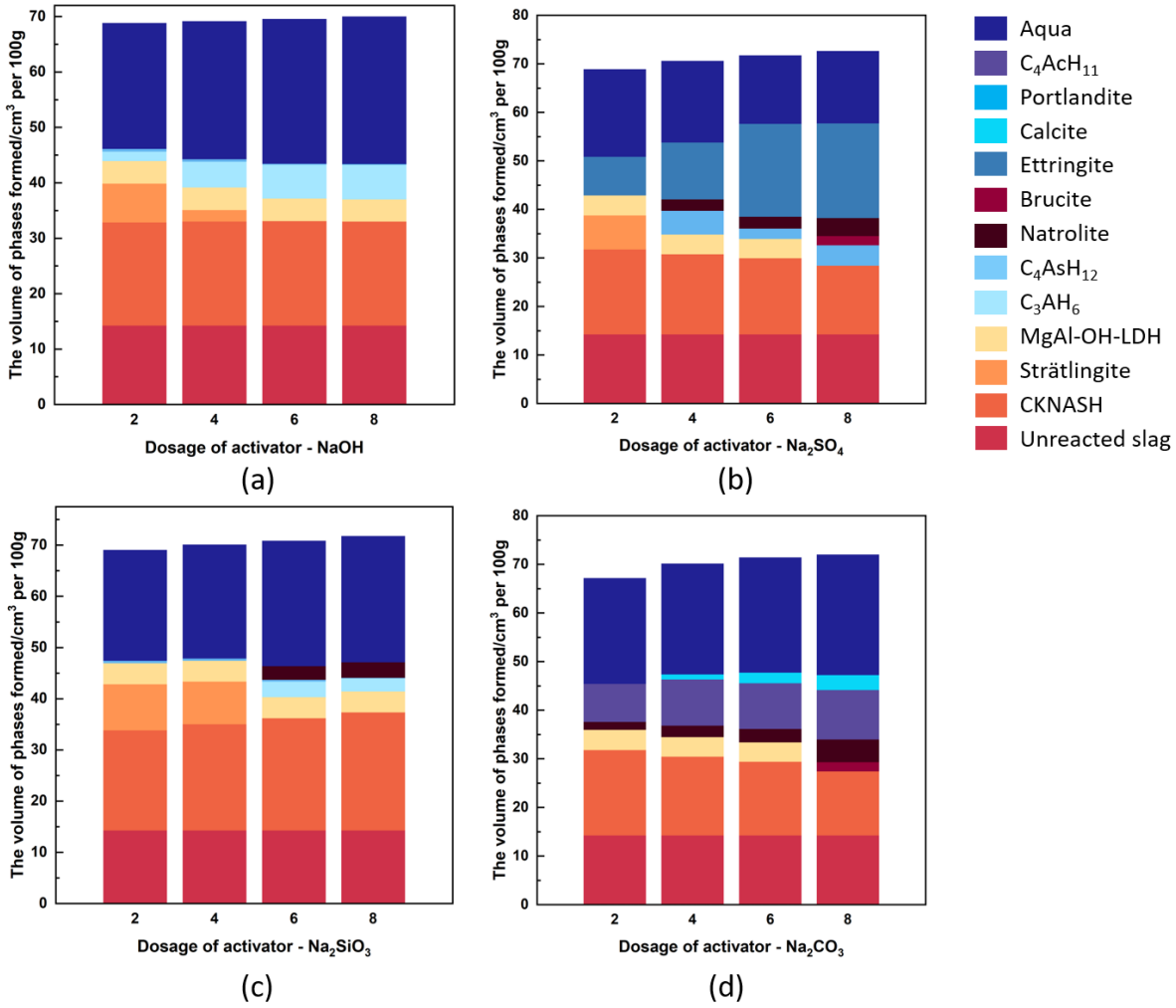

Figure 5-1. The simulated phase assemblages resulting from GGBFS activation by four activators with various dosages

For the AAM with the highest dosage of NaOH, portlandite can be seen in Figure 5-1a although its volume is minor. Brucite is predicted to precipitate in the activation of GGBFS by Na_2SO_4

and Na_2CO_3 at dosages of 8% equivalent Na_2O, which contrasts with the results of experimental research where there is no brucite formed (Ben Haha et al., 2011; Richardson et al., 1994). The reason for this difference is due to lack of the thermodynamic data for low Mg/Al ratio Mg-Al-OH-LDH_ss and M-S-H (magnesium silicate hydrate) (Myers et al., 2017). The GGBFS used here contains a high amount of MgO, resulting in the formation of brucite as the Mg is not accommodated in other potential reaction product phases. Natrolite is predicted to form in AAMs, except when NaOH is used as an activator, and appears to be a proxy also for the disordered N-A-S-H type products which form in alkali-activated cements, which have chemical structures and energetics resembling those of zeolites. This zeolite-type product is also predicted to form in the simulation work of Myers et. al and Mundra et. al (Mundra et al., 2020; Myers et al., 2015, 2017), who reported that the formation of natrolite indicates the coexistence of C-N-A-S-H gel and N-A-S-H gel.

The phase assemblage of AAMs with different modulus waterglass activators at different equivalent Na_2O doses is shown in Figure 5-2. The formation of C-S-H increases gradually when increasing the modulus of waterglass, which is consistent with refs. (Mundra et al., 2020; Myers et al., 2017) who considered the effects of Na_2SiO_3 and $Na_2Si_2O_5$ as activators on the phase assemblage of AAM. Strätlingite is predicted to form at lower activator dosages, and also precipitates in the silicate-activated systems shown in Figure 5-2c with higher modulus. In turn, the formation of katoite can be seen when there is a relatively low amount of strätlingite (e.g. 0.5% activator dosage in Figure 5-2b) or in the absence of strätlingite. Myers et. al (Myers et al., 2017) stated that it is more likely to form strätlingite in the activation of slags with low or moderate Si contents, and this may be used to explain the absence of this phase the higher silicate activator dosages due to the additional silica present in those cements. However, the reasons for the transformation of strätlingite and katoite may be attributed to the use of different thermodynamic databases between the two studies (Lothenbach et al., 2008, 2019). The formation of zeolite (natrolite) is expected when increasing the modulus and dosage of the silicate activator.

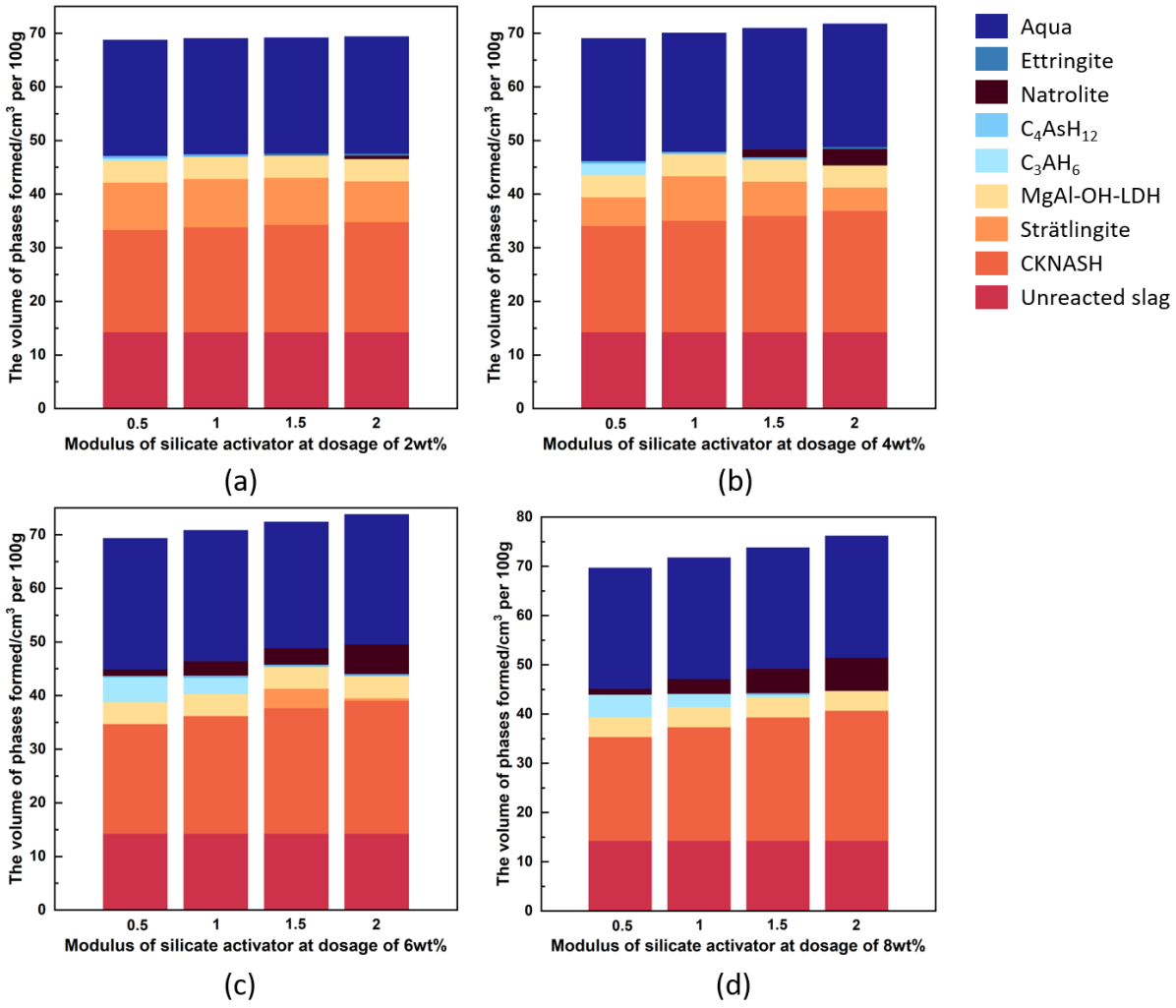

Figure 5-2. The phase assemblage of GGBFS activated by different dosage of waterglass with various modulus values

5.3.2 Pore solution chemistry

Considering the effect of various dosages of the four activators on solution chemistry in AAMs after hydration (stage 1 of the two-step reaction process, before the ASR simulation is initiated), the concentrations of the elements that can participate in formation of ASR products, and hydroxyl ions, in the pore solution are shown in Figure 5-3. When increasing the activator dosage, the concentration of Na increases dramatically in all AAM samples. A similar trend is seen with respect to the change of concentration of hydroxyl ions, largely for reasons of charge balance, resulting in a stronger alkaline environment and more new phases formed, which is consistent with the results shown in Figure 5-1.

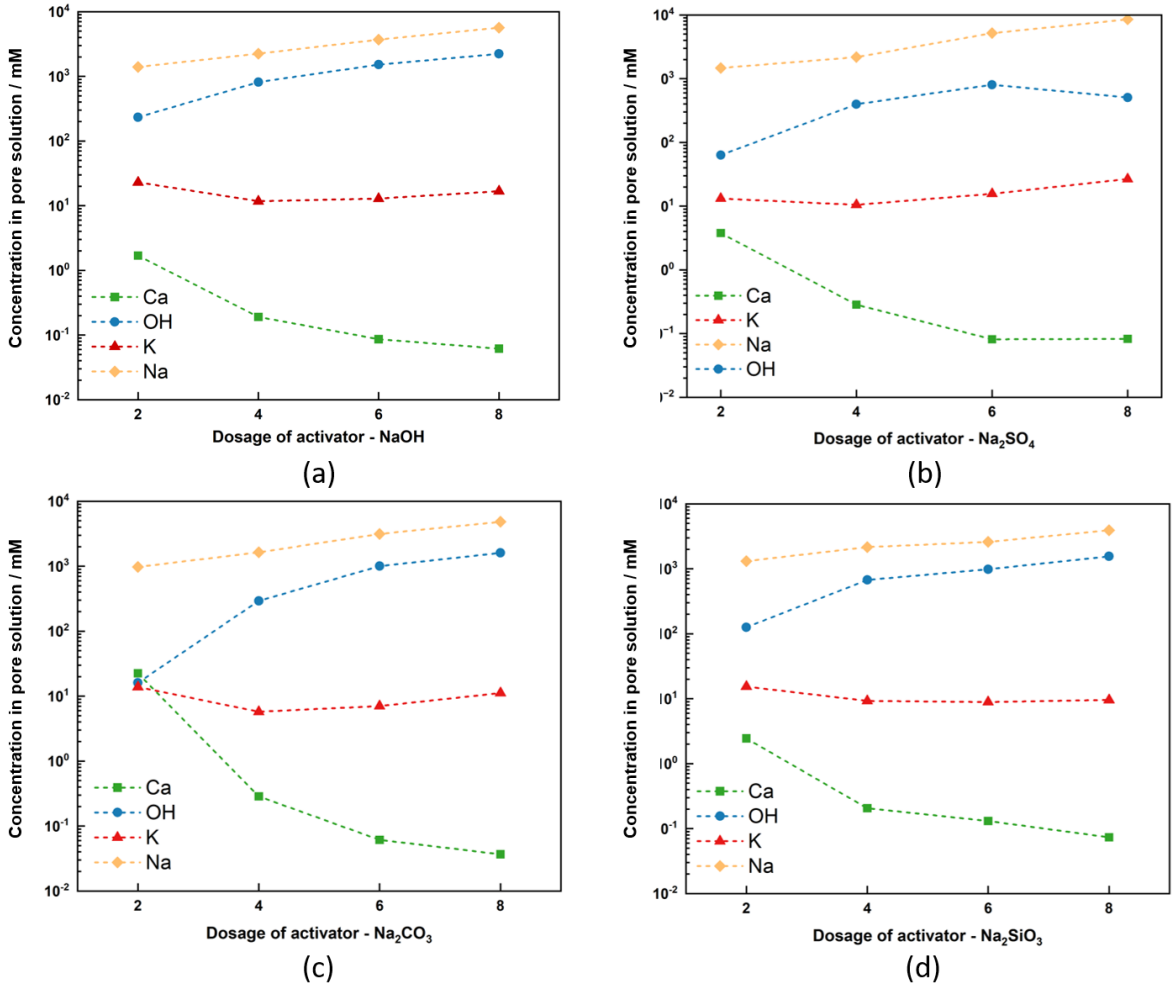

Figure 5-3 . The concentrations of Ca, K, Na and OH^- calculated to remain in the pore solution after hydration, for GGBFS activated by different dosages of four activators. Other anions such as sulfate that do not participate in ASR are not plotted; more detailed information is given in Appendix B.

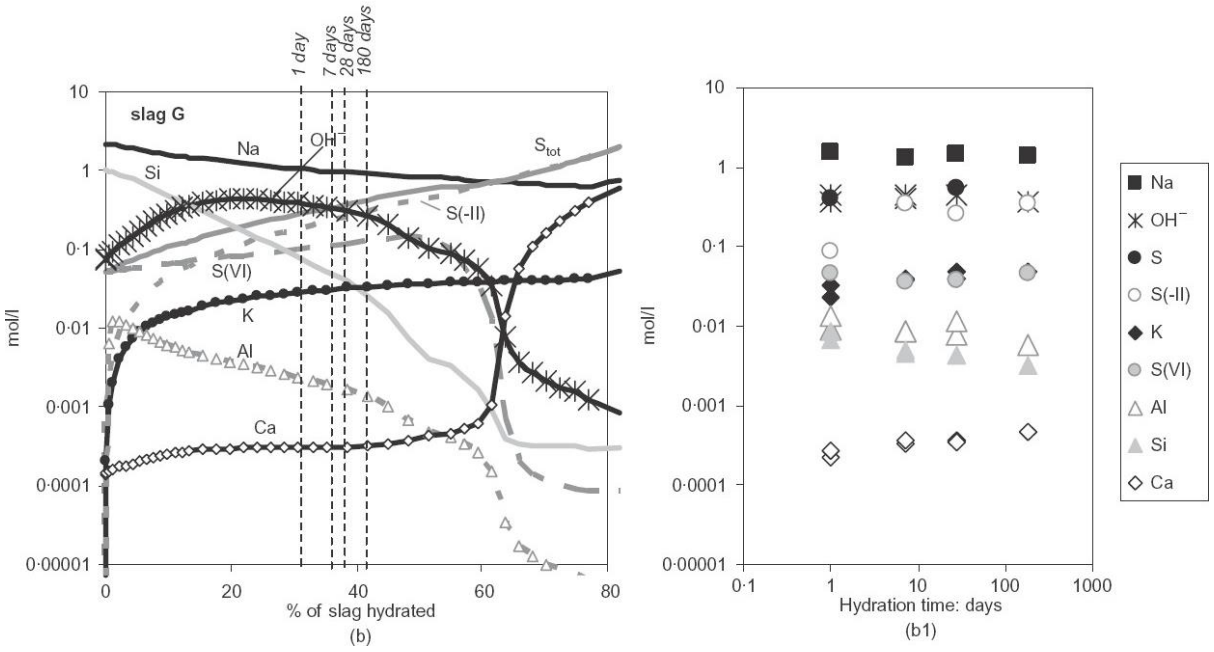

Figure 5-4 Calculated composition of the pore solution of Na-silicate-activated slag, compared to the measured compositions. Adapted from (Lothenbach & Gruskovnjak, 2007)

The higher concentration of alkalis in AAMs is sometimes claimed to be a detrimental factor causing a higher risk of formation of ASR products, or alkaline dissolution of the aggregates, compared to Portland cement. The simulation here covers this relationship, which will be discussed in section 5.3.3. It is also potentially notable that the concentration of hydroxyl ions reduces at an Na_2SO_4 dosage of 8% Na_2O equivalent. This may be attributed to precipitation of brucite (Figure 5-1b) which may lead to a decrease in the concentration of hydroxyl ions in the pore solution. However, a different trend was found in Na_2CO_3-activated slag, which also forms brucite at higher dosages; the rise in the concentration of hydroxyl ions with increasing Na_2CO_3 dosage is due to the transformation from MgAl-OH-LDH to $Mg(OH)_2$.

Several experimentally-oriented papers have reported the concentrations of elements in the pore solution of AAMs, either as a function of curing time, or with different dosages of waterglass or NaOH activators (Dai et al., 2022; Lloyd et al., 2010; Puertas et al., 2004; Song & Jennings, 1999). The near-neutral salt activators Na_2CO_3 and Na_2SO_4 have slower hydration kinetics when they are used as activators (Bernal et al., 2015; Rashad et al., 2013), and are relatively less studied in terms of pore fluid chemistry. Lothenbach and Gruskovnjak (Lothenbach & Gruskovnjak, 2007) considered the degree of reaction of GGBFS and predicted the solution chemistry via thermodynamic modelling, which is shown in the Figure 5-4. Myers

et. al (Myers et al., 2014) also simulated the concentration of elements in activated GGBFS binders using their C-N-A-S-H model and compared with experimental results from the references above. In this study, the simulation trends are generally in agreement with the results of Lothenbach and Gruskovnjak, but the quantities are under-predicted (Lothenbach & Gruskovnjak, 2007): the line representing the concentration of Ca is always at the lowest level while the increased trend for the concentration of Na can be seen as growing the dosage of activators. The reason for underestimation may be related to the experimental system not reaching equilibrium (i.e. an immature binder tested at early age) and the conservative degree of reaction of GGBFS used here (70-80% reacted in experiments (Durdziński et al., 2017)). However, the simulation results are still valuable for discussion of ASR, as this process takes quite a long time after hydration has largely stabilised.

Figure 5-5 displays the concentrations of Ca, K, Na and OH^- calculated to remain in the pore solution after hydration of GGBFS. The results for waterglass at 2% dosage with different modulus values are shown here; the other dosages of silicate activators because they have similar trends (data given in Appendix B). It can be seen that the concentration of Na decreases when increasing the modulus of waterglass, while the concentration of Ca increases, which is in agreement with the trends gained from experiments (Zuo et al., 2019). Combined with the results in Figure 5-2 regarding the phase assemblage formed in each silicate-activated AAM, the fall in the concentration of K may be because the additional C-A-S-H formed at a higher modulus binds more K. Ca-bearing phases such as strätlingite, C_3AH_6 and C_4AsH_{12} formed at lower modulus are replaced by ettringite, as the sulfide from the slag becomes partially oxidised in the simulation. Therefore, this is main reason for the increase in the concentration of Ca in the pore solution shown in Figure 5-5. The concentration of hydroxyl ions also decreases when the modulus of waterglass increases from 0.5 to 2 due to more soluble SiO_2 in the system, which acts as a polyprotic acid (Swaddle, 2001).

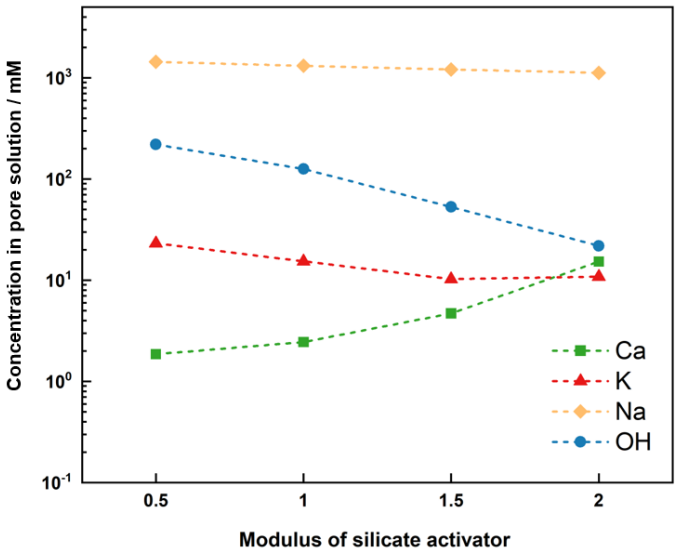

Figure 5-5. The concentrations of Ca, K, Na and OH^- in the pore solution after activation of GGBFS by waterglass at different modulus values, at a dosage of 2% equivalent Na_2O

5.3.3 ASR product formation

5.3.3.1 The effect of activator type and dosage on the volumes of ASR products formed

Table 5-3. The effect of dosage on the volume of shlykovite-type products formed in the cement systems simulated, in cm^3 per 100 g GGBFS. The Na_2O_{eq} content of the Portland cement is taken from Table 5-1.

$Na_2O_{(eq)}$	PC	NaOH	Na_2SiO_3**	Na_2CO_3	Na_2SO_4
2%	-	*0.0030*	*0.0064*	*0.078*	*0.0096*
4%	-	*0*	*0*	*0*	*0*
6%	-	*0*	*0*	*0*	*0*
8%	-	*0.45*	*0*	*0*	*0*
0.29	0.99 (0.72 K; 0.27 Na) *	-	-	-	-

* In all cases, the Na-shlykovite form dominates the ASR products, except for PC (Jin et al., 2024).

** The waterglass activation here is simulated with an activator modulus of 1.0, giving a composition of Na_2SiO_3

The volumes of two possible ASR products formed in the AAM system with four activators are shown in Table 5-3, with PC as a comparison. K-shlykovite only appears in the PC mortar; none of the AAMs precipitated this ASR product due to the lack of potassium in the composition of GGBFS. Na-shlykovite formed in some of the AAM simulations, but the volume of shlykovite-type products produced in all AAMs is much less than in the Portland cement mortar, regardless of the nature or dose of the activator. Na_2CO_3-activated GGBFS is the sample that contains the most Na-shlykovite compared with other AAM samples, forming almost 0.01 cm^3 per 100 g GGBFS.

According to the results of Chen et al., also considering the effect of type of activators on ASR, they observed the following order based on the ASR expansion experiments: waterglass, Na_2CO_3, Na_2SO_4, NaOH (Chen et al., 2002). In the current study, however, the ranking of waterglass is changed, to come behind Na_2SO_4. The reason behind this may be because the modulus of waterglass in the Chen et al. study (3.29) was much higher than that in the modelling, which may provide an additional silica source when ASR is taking place. Krivenko et al. (Krivenko et al., 2014) also investigated the ASR expansion of GGBFS activated by sodium carbonate and sodium metasilicate, and found that Na_2CO_3-activated GGBFS is more affected by ASR than when the GGBFS is activated by sodium metasilicate. The modelling work in in agreement with these findings.

The simulation results here also support the idea that AAM has better performance in resisting ASR in comparison with PC, despite containing a much higher content of alkalis. Unlike the results of Talling and Brandstetr (Talling & Brandstetr, 1989) who reported that there was no ASR expansion observed in AAMs, the findings presented here indicate that ASR can exist, but is less prevalent compared with the situation in PC (García-Lodeiro et al., 2007; P.M. Gifford;J.E. Gillott, 1996).

In terms of the effect of activator dose, the ASR product is only predicted to form when GGBFS is activated by activators with 2% equivalent Na_2O dosage (for all activators), and also when GGBFS is activated by the highest dosage of NaOH. In other words, increasing the dosage of activators does not directly increase the formation of ASR products in the cements studied here. When the dosage of NaOH increases to 8% of equivalent Na_2O, pH increases, resulting in the combination between Ca ion and hydroxyl ions, leading to portlandite precipitation which although minor (Figure 5-1), needs to be considered in simulating the process of ASR (Jin et al., 2024). This is the main reason for formation of more Na-shlykovite, as additional Ca becomes available for ASR processes. It should be noted that the two-step ASR simulation methodology applied here does not consider the C-S-H-type binding gels as a potential source of calcium for shlykovite formation, and so the only other Ca made available for this reaction is the residual Ca in the pore fluid after hydration.

Shi *et al.* (Shi et al., 2015; Shi, Shi, Wan, et al., 2018) concluded that the expansion caused by ASR decreased when increasing the concentration of NaOH from 4 wt% to 8 wt% in NaOH-activated GGBFS, which is incompatible with simulation results. Similarly, the experimental results obtained from Yang's and Al-Otaibi's research also are conflicting with the prediction (Al-Otaibi, 2008; Yang et al., 1999a, 1999b). The difference between these findings may be attributed to testing methods and kinetic issues. For ASR research in AAMs, ASTM C1260 or similar rapid testing methods are applied, in which expansion is determined after 14 days at high temperature immersed in NaOH solution (ASTM International, 2007). However, here the author simulates ASR under ambient temperature conditions and after AAM hydration, resulting in the binding of relevant ions in hydration products so that they no longer participate in the process of ASR, especially for calcium. The differences in temperature and highly alkaline immersion environment may also be important. Also, the conservative assumptions about the degree of reaction of GGBFS used in the modelling may mitigate the formation of more ASR products.

The results shown here seem to be supported by the previous work (Jin et al., 2023) to generate and analyse the $(Na,K)_2O$-SiO_2-CaO ternary phase diagram to assess shlykovite stability and formation. That study (Chapter 3) concluded that the presence of more alkalis in the system

does not necessarily improve the formation of shlykovite-type phases. Instead, there is a threshold concentration of alkali, which is less than 0.56 mol/L. Increasing the dosage of activators here does lead to a growth in the concentration of alkalis in the pore solution, which may instead suppress the formation of Na-shlykovite.

5.3.3.2 The effect of modulus and dosage of waterglass on ASR products

The effects of modulus (molar ratio SiO_2/Na_2O) and dosage of waterglass on the simulated formation of ASR products are shown in Table 5-4. Similar to the results in Table 5-3, the formation of Na-shlykovite is only predicted at the lowest dosage (2%) for each given modulus. The volume of ASR product increases with an increase in the modulus at this dosage. Increasing in the modulus provides extra silica source to react with alkali ions and form ASR product. The experimental results are contradictory regarding this point. Tänzer et al. (Tänzer et al., 2017) presented the same trend as simulation results, while Shi et. al (Shi et al., 2018) gained different outcomes with different waterglass dosages. At a lower dosage (4% Na_2O) there is a pessimum expansion when the modulus is 1, and similar trends are observed at dosages of 6% and 8% Na_2O. They attributed this to the alkalinity of the pore solution. However, the calculated concentrations of hydroxyl ions after AAM hydration reduced (Figure 5-5), even at 4% equivalent Na_2O, which indicates that there must be another mechanism controlling this.

Table 5-4. The effect of modulus and dosage of waterglass on the quantity of Na-shlykovite formed in GGBFS activated by waterglass, expressed in cm^3/100 g GGBFS

SiO_2/Na_2O	2% Na_2O	4% Na_2O	6% Na_2O	8% Na_2O
0.5	0.0036	0	0	0
1.0	0.0064	0	0	0
1.5	0.015	0	0	0
2.0	0.053	0	0	0

3.3.3 Phases formed in the process of ASR

Apart from Na-shlykovite, at the higher dosage and modulus of activators, zeolite-like phases (represented as natrolite) and Ca-heulandite are precipitated in minor amounts instead of ASR products. The rest of the dissolved silica either remains in the pore solution, or forms amorphous silica. Myers et al. (Myers et al., 2017) concluded that these two phases are prone to form in the alkali-activation of lower-Al, Si-rich slags. Although they are not predicted to form in the hydration modelling, the ASR process creates a similar environment, and this is an important reason for the suppression of the formation of ASR products. In addition, combining the information obtained here about the phase assemblages formed with different modulus values of waterglass at same dosage, it appears that increasing the modulus leads to precipitation of natrolite before the process of ASR, which consumes part of the Na from the pore solution. Therefore, the volume of this zeolite decreases in the second stage (see Appendix B).

5.4 Discussion

Opinions on the performance of AAMs regarding ASR resistance are currently contradictory. In this study, the results from thermodynamic modelling indicate that a minor amount of ASR products formed in alkali-activated slag-based cements with different activators compared with PC. Although the actual degree of expansion caused by ASR depends on various factors such as the rate of reaction (dissolution) of the aggregate, viscosity and water uptake of ASR products and dense of paste, it is nonetheless important to consider the extent of ASR product formation as a prerequisite for any expansion to occur. Combining the pore solution chemistry and volume of ASR products shown in Figure 5-3 and Table 5-3, due to the very limited availability of K in the AAMs, no K-shlykovite is predicted to form in these AAMs. The concentration of Na increases dramatically when using the four Na-bearing activators. Nevertheless, this higher concentration of Na in the pore solution does not result in the formation of more Na-shlykovite in the simulations: compared with NaOH- and Na_2CO_3-activated GGBFS at 2% equivalent Na_2O, the predicted concentration of Na in the former pore fluid (1400.2 mmol/L) is higher than in the latter (976.2 mmol/L), but the formation of Na-shlykovite in the Na_2CO_3-activated GGBFS was the greatest in simulations. This indicates that the concentration of alkalis in the pore solution is not the sole factor controlling the formation of ASR products.

In the work of Shi et al. (Shi, Shi, Wan, et al., 2018), a linear relationship was observed between the concentration of hydroxyl ions and the ASR expansion, when considering different dosages of the activator. In the simulation methodology applied here, the concentration of OH^- appears to have at most an indirect impact on the formation of ASR products. This can be seen by comparison of activators: for Na_2SO_4- and Na_2CO_3-activated AAMs, the concentration of OH^- is lower than the other mixes because these two activators are near-neutral salts with less alkaline pH, but the content of Na-shlykovite predicted to be formed in these two systems is higher than for the NaOH- and $Na_2O.nSiO_2$-activated formulations. Also, in terms of the effect of activator dosage, the concentration of hydroxyl ions increases to almost 2 mol/L when increasing the dosage of each activator to 8%. However, no Na-shlykovite forms even at such a high concentration of hydroxyl ions.

With respect to Ca, many works have proven that the concentration of Ca in the pore solution plays an important role in the formation and composition of ASR products (Chatterji, 1979; Guo et al., 2019; Kim et al., 2015; Leemann et al., 2011). The concentration of Ca in the pore fluids reaches a maximum with a 2% dosage of Na_2O, Figure 5-3, consistent with the rank order of the volumes of Na-shlykovite predicted to form (Table 5-3), which always reaches a maximum at that dosage of 2% among those tested here. The higher the concentration of Ca left in the pore solution in AAM samples, the more Na-shlykovite is formed. Likewise, increasing in the modulus of sodium silicate leads to increase the amount of Ca ions in the pore solution, which also simulates more ASR products formed there. The higher activator dosages suppress Ca concentrations to the point where there is no longer any ASR product formed. It can be seen in Figure 5-6, that in additional simulations with further reductions in the dosage of NaOH, the relationship between the concentration of Ca and the volume of ASR products is clearer: the lower the dosage used, the higher the concentration of Ca in the pore solution, and the more ASR products formed. This indicates that the lack of an available Ca source may result in the suppression of ASR product formation, even in these binders which do contain Ca in their hydrate phase assemblage, if that Ca is not available to redissolve and trigger an ASR process. The amorphous silica that dissolves from reactive aggregates may be soluble and left in the pore solution, or may react with alkalis to form zeolites or related phases in the absence of enough available Ca (Diamond, 1989; Skalny et al., 2001). It could be argued that the other

Ca-containing phases present, such as C-A-S-H, may also provide a reservoir of available Ca for reaction, but it is likely that the Ca will be rather tightly held by C-A-S-H at the low Ca/Si ratios present in AAMs, so this potential pathway was not included in the simulation methodology here.

In comparison with the pore solution of Portland cement, the concentration of Ca remains higher for these four AAM samples (see data in Appendix B). However, in the Portland cement system, portlandite ($Ca(OH)_2$) as one of the main hydration products provides most of the Ca required for ASR, in addition to the concentration of Ca in the pore solution. This indicates again that in this case, the Ca source rather than the alkali content in the pore solution is the key factor controlling the formation of ASR products. As in the case of the PC, the presence of $Ca(OH)_2$ in the highest-dosage NaOH-activated sample triggers the process of ASR and the formation of more ASR products. This can be used to explain the results in Table 5.3 where there is the highest volume of Na-shlykovite formed in this cement among all the AAMs simulated.

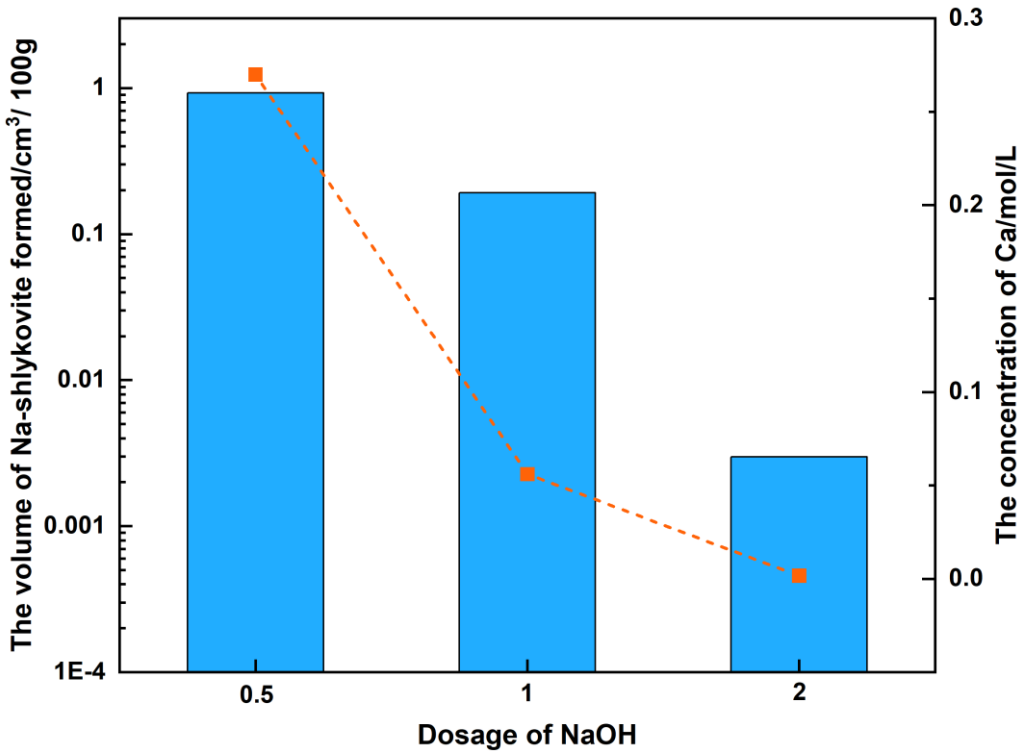

Figure 5-6. The relationship between the concentration of Ca in the pore solution of AAM and the volume of Na-shlykovite formed in the process of ASR, with different dosages of NaOH. The dosages where no ASR products form are not displayed here.

The role of Al in mitigating ASR in blended cement is widely reported, and it can act either by slowing the dissolution of soluble silica from reactive aggregates (Bickmore et al., 2006; Shi et al., 2021), or because it decreases the available alkali in the pore solution by dilution effects (Chappex & Scrivener, 2012a, 2012b; L'Hôpital, Lothenbach, Scrivener, et al., 2016). This inhibition is more notable in the presence of Al-rich supplementary cementitious materials such as metakaolin and fly ash. However, the studies here focus on GGBFS with intermediate Al content, and according to the phase assemblages shown in Figure 5-1, most of the Al reacts with other ions to form hydrate phases rather than remaining available for interactions in ASR-related processes. Therefore, this study does not cover detailed discussion of the role of Al.

The simulation results here indicate that the restricted Ca availability, in conjunction with the alkali ions, has a greater influence on ASR than the higher alkalinity of pore solution. The presence of less Ca in the AAM precursors such as GGBFS may become an advantage instead. Although experimental results do not often quantity the amount of ASR products, the relatively limited formation of shlykovite-type phases in AAM simulations supports the observed better performance in terms of ASR resistance for AAMs than PC.

5.5 Conclusions

The development of thermodynamic modelling approaches based on an updated database for ASR products allows researchers to make comparison between experiment and modelling. In this study the author investigated ASR in alkali-activated slag cements by changing the types, dosages, and modulus of activators (NaOH, Na_2SO_4, Na_2CO_3, Na_2SiO_3), using a two-step simulation method. The solution chemistry and phase assemblage after hydration were obtained and analysed to further explain the trends for the formation of ASR products. The conclusions are as follows:

1) Compared with Portland cement, there is no K-shlykovite and much less Na-shlykovite formed in the simulations of alkali activated cement. Na-shlykovite was formed only with 0.5-2% and 8% equivalent Na_2O added as NaOH, and only formed at the lowest dosage simulated (2%) for the rest of the activators. For waterglass activation, the volume of ASR products increases when increasing the waterglass modulus.

2) Combining the results of solution chemistry and phase assemblages, for those samples which form Na-shlykovite, the main reason for this is the higher concentration of Ca in the pore solution after hydration, and the formation of less potentially-reactive Ca-bearing hydration products. This reason can also apply for the silicate-activated GGBFS with different modulus values that influence the availability of soluble SiO_2. The concentration of alkali is not the sole controlling factor for the formation of ASR products, even though there is a much higher concentration of alkali in the pore solution of alkali-activated cement. Portlandite was found in the simulated phase assemblage when the dosage of NaOH increased to 8% equivalent Na_2O, which also triggers the process of ASR.

Chapter 6 CONCLUSIONS AND FUTURE WORK

6.1 Conclusions

The results discussed in the previous chapters indicated that thermodynamic modelling is a potential method that can be used in the prediction of alkali silica reaction (ASR) in concrete, associated with an accurate database for ASR products. This method can be applied regardless of the composition of cement and other supplementary cementitious materials (SCMs) blended. The application of a corresponding approach to alkali activated cements also demonstrated that this is not limited by the specific cement system.

6.1.1 Estimation of thermodynamic parameters of ASR products

Based on the recent synthesis of shlykovite-type ASR products, and improvements in consideration of temperature effects, a more completed database was established. In the calculation of the solubility products of these phases, a previously estimated pH value in the ionic solution has been refined using GEMS, thus resulting in obtaining more accurate solubility products with smaller error bars. Parameters such as entropy and heat capacity are calculated based on the molar volumes of ASR products. This can be used in the predictions considering different concentrations and temperatures.

ASR products with other phases were simulated in in the $(Na, K)_2O$-CaO–SiO_2-H_2O system. There is no ASR product found in the absence of alkalis. Shlykovite phases are found with an increase in the concentration of alkalis, and regions that form this ASR product occupy areas that formed C-S-H and amorphous silica without alkalis, which means that there exists an order of the formation of ASR products and C-S-H. The ASR product can co-exist with C-S-H when further increasing the concentration of CaO. However, adding more Na does not always mean the formation of more ASR products. There is a maximum concentration of alkalis that enables the formation of shlykovite phases. For example, beyond 1.48 mol/kg of Na_2O, this type of ASR product is no longer predicted to form, due to the suppression of calcium solubility. Solubility chemistry results proved that adding more Na_2O increases the pH of the solution, thus increasing the dissolution of Si and further forming more Na-shlykovite. Less Ca takes

part in the reaction due to the suppression of calcium solubility, and the Si source starts to react with Na_2O and CaO to form C-S-H instead of shlykovite-group minerals.

When considering the effect of temperature on the formation of ASR products, 38°C, 60°C, and 80°C were selected to represent the temperatures used in the common ASR tests. Phase diagrams show that the areas presenting phase formation were similar, while the threshold of alkali concentration for precipitating ASR products decreased with increasing temperature. This may provide a new insight into explaining different results obtained from different tests.

6.1.2 Using thermodynamic modelling in studying ASR in cement with or without SCMs

The use of SCMs in mitigating expansion caused by ASR is extensively reported in the literature, and this efficiency is verified via a two-step modelling method used in this study. This new method separates the cement hydration process and the ASR process in time, and allows only the pore solution and $Ca(OH)_2$ resulting from cement (or blended cement) hydration to react with silica in ASR processes, trying to build up a relationship among them.

The consumption of $Ca(OH)_2$ in SCM hydration (latent hydraulic or pozzolanic) is considered to be the main reason explaining the role of SCMs in reducing the volume of K- and Na-shlykovite products formed. However, precipitation of ASR products also depends on the content of alkalis available in the pore solution after cement hydration. Different SCMs have different mechanisms of action:

- Incorporating slag and metakaolin into cement, thus leading to a reduction in the alkalis available to participate in the ASR process, is responsible for dilution effects.
- Due to the relatively high K content in the silica fume used in the simulations here, the amount of K inputted into the cement hydration modelling remains constant at all silica fume contents simulated. The simulation indicates that incorporating silica fume into cement increases the formation of K-containing end-members, which is favoured by lower Ca/Si ratios that lead to higher chain lengths, and indicates that the ability to bind alkalis in C-S-H improves in the presence of silica fume.
- Fly ash, however, does not mitigate the formation of ASR products in these simulation due to its higher alkali contents, which is incompatible with literature. The controversy

related to these results may emphasise the kinetic role of Al that is often discussed in experiment-based papers, because the thermodynamic predictions are not able to explain the observed behaviour.

Considering the role of Al, there is a tendency toward zeolite precipitation in preference to ASR products when considering a situation where Al is added alone, and after the cement hydration simulation has been completed. However, this does not take place in the cements incorporating Al-rich SCMs. The reason for this appears to be because ettringite, hydrogarnet, or AFm phases form in the early hydration stages, consuming the Al and meaning that it is not available to play a similar role in the later-age simulations of ASR. These modelling results seem to indirectly support the hypothesis that the main role of Al is to reduce the rate of dissolution of reactive aggregate.

6.1.3 Investigation of ASR in AAS

The thermodynamic modelling of ASR processes is also applied for alkali-activated slag cements. By changing the types, dosages, and modulus of activators (NaOH, Na_2SO_4, Na_2CO_3, Na_2SiO_3), the volume of shlykovite-type products was investigated and compared to those formed in Portland cement.

Much less of the shlykovite-type phases formed in the simulations of alkali activated cements compared with Portland cement. Na-shlykovite was formed only with 0.5-2% and 8% equivalent Na_2O added as NaOH, and only formed at the lowest dosage simulated (2%) for the rest of the activators. For waterglass activation, the volume of ASR products increases when increasing the waterglass modulus.

Combining the results of solution chemistry and phase assemblages, for those samples which form Na-shlykovite, the main reason for this is the higher concentration of Ca in the pore solution after hydration, and the formation of less potentially-reactive Ca-bearing hydration products. This reason can also apply for the silicate-activated GGBFS with different modulus values that influence the availability of soluble SiO_2. The concentration of alkali is not the sole

controlling factor for the formation of ASR products, even though there is a much higher concentration of alkali in the pore solution of alkali-activated cement. Portlandite was found in the simulated phase assemblage when the dosage of NaOH increased to 8% equivalent Na_2O, which also triggers the process of ASR.

6.2 Directions for future work

The simulations presented here provide new thermodynamic insight into research on ASR, which can guide preliminary experiments when selecting raw materials. For further developing the simulations used in studying ASR, there are still a number of open questions that need to be solved:

- Different types of ASR products may still exist in field concretes. Relying on advanced measurements and equipment, the structure and transformation process are valuable to investigate. Changes in the types and amount of binding of alkalis, and binding of water molecules, need to be observed. After gaining deeper understanding about different types of ASR products, a database for them also needs to be completed.
- A relationship between expansion and the volume of ASR products formed should be built up, after completing the database for ASR products. A practical model to connect expansion and volume of ASR products is needed.
- Changes in the structure of ASR products from amorphous to crystalline have been observed. A kinetic model for this transformation could be developed, as a function of the reaction time and reactive silica dissolved from aggregate. Also, another kinetic model for the dissolution of aggregate is required, considering not only the size and types of aggregates, but also the role of Al in slowing the dissolution stage.
- The roles of SCMs in mitigating ASR have been presented here, and this is also relevant when changing the composition of SCMs. However, more work should be done to explain the role of Al-rich SCMs such as metakaolin and fly ash. The simulation of fly ash hydration is also another difficult topic. In the future these two aspects should be combined to further explain the observed better ASR-resisting performance in the presence of Al-rich SCMs.

In summary, this study presents a modelling-based investigation compared with experimental results. Some assumptions were made to simplify the process of simulation. Therefore, there are still lines of work to be followed, before guiding experiments based on modelling outcomes. The results presented here have indeed pushed the boundaries of knowledge in the field of ASR modelling, and paved the way for future advancements.

References

Al-Otaibi, S. (2008). Durability of concrete incorporating GGBS activated by water-glass. *Construction and Building Materials*, *22*(10), 2059–2067. https://doi.org/10.1016/j.conbuildmat.2007.07.023

Aquino, W., Lange, D. A., & Olek, J. (2001). The influence of metakaolin and silica fume on the chemistry of alkali–silica reaction products. *Cement and Concrete Composites*, *23*(6), 485–493. https://doi.org/10.1016/S0958-9465(00)00096-2

Arano, N., & Kawamura, M. (2000). Comparative consideration on the mechanisms of ASR suppression due to different mineral admixtures. *11th International Conference on Alkali–Aggregate Reaction in Concrete, Quebec, Canada*, 553–562.

ASTM International. (2023). *ASTM C1260-23: Standard test method for potential alkali reactivity of aggregates (mortar–bar method)*. ASTM International, West Conshohocken, PA, USA.

ASTM International. (2023). *ASTM C1293-23, Standard Test Method for Determination of Length Change of Concrete Due to Alkali-Silica Reaction*. ASTM International, West Conshohocken, PA, USA.

Aydın, S., & Baradan, B. (2012). Mechanical and microstructural properties of heat cured alkali-activated slag mortars. *Materials & Design*, *35*, 374–383. https://doi.org/10.1016/j.matdes.2011.10.005

Bagheri, M., Lothenbach, B., & Scrivener, K. (2022). The effect of paste composition, aggregate mineralogy and temperature on the pore solution composition and the extent of ASR expansion. *Materials and Structures*, *55*(7), 192. https://doi.org/10.1617/s11527-022-02015-6

Bagheri, M., Lothenbach, B., Shakoorioskooie, M., & Scrivener, K. (2022). Effect of different ions on dissolution rates of silica and feldspars at high pH. *Cement and Concrete Research*, *152*, 106644. https://doi.org/10.1016/j.cemconres.2021.106644

Bakharev, T., Sanjayan, J. G., & Cheng, Y. B. (2001). Resistance of alkali-activated slag concrete to alkali-aggregate reaction. *Cement and Concrete Research*, *31*(10), 331–334. https://doi.org/10.1016/S0008-8846(03)00125-X

Bakharev, T., Sanjayan, J. G., & Cheng, Y.-B. (2002). Sulfate attack on alkali-activated slag concrete. *Cement and Concrete Research*, *32*(2), 211–216. https://doi.org/10.1016/S0008-8846(01)00659-7

Bakharev, T., Sanjayan, J. G., & Cheng, Y.-B. (2003). Resistance of alkali-activated slag concrete to acid attack. *Cement and Concrete Research*, *33*(10), 1607–1611. https://doi.org/10.1016/S0008-8846(03)00125-X

Balachandran, C., Muñoz, J. F., & Arnold, T. (2017). Characterization of alkali silica reaction gels using Raman spectroscopy. *Cement and Concrete Research*, *92*, 66–74. https://doi.org/10.1016/j.cemconres.2016.11.018

Baquerizo, L. G., Matschei, T., & Scrivener, K. L. (2016). Impact of water activity on the stability of ettringite. *Cement and Concrete Research*, *79*, 31–44. https://doi.org/10.1016/j.cemconres.2015.07.008

Barrer, R. M., & Mainwaring, D. E. (1972). Chemistry of soil minerals. Part XI. Hydrothermal transformations of metakaolinite in potassium hydroxide. *Journal of the Chemical Society, Dalton Transactions*, *12*, 1254–1259. https://doi.org/10.1039/DT9720001254

Bazant, Z. P., & Steffens, A. (2000). Mathematical model for kinetics of alkali-silica reaction in concrete. *Cement and Concrete Research*, *30*(3), 419–428. https://doi.org/10.1016/S0008-8846(99)00270-7

Bektas, F., Turanli, L., & Monteiro, P. J. M. (2005). Use of perlite powder to suppress the alkali-silica reaction. *Cement and Concrete Research*, *35*(10), 2014–2017. https://doi.org/10.1016/j.cemconres.2004.10.029

Ben Haha, M., Le Saout, G., Winnefeld, F., & Lothenbach, B. (2011). Influence of activator type on hydration kinetics, hydrate assemblage and microstructural development of alkali activated blast-furnace slags. *Cement and Concrete Research*, *41*(3), 301–310. https://doi.org/10.1016/j.cemconres.2010.11.016

Bernal, S. A., Provis, J. L., Myers, R. J., San Nicolas, R., & van Deventer, J. S. J. (2015). Role of carbonates in the chemical evolution of sodium carbonate-activated slag binders. *Materials and Structures*, *48*(3), 517–529. https://doi.org/10.1617/s11527-014-0412-6

Bernard, E., Yan, Y., & Lothenbach, B. (2021). Effective cation exchange capacity of calcium silicate hydrates (C-S-H). *Cement and Concrete Research*, *143*, 106393. https://doi.org/10.1016/j.cemconres.2021.106393

Bérubé, M. A., Dorion, J. F., Duchesne, J., Fournier, B., & Vézina, D. (2003). Laboratory and field investigations of the influence of sodium chloride on alkali-silica reactivity. *Cement and Concrete Research*, *33*(1), 77–84. https://doi.org/10.1016/S0008-8846(02)00926-2

Bérubé, M. A., Duchesne, J., Dorion, J. F., & Rivest, M. (2002). Laboratory assessment of alkali contribution by aggregates to concrete and application to concrete structures affected by alkali-silica reactivity. *Cement and Concrete Research*, *32*(8), 1215–1227. https://doi.org/10.1016/S0008-8846(02)00766-4

Bérubé, M.-A., Chouinard, D., Pigeon, M., Frenette, J., Boisvert, L., & Rivest, M. (2002). Effectiveness of sealers in counteracting alkali-silica reaction in plain and air-

entrained laboratory concretes exposed to wetting and drying, freezing and thawing, and salt water. *Canadian Journal of Civil Engineering*, *29*(2), 289–300.

Bérubé, M.-A., & Fournier, B. (1993). Canadian experience with testing for alkali-aggregate reactivity in concrete. *Cement and Concrete Composites*, *15*(1), 27–47. https://doi.org/10.1016/0958-9465(93)90037-A

Bich, Ch., Ambroise, J., & Péra, J. (2009). Influence of degree of dehydroxylation on the pozzolanic activity of metakaolin. *Applied Clay Science*, *44*(3), 194–200. https://doi.org/10.1016/j.clay.2009.01.014

Bickmore, B. R., Nagy, K. L., Gray, A. K., & Brinkerhoff, A. R. (2006). The effect of $Al(OH)_4^-$ on the dissolution rate of quartz. *Geochimica et Cosmochimica Acta*, *70*(2), 290–305. https://doi.org/10.1016/j.gca.2005.09.017

Boddy, A. M., Hooton, R. D., & Thomas, M. D. A. (2000). The effect of product form of silica fume on its ability to control alkali–silica reaction. *Cement and Concrete Research*, *30*(7), 1139–1150. https://doi.org/10.1016/S0008-8846(00)00297-0

Boddy, A. M., Hooton, R. D., & Thomas, M. D. A. (2003). The effect of the silica content of silica fume on its ability to control alkali-silica reaction. *Cement and Concrete Research*, *33*(8), 1263–1268. https://doi.org/10.1016/S0008-8846(03)00058-9

Boehm-Courjault, E., Barbotin, S., Leemann, A., & Scrivener, K. (2020). Microstructure, crystallinity and composition of alkali-silica reaction products in concrete determined by transmission electron microscopy. *Cement and Concrete Research*, *130*, 105988. https://doi.org/10.1016/j.cemconres.2020.105988

Automatic citation updates are disabled. To see the bibliography, click Refresh in the Zotero tab.BRE, *Alkali-silica reaction in concrete. BRE Digest 330 (Parts 1 to 4)*. (2004).

Briki, Y., Avet, F., Zajac, M., Bowen, P., Haha, M. B., & Scrivener, K. (2021). Understanding of the factors slowing down metakaolin reaction in limestone calcined

clay cement (LC3) at late ages. *Cement and Concrete Research*, *146*, 106477. https://doi.org/10.1016/j.cemconres.2021.106477

Brown, P. W. (1990). The System Na_2O-CaO-SiO_2-H_2O. *Journal of the American Ceramic Society 61*(6), 3457–3461.

BSI, *BS 812-123:1999 Testing aggregates. Method of determination of alkali-silica reactivity—Concrete prism method (incorporating corrigendum No.1)*. (1999). https://www.thenbs.com/PublicationIndex/documents/details?DocId=247678

Canham, I., Page, C. L., & Nixon, P. J. (1987). Aspects of the pore solution chemistry of blended cements related to the control of alkali silica reaction. *Cement and Concrete Research 17*, 839–844.

Chappex, T., & Scrivener, K. (2012a). Alkali fixation of C-S-H in blended cement pastes and its relation to alkali silica reaction. *Cement and Concrete Research*, *42*(8), 1049–1054. https://doi.org/10.1016/j.cemconres.2012.03.010

Chappex, T., & Scrivener, K. L. (2012b). The influence of aluminium on the dissolution of amorphous silica and its relation to alkali silica reaction. *Cement and Concrete Research*, *42*(12), 1645–1649. https://doi.org/10.1016/j.cemconres.2012.09.009

Chappex, T., & Scrivener, K. L. (2013). The effect of aluminum in solution on the dissolution of amorphous silica and its relation to cementitious systems. *Journal of the American Ceramic Society*, *96*(2), 592–597. https://doi.org/10.1111/jace.12098

Chatterji, S. (1979). The role of $Ca(OH)_2$ in the breakdown of Portland cement concrete due to alkali-silica reaction. *Cement and Concrete Research*, *9*(2), 185–188. https://doi.org/10.1016/0008-8846(79)90024-3

Chatterji, S., & Clausson-Kaas, N. F. (1984). Prevention of alkali-silica expansion by using slag-Portland cement. *Cement and Concrete Research*, *14*(6), 816–818. https://doi.org/10.1016/0008-8846(84)90006-1

Chatterji, S., Jensen, A. D., Thaulow, N., & Christensen, P. (1986). Studies of alkali-silica reaction. Part 3. Mechanisms by which NaCl and $Ca(OH)_2$ affect the reaction. *Cement and Concrete Research*, *16*(2), 246–254. https://doi.org/10.1016/0008-8846(86)90141-9

Chatterji, S., Thaulow, N., & Jensen, A. D. (1987). Studies of alkali-silica reaction. part 4. effect of different alkali salt solutions on expansion. *Cement and Concrete Research*, *17*, 777–783.

Chatterji, S., Thaulow, N., & Jensen, A. D. (1988). Studies of alkali-silica reaction, part 6. practical implications of a proposed reaction mechanism. *Cement and Concrete Research 18*, 363–366.

Chatterji, S., Thaulow, N., & Jensen, A. D. (1989). Studies of alkali-silica reaction. Part 5. Verification of a newly proposed reaction mechanism. *Cement and Concrete Research*, *19*(2), 177–183. https://doi.org/10.1016/0008-8846(89)90081-1

Chen, Y. Z., Pu, X. C., Yang, C. H., & Ding, Q. J. (2002). Alkali aggregate reaction in alkali slag cement mortars. *Journal of Wuhan University of Technology, Materials Science Edition*, *17*(3), 3–6. https://doi.org/10.1007/bf02838542

Chindaprasirt, P., Rattanasak, U., & Taebuanhuad, S. (2013). Resistance to acid and sulfate solutions of microwave-assisted high calcium fly ash geopolymer. *Materials and Structures*, *46*(3), 375–381. https://doi.org/10.1617/s11527-012-9907-1

Cole, W. F., & Lancucki, C. J. (1983). Products formed in an aged concrete: the occurrence of okenite. *Cement and Concrete Research*, *13*(5), 611–618. https://doi.org/10.1016/0008-8846(83)90049-2

Collins, C. L., Ideker, J. H., Willis, G. S., & Kurtis, K. E. (2004). Examination of the effects of LiOH, LiCl, and $LiNO_3$ on alkali-silica reaction. *Cement and Concrete Research*, *34*(8), 1403–1415. https://doi.org/10.1016/j.cemconres.2004.01.011

Collins, R. J. (1989). Alkali aggregate reactivity in dense concretes containing synthetic or porous natural aggregate. *Cement and Concrete Research*, *19*(2), 278–288. https://doi.org/10.1016/0008-8846(89)90092-6

Dai, X., Aydin, S., Yardimci, M. Y., Lesage, K., & De Schutter, G. (2022). Early age reaction, rheological properties and pore solution chemistry of NaOH-activated slag mixtures. *Cement and Concrete Composites*, *133*, 104715. https://doi.org/10.1016/j.cemconcomp.2022.104715

Davies, G., & Oberholster, R. E. (1988). Alkali-silica reaction products and their development. *Cement and Concrete Research*, *18*(4), 621–635. https://doi.org/10.1016/0008-8846(88)90055-5

De Ceukelaire, L. (1991). The determination of the most common crystalline alkali-silica reaction product. *Materials and Structures*, *24*(3), 169–171. https://doi.org/10.1007/BF02472981

De Souza, D. J., & Sanchez, L. F. M. (2023). Evaluating the efficiency of SCMs to avoid or mitigate ASR-induced expansion and deterioration through a multi-level assessment. *Cement and Concrete Research*, *173*, 107262. https://doi.org/10.1016/j.cemconres.2023.107262

Dent Glasser, L. S., & Kataoka, N. (1981). The chemistry of 'alkali-aggregate' reaction. *Cement and Concrete Research*, *11*(1981), 1–9.

Deschenes Jr, R. A., Murray, C. D., & Hale, W. M. (2017). Mitigation of alkali-silica reaction and freezing and thawing through surface treatment. *ACI Materials Journal*, *114*(2), 307-314.

Diamond, S. (1975). A review of alkali-silica reaction and expansion mechanisms 1. Alkalies in cements and in concrete pore solutions. *Cement and Concrete Research*, *5*(4), 329–345. https://doi.org/10.1016/0008-8846(75)90089-7

Diamond, S. (1976). *A review of alkali-silica reaction and expansion mechanisms 2. Reactive aggregates*. *6*, 549–560.

Diamond, S. (1989). ASR-another look at mechanisms. *Proceedings of the 8th International Conference on Alkali-Aggregate Reaction in Concrete*, Kyoto, Japan, 83–94.

Dilnesa, B. Z., Lothenbach, B., Renaudin, G., Wichser, A., & Kulik, D. (2014). Synthesis and characterization of hydrogarnet $Ca_3(Al_xFe_{1-x})_2(SiO4)_y(OH)_{4(3-y)}$. *Cement and Concrete Research*, *59*, 96–111. https://doi.org/10.1016/j.cemconres.2014.02.001

Ding, Y., Dai, J.-G., & Shi, C.-J. (2016). Mechanical properties of alkali-activated concrete: A state-of-the-art review. *Construction and Building Materials*, *127*, 68–79. https://doi.org/10.1016/j.conbuildmat.2016.09.121

Dron, R., & Brivot, F. (1992). Thermodynamic and kinetic approach to the ASR Part 1—Concepts. *Cement and Concrete Research*, *22*, 941–948.

Dron, R., & Brivot, F. (1993). Thermodynamic and kinetic approach to the alkali-silica reaction. Part 2: Experiment. *Cement and Concrete Research*, *23*(1), 93–103. https://doi.org/10.1016/0008-8846(92)90118-F

Duchesne, J., & Bérubé, M. A. (1994a). The effectiveness of supplementary cementing materials in suppressing expansion due to ASR: Another look at the reaction mechanisms part 1: Concrete expansion and portlandite depletion. *Cement and Concrete Research*, *24*(1), 73–82. https://doi.org/10.1016/0008-8846(94)90084-1

Duchesne, J., & Bérubé, M. A. (1994b). The effectiveness of supplementary cementing materials in suppressing expansion due to ASR: Another look at the reaction mechanisms part 2: Pore solution chemistry. *Cement and Concrete Research*, *24*(2), 221–230. https://doi.org/10.1016/0008-8846(94)90047-7

Duchesne, J., & Bérubé, M.-A. (2001). Long-term effectiveness of supplementary cementing materials against alkali–silica reaction. *Cement and Concrete Research, 31*(7), 1057–1063. https://doi.org/10.1016/S0008-8846(01)00538-5

Dunant, C. F., & Scrivener, K. L. (2012). Effects of aggregate size on alkali-silica-reaction induced expansion. *Cement and Concrete Research, 42*(6), 745–751. https://doi.org/10.1016/j.cemconres.2012.02.012

Duncan, M. A. G., Gillott, J. E., & Swenson, E. G. (1973). Alkali-aggregate reaction in Nova Scotia II. Field and petrographic studies. *Cement and Concrete Research*. *3*, 119–128.

Durdziński, P. T., Ben Haha, M., Bernal, S. A., De Belie, N., Gruyaert, E., Lothenbach, B., Menéndez Méndez, E., Provis, J. L., Schöler, A., Stabler, C., Tan, Z., Villagrán Zaccardi, Y., Vollpracht, A., Winnefeld, F., Zając, M., & Scrivener, K. L. (2017). Outcomes of the RILEM round robin on degree of reaction of slag and fly ash in blended cements. *Materials and Structures*, *50*(2), 135. https://doi.org/10.1617/s11527-017-1002-1

Durdziński, P. T., Dunant, C. F., Ben Haha, M., & Scrivener, K. L. (2015). A new quantification method based on SEM-EDS to assess fly ash composition and study the reaction of its individual components in hydrating cement paste. *Cement and Concrete Research, 73,* 111–122. https://doi.org/10.1016/j.cemconres.2015.02.008

Durdziński, P. T., Snellings, R., Dunant, C. F., Ben Haha, M., & Scrivener, K. L. (2015). Fly ash as an assemblage of model Ca–Mg–Na-aluminosilicate glasses. *Cement and Concrete Research, 78,* 263–272. https://doi.org/10.1016/j.cemconres.2015.08.005

Feng, X., Thomas, M. D. A., Bremner, T. W., Balcom, B. J., & Folliard, K. J. (2005). Studies on lithium salts to mitigate ASR-induced expansion in new concrete: A critical review. *Cement and Concrete Research*, *35*(9), 1789–1796. https://doi.org/10.1016/j.cemconres.2004.10.013

Feng, X., Thomas, M. D. A., Bremner, T. W., Folliard, K. J., & Fournier, B. (2010). New observations on the mechanism of lithium nitrate against alkali silica reaction (ASR). *Cement and Concrete Research*, *40*(1), 94–101. https://doi.org/10.1016/j.cemconres.2009.07.017

Fernández-Jiménez, A., & Puertas, F. (2002). The alkali-silica reaction in alkali-activated granulated slag mortars with reactive aggregate. *Cement and Concrete Research*, *32*(7), 1019–1024. https://doi.org/10.1016/S0008-8846(01)00745-1

Figueira, R. B., Sousa, R., Coelho, L., Azenha, M., de Almeida, J. M., Jorge, P. A. S., & Silva, C. J. R. (2019). Alkali-silica reaction in concrete: Mechanisms, mitigation and test methods. *Construction and Building Materials*, *222*, 903–931. https://doi.org/10.1016/j.conbuildmat.2019.07.230

Gao, X. X., Multon, S., Cyr, M., & Sellier, A. (2013). Alkali-silica reaction (ASR) expansion: Pessimum effect versus scale effect. *Cement and Concrete Research*, *44*, 25–33. https://doi.org/10.1016/j.cemconres.2012.10.015

Garcia-Diaz, E., Bulteel, D., Monnin, Y., Degrugilliers, P., & Fasseu, P. (2010). ASR pessimum behaviour of siliceous limestone aggregates. *Cement and Concrete Research*, *40*(4), 546–549. https://doi.org/10.1016/j.cemconres.2009.08.011

Garcia-Diaz, E., Riche, J., Bulteel, D., & Vernet, C. (2006). Mechanism of damage for the alkali-silica reaction. *Cement and Concrete Research*, *36*(2), 395–400. https://doi.org/10.1016/j.cemconres.2005.06.003

García-Lodeiro, I., Palomo, A., & Fernández-Jiménez, A. (2007). Alkali–aggregate reaction in activated fly ash systems. *Cement and Concrete Research*, *37*(2), 175–183. https://doi.org/10.1016/j.cemconres.2006.11.002

Geng, G., Barbotin, S., Shakoorioskooie, M., Shi, Z., Leemann, A., Sanchez, D. F., Grolimund, D., Wieland, E., & Dähn, R. (2021). An in-situ 3D micro-XRD

investigation of water uptake by alkali-silica-reaction (ASR) product. *Cement and Concrete Research*, *141*, 106331. https://doi.org/10.1016/j.cemconres.2020.106331

Geng, G., Shi, Z., Leemann, A., Borca, C., Huthwelker, T., Glazyrin, K., Pekov, I. V., Churakov, S., Lothenbach, B., Dähn, R., & Wieland, E. (2020). Atomistic structure of alkali-silica reaction products refined from X-ray diffraction and micro X-ray absorption data. *Cement and Concrete Research*, *129*, 105958. https://doi.org/10.1016/j.cemconres.2019.105958

Geng, G., Shi, Z., Leemann, A., Glazyrin, K., Kleppe, A., Daisenberger, D., Churakov, S., Lothenbach, B., Wieland, E., & Dähn, R. (2020). Mechanical behavior and phase change of alkali-silica reaction products under hydrostatic compression. *Acta Crystallographica Section B, Structural Science, Crystal Engineering and Materials*, *76*, 674–682. https://doi.org/10.1107/S205252062000846X

Ghazizadeh, S., Hanein, T., Provis, J. L., & Matschei, T. (2020). Estimation of standard molar entropy of cement hydrates and clinker minerals. *Cement and Concrete Research*, *136*(April), 106188. https://doi.org/10.1016/j.cemconres.2020.106188

Gifford, P. M. & Gillott, J. E. (1996). Alkali-silica reaction (ASR) and alkali-carbonate reaction (ACR) in activated blast furnace slag cement (ABFSC) concrete. *Cement and Concrete Research*, *26*, 21–26.

Gillott, J. E. (1975). Alkali--aggregate reactions in concrete. *Engineering Geology*, *9*, 303–326.

Glasser, L., & Jenkins, H. D. B. (2011). Ambient isobaric heat capacities, Cp,m, for ionic solids and liquids: an application of volume-based thermodynamics (VBT). *Inorganic Chemistry*, *50*(17), 8565–8569.

Glosser, D., Suraneni, P., Isgor, O. B., & Weiss, W. J. (2021). Using glass content to determine the reactivity of fly ash for thermodynamic calculations. *Cement and*

Concrete Composites, *115*, 103849. https://doi.org/10.1016/j.cemconcomp.2020.103849

Goguel, R. (1995). Alkali release by volcanic aggregates in concrete. *Cement and Concrete Research*, *25*(4), 841–852. https://doi.org/10.1016/0008-8846(95)00075-N

Gudmundsson, G., & Olafsson, H. (1999). Alkali-silica reactions and silica fume: 20 years of experience in Iceland. *Cement and Concrete Research*, *29*(8), 1289–1297. https://doi.org/10.1016/S0008-8846(98)00239-7

Guo, S., Dai, Q., & Si, R. (2019). Effect of calcium and lithium on alkali-silica reaction kinetics and phase development. *Cement and Concrete Research*, *115*, 220–229. https://doi.org/10.1016/j.cemconres.2018.10.007

Guthrie, G. D., & Carey, J. W. (2015). A thermodynamic and kinetic model for paste-aggregate interactions and the alkali-silica reaction. *Cement and Concrete Research*, *76*, 107–120. https://doi.org/10.1016/j.cemconres.2015.05.004

Habert, G., Miller, S. A., John, V. M., Provis, J. L., Favier, A., Horvath, A., & Scrivener, K. L. (2020). Environmental impacts and decarbonization strategies in the cement and concrete industries. *Nature Reviews Earth & Environment*, *1*(11), 559–573. https://doi.org/10.1038/s43017-020-0093-3

Hassan, A., Arif, M., & Shariq, M. (2019). Use of geopolymer concrete for a cleaner and sustainable environment – A review of mechanical properties and microstructure. *Journal of Cleaner Production*, *223*, 704–728. https://doi.org/10.1016/j.jclepro.2019.03.051

Hay, R., & Ostertag, C. P. (2019). On utilization and mechanisms of waste aluminium in mitigating alkali-silica reaction (ASR) in concrete. *Journal of Cleaner Production*, *212*, 864–879. https://doi.org/10.1016/j.jclepro.2018.11.288

Hay, R., & Ostertag, C. P. (2021). New insights into the role of fly ash in mitigating alkali-silica reaction (ASR) in concrete. *Cement and Concrete Research*, *144*, 106440. https://doi.org/10.1016/j.cemconres.2021.106440

Helgeson, H. C., Kirkham, D. H., & Flowers, G. C. (1981). Theoretical prediction of the thermodynamic behavior of aqueous electrolytes by high pressures and temperatures; IV, Calculation of activity coefficients, osmotic coefficients, and apparent molal and standard and relative partial molal properties to 600°C and 5kb. *American Journal of Science, 281*, 1249-1516.

Hench, L. L., & Clark, D. E. (1978). Physical chemistry of glass surfaces. *Journal of Non-Crystalline Solids*, *28*(1), 83–105. https://doi.org/10.1016/0022-3093(78)90077-7

Hester, D., McNally, C., & Richardson, M. (2005). A study of the influence of slag alkali level on the alkali–silica reactivity of slag concrete. *Construction and Building Materials*, *19*(9), 661–665. https://doi.org/10.1016/j.conbuildmat.2005.02.016

Hobbs, D. W. (1986). Deleterious expansion of concrete due to alkali-silica reaction: Influence of pfa and slag. *Magazine of Concrete Research*, *38*(137), 191–205. https://doi.org/10.1680/macr.1986.38.137.191

Hobbs, D. W. (1988). *Alkali-silica reaction in concrete*. Thomas Telford Publishing.

Hong, S. Y., & Glasser, F. P. (2002). Alkali sorption by C-S-H and C-A-S-H gels: Part II. Role of alumina. *Cement and Concrete Research*, *32*(7), 1101–1111. https://doi.org/10.1016/S0008-8846(02)00753-6

Hong, S.-Y., & Glasser, F. P. (1999). Alkali binding in cement pastes: Part I. The C-S-H phase. *Cement and Concrete Research*, *29*(12), 1893–1903. https://doi.org/10.1016/S0008-8846(99)00187-8

Honorio, T., Chemgne Tamouya, O. M., Shi, Z., & Bourdot, A. (2020). Intermolecular interactions of nanocrystalline alkali-silica reaction products under sorption. *Cement*

and Concrete Research, *136*, 106155. https://doi.org/10.1016/j.cemconres.2020.106155

Hou, X., Kirkpatrick, R. J., Struble, L. J., & Monteiro, P. J. M. (2005). Structural investigations of alkali silicate gels. *Journal of the American Ceramic Society*, *88*(4), 943–949. https://doi.org/10.1111/j.1551-2916.2005.00145.x

Hou, X., Struble, L. J., & Kirkpatrick, R. J. (2004). Formation of ASR gel and the roles of C-S-H and portlandite. *Cement and Concrete Research*, *34*(9), 1683–1696. https://doi.org/10.1016/j.cemconres.2004.03.026

Hünger, K.-J. (2007). The contribution of quartz and the role of aluminum for understanding the AAR with greywacke. *Cement and Concrete Research*, *37*(8), 1193–1205. https://doi.org/10.1016/j.cemconres.2007.05.009

Ichikawa, T. (2009). Alkali-silica reaction, pessimum effects and pozzolanic effect. *Cement and Concrete Research*, *39*(8), 716–726. https://doi.org/10.1016/j.cemconres.2009.06.004

Ichikawa, T., & Miura, M. (2007). Modified model of alkali-silica reaction. *Cement and Concrete Research*, *37*(9), 1291–1297. https://doi.org/10.1016/j.cemconres.2007.06.008

Jin, H., Ghazizadeh, S., & Provis, J. L. (2023). Assessment of the thermodynamics of Na,K-shlykovite as potential alkali-silica reaction products in the $(Na,K)_2O$-CaO–SiO_2-H_2O system. *Cement and Concrete Research*, *172*, 107253. https://doi.org/10.1016/j.cemconres.2023.107253

Jin, H., Ghazizadeh, S., & Provis, J. L. (2024). *Thermodynamic modelling of alkali-silica reaction in blended cements*. Under review.

Jones, J. B., & Segnit, E. R. (1971). The nature of opal I. nomenclature and constituent phases. *Journal of the Geological Society of Australia*, *18*(1), 57–68. https://doi.org/10.1080/00167617108728743

Jones, T. R., Walters, G. V., & Kostuch, J. A. (1992). Role of metakaolin in suppressing ASR in concrete containing reactive aggregate and exposed to saturated NaCl solution. *Proceedings of the 9th International Conference on Alkali-Aggregate Reaction in Concrete*, London, UK, 12 pp.

Juenger, M. C. G., & Ostertag, C. P. (2004). Alkali-silica reactivity of large silica fume-derived particles. *Cement and Concrete Research*, *34*(8), 1389–1402. https://doi.org/10.1016/j.cemconres.2004.01.001

Kakali, G., Perraki, T., Tsivilis, S., & Badogiannis, E. (2001). Thermal treatment of kaolin: The effect of mineralogy on the pozzolanic activity. *Applied Clay Science*, *20*(1), 73–80. https://doi.org/10.1016/S0169-1317(01)00040-0

Kandasamy, S., & Shehata, M. H. (2014). The capacity of ternary blends containing slag and high-calcium fly ash to mitigate alkali silica reaction. *Cement and Concrete Composites*, *49*, 92–99. https://doi.org/10.1016/j.cemconcomp.2013.12.008

Kawabata, Y., & Yamada, K. (2017). The mechanism of limited inhibition by fly ash on expansion due to alkali–silica reaction at the pessimum proportion. *Cement and Concrete Research*, *92*, 1–15. https://doi.org/10.1016/j.cemconres.2016.11.002

Ke, X., Bernal, S. A., Provis, J. L., & Lothenbach, B. (2020). Thermodynamic modelling of phase evolution in alkali-activated slag cements exposed to carbon dioxide. *Cement and Concrete Research*, *136*, 106158. https://doi.org/10.1016/j.cemconres.2020.106158

Kim, T., & Olek, J. (2014). Chemical sequence and kinetics of alkali-silica reaction part II. A thermodynamic model. *Journal of the American Ceramic Society*, *97*(7), 2204–2212. https://doi.org/10.1111/jace.12830

Kim, T., Olek, J., & Jeong, H. G. (2015). Alkali-silica reaction: Kinetics of chemistry of pore solution and calcium hydroxide content in cementitious system. *Cement and Concrete Research*, *71*, 36–45. https://doi.org/10.1016/j.cemconres.2015.01.017

Krivenko, P., Drochytka, R., Gelevera, A., & Kavalerova, E. (2014). Mechanism of preventing the alkali–aggregate reaction in alkali activated cement concretes. *Cement and Concrete Composites*, *45*, 157–165. https://doi.org/10.1016/j.cemconcomp.2013.10.003

Krüger, M. E., Heisig, A., Hilbig, H., Eickhoff, H., Heinz, D., & Machner, A. (2023). Effect of aluminum on the structure of synthetic alkali-silica gels. *Cement and Concrete Research*, *166*, 107088. https://doi.org/10.1016/j.cemconres.2022.107088

Kulik, D. A., Miron, G. D., & Lothenbach, B. (2022). A structurally-consistent CASH+ sublattice solid solution model for fully hydrated C-S-H phases: Thermodynamic basis, methods, and Ca-Si-H_2O core sub-model. *Cement and Concrete Research*, *151*, 106585. https://doi.org/10.1016/j.cemconres.2021.106585

Kulik, D. A., Wagner, T., Dmytrieva, S. V., Kosakowski, G., Hingerl, F. F., Chudnenko, K. V., & Berner, U. R. (2013). GEM-Selektor geochemical modeling package: Revised algorithm and GEMS3K numerical kernel for coupled simulation codes. *Computational Geosciences*, *17*(1), 1–24. https://doi.org/10.1007/s10596-012-9310-6

Kunther, W., Dai, Z., & Skibsted, J. (2016). Thermodynamic modeling of hydrated white Portland cement–metakaolin–limestone blends utilizing hydration kinetics from ^{29}Si MAS NMR spectroscopy. *Cement and Concrete Research*, *86*, 29–41. https://doi.org/10.1016/J.CEMCONRES.2016.04.012

Lane, D. S., & Ozyildirim, C. (1999). Preventive measures for alkali-silica reactions (binary and ternary systems). *Cement and Concrete Research*, *29*(8), 1281–1288. https://doi.org/10.1016/S0008-8846(98)00242-7

Leemann, A. (2017). Raman microscopy of alkali-silica reaction (ASR) products formed in concrete. *Cement and Concrete Research*, *102*, 41–47. https://doi.org/10.1016/j.cemconres.2017.08.014

Leemann, A., Katayama, T., Fernandes, I., & Broekmans, M. A. T. M. (2016). Types of alkali-aggregate reactions and the products formed. *Proceedings of the Institution of Civil Engineers: Construction Materials*, *169*(3), 128–135. https://doi.org/10.1680/jcoma.15.00059

Leemann, A., Le Saout, G., Winnefeld, F., Rentsch, D., & Lothenbach, B. (2011). Alkali-silica reaction: The influence of calcium on silica dissolution and the formation of reaction products. *Journal of the American Ceramic Society*, *94*(4), 1243–1249. https://doi.org/10.1111/J.1551-2916.2010.04202.X

Leemann, A., Lörtscher, L., Bernard, L., Le Saout, G., Lothenbach, B., & Espinosa-Marzal, R. M. (2014). Mitigation of ASR by the use of $LiNO_3$—Characterization of the reaction products. *Cement and Concrete Research*, *59*, 73–86. https://doi.org/10.1016/j.cemconres.2014.02.003

Leemann, A., & Merz, C. (2013). An attempt to validate the ultra-accelerated microbar and the concrete performance test with the degree of AAR-induced damage observed in concrete structures. *Cement and Concrete Research*, *49*, 29–37. https://doi.org/10.1016/j.cemconres.2013.03.014

Leemann, A., Shi, Z., & Lindgård, J. (2020). Characterization of amorphous and crystalline ASR products formed in concrete aggregates. *Cement and Concrete Research*, *137*(June), 106190. https://doi.org/10.1016/j.cemconres.2020.106190

L'Hôpital, E., Lothenbach, B., Kulik, D. A., & Scrivener, K. (2016). Influence of calcium to silica ratio on aluminium uptake in calcium silicate hydrate. *Cement and Concrete Research, 85,* 111–121. https://doi.org/10.1016/j.cemconres.2016.01.014

L'Hôpital, E., Lothenbach, B., Le Saout, G., Kulik, D., & Scrivener, K. (2015). Incorporation of aluminium in calcium-silicate-hydrates. *Cement and Concrete Research, 75,* 91–103. https://doi.org/10.1016/j.cemconres.2015.04.007

L'Hôpital, E., Lothenbach, B., Scrivener, K., & Kulik, D. A. (2016). Alkali uptake in calcium alumina silicate hydrate (C-A-S-H). *Cement and Concrete Research, 85,* 122–136. https://doi.org/10.1016/j.cemconres.2016.03.009

Lindgård, J., Sellevold, E. J., Thomas, M. D. A., Pedersen, B., Justnes, H., & Rønning, T. F. (2013). Alkali-silica reaction (ASR)—Performance testing: Influence of specimen pre-treatment, exposure conditions and prism size on concrete porosity, moisture state and transport properties. *Cement and Concrete Research, 53,* 145–167. https://doi.org/10.1016/j.cemconres.2013.05.020

Lindgård, J., Thomas, M. D. A., Sellevold, E. J., Pedersen, B., Andiç-Çakır, Ö., Justnes, H., & Rønning, T. F. (2013). Alkali–silica reaction (ASR)—performance testing: Influence of specimen pre-treatment, exposure conditions and prism size on alkali leaching and prism expansion. *Cement and Concrete Research, 53,* 68–90. https://doi.org/10.1016/j.cemconres.2013.05.017

Lloyd, R. R., Provis, J. L., & Van Deventer, J. S. J. (2010). Pore solution composition and alkali diffusion in inorganic polymer cement. *Cement and Concrete Research, 40*(9), 1386–1392. https://doi.org/10.1016/j.cemconres.2010.04.008

Lorenzo, P., Gñoni, S., Hernández, S., & Guerrero, A. (1996). Effect of fly ashes with high total alkali content on the alkalinity of the pore solution of hydrated Portland cement

paste. *Journal of the American Ceramic Society*, *79*(2), 470–474. https://doi.org/10.1111/j.1151-2916.1996.tb08146.x

Lothenbach, B., Bernard, E., & Mäder, U. (2017). Zeolite formation in the presence of cement hydrates and albite. *Physics and Chemistry of the Earth, Parts A/B/C*, *99*, 77-94. https://doi.org/10.1016/j.pce.2017.02.006

Lothenbach, B. (2010). Thermodynamic equilibrium calculations in cementitious systems. *Materials and Structures/Materiaux et Constructions*, *43*(10), 1413–1433. https://doi.org/10.1617/s11527-010-9592-x

Lothenbach, B., & Gruskovnjak, A. (2007). Hydration of alkali-activated slag: Thermodynamic modelling. *Advances in Cement Research*, *19*(2), 81–92. https://doi.org/10.1680/adcr.2007.19.2.81

Lothenbach, B., Kulik, D. A., Matschei, T., Balonis, M., Baquerizo, L., Dilnesa, B., Miron, G. D., & Myers, R. J. (2019). Cemdata18: A chemical thermodynamic database for hydrated Portland cements and alkali-activated materials. *Cement and Concrete Research*, *115*, 472–506. https://doi.org/10.1016/j.cemconres.2018.04.018

Lothenbach, B., Matschei, T., Möschner, G., & Glasser, F. P. (2008). Thermodynamic modelling of the effect of temperature on the hydration and porosity of Portland cement. *Cement and Concrete Research*, *38*(1), 1–18. https://doi.org/10.1016/J.CEMCONRES.2007.08.017

Lothenbach, B., Scrivener, K., & Hooton, R. D. (2011). Supplementary cementitious materials. *Cement and Concrete Research*, *41*(12), 1244–1256. https://doi.org/10.1016/j.cemconres.2010.12.001

Lothenbach, B., & Winnefeld, F. (2006). Thermodynamic modelling of the hydration of Portland cement. *Cement and Concrete Research*, *36*(2), 209–226. https://doi.org/10.1016/J.CEMCONRES.2005.03.001

Lothenbach, B., & Zajac, M. (2019). Application of thermodynamic modelling to hydrated cements. *Cement and Concrete Research*, *123*, 105779. https://doi.org/10.1016/j.cemconres.2019.105779

Ma, B., & Lothenbach, B. (2021). Synthesis, characterization, and thermodynamic study of selected K-based zeolites. *Cement and Concrete Research*, *148*, 106537. https://doi.org/10.1016/J.CEMCONRES.2021.106537

Maas, A. J., Ideker, J. H., & Juenger, M. C. G. (2007). Alkali silica reactivity of agglomerated silica fume. *Cement and Concrete Research*, *37*(2), 166–174. https://doi.org/10.1016/j.cemconres.2006.10.011

Maraghechi, H. (2014). *Development and assessment of alkali activated recycled glass-based concretes for civil infrastructure*. The Pennsylvania State University.

Maraghechi, H., Rajabipour, F., Pantano, C. G., & Burgos, W. D. (2016). Effect of calcium on dissolution and precipitation reactions of amorphous silica at high alkalinity. *Cement and Concrete Research*, *87*, 1–13. https://doi.org/10.1016/j.cemconres.2016.05.004

Maraghechi, H., Shafaatian, S. M. H., Fischer, G., & Rajabipour, F. (2012). The role of residual cracks on alkali silica reactivity of recycled glass aggregates. *Cement and Concrete Composites*, *34*(1), 41–47. https://doi.org/10.1016/j.cemconcomp.2011.07.004

Marusin, S. L., & Shotwell, L. B. (2000). Alkali-silica reaction in concrete caused by densified silica fume lumps: a case study. *Cement, Concrete, and Aggregates*, *22*(2), 90–94. https://doi.org/10.1520/CCA10468J

Matschei, T., Lothenbach, B., & Glasser, F. P. (2007a). The AFm phase in Portland cement. *Cement and Concrete Research*, *37*(2), 118–130. https://doi.org/10.1016/j.cemconres.2006.10.010

Matschei, T., Lothenbach, B., & Glasser, F. P. (2007b). Thermodynamic properties of Portland cement hydrates in the system $CaO–Al_2O_3–SiO_2–CaSO_4–CaCO_3–H_2O$. *Cement and Concrete Research*, *37*(10), 1379–1410. https://doi.org/10.1016/j.cemconres.2007.06.002

McCoy, W. J., & Caldwell, A. G. (1951). New approach to inhibiting alkali-aggregate expansion. *ACI Journal Proceedings*, *47*(5), 693–706.

Menéndez, E., Silva, A. S., & Duchesne, J. (2021). Recommendation of RILEM TC 258-AAA: RILEM AAR-8: determination of potential releasable alkalis by aggregates in concrete. *Materials and Structures*, *54*(6), 205. https://doi.org/10.1617/s11527-021-01682-1

Min, D., & Mingshu, T. (1993). Measures to inhibit alkali-dolomite reaction. *Cement and Concrete Research*, *23*(5), 1115–1120. https://doi.org/10.1016/0008-8846(93)90171-5

Min, D., Zhongzi, X., Xianghui, L., Sufen, H., & Mingshu, T. (1996). Microstructures of some alkali-silica reactive aggregates in China. *Cement and Concrete Reseacch*, *26*(5), 663–668.

Mo, X. (2005). Laboratory study of LiOH in inhibiting alkali-silica reaction at 20 °C: A contribution. *Cement and Concrete Research*, *35*(3), 499–504. https://doi.org/10.1016/j.cemconres.2004.06.003

Monnin, Y., Dégrugilliers, P., Bulteel, D., & Garcia-Diaz, E. (2006). Petrography study of two siliceous limestones submitted to alkali-silica reaction. *Cement and Concrete Research*, *36*(8), 1460–1466. https://doi.org/10.1016/j.cemconres.2006.03.025

Moser, R. D., Jayapalan, A. R., Garas, V. Y., & Kurtis, K. E. (2010). Assessment of binary and ternary blends of metakaolin and Class C fly ash for alkali-silica reaction mitigation in concrete. *Cement and Concrete Research*, *40*(12), 1664–1672. https://doi.org/10.1016/j.cemconres.2010.08.006

Multon, S., Cyr, M., Sellier, A., Diederich, P., & Petit, L. (2010). Effects of aggregate size and alkali content on ASR expansion. *Cement and Concrete Research*, *40*(4), 508–516. https://doi.org/10.1016/j.cemconres.2009.08.002

Multon, S., Cyr, M., Sellier, A., Leklou, N., & Petit, L. (2008). Coupled effects of aggregate size and alkali content on ASR expansion. *Cement and Concrete Research*, *38*(3), 350–359. https://doi.org/10.1016/j.cemconres.2007.09.013

Multon, S., & Sellier, A. (2016). Multi-scale analysis of alkali-silica reaction (ASR): Impact of alkali leaching on scale effects affecting expansion tests. *Cement and Concrete Research*, *81*, 122–133. https://doi.org/10.1016/j.cemconres.2015.12.007

Multon, S., & Toutlemonde, F. (2010). Effect of moisture conditions and transfers on alkali silica reaction damaged structures. *Cement and Concrete Research*, *40*(6), 924–934. https://doi.org/10.1016/j.cemconres.2010.01.011

Mundra, S., Prentice, D. P., Bernal, S. A., & Provis, J. L. (2020). Modelling chloride transport in alkali-activated slags. *Cement and Concrete Research*, *130*, 106011. https://doi.org/10.1016/j.cemconres.2020.106011

Myers, R. J., Bernal, S. A., & Provis, J. L. (2014). A thermodynamic model for C-(N-)A-S-H gel: CNASH_ss. Derivation and validation. *Cement and Concrete Research*, *66*, 27–47. https://doi.org/10.1016/J.CEMCONRES.2014.07.005

Myers, R. J., Bernal, S. A., & Provis, J. L. (2017). Phase diagrams for alkali-activated slag binders. *Cement and Concrete Research*, *95*, 30–38. https://doi.org/10.1016/j.cemconres.2017.02.006

Myers, R. J., Bernal, S. A., San Nicolas, R., & Provis, J. L. (2013). Generalized structural description of calcium-sodium aluminosilicate hydrate gels: The cross-linked substituted tobermorite model. *Langmuir*, *29*(17), 5294–5306. https://doi.org/10.1021/la4000473

Myers, R. J., Lothenbach, B., Bernal, S. A., & Provis, J. L. (2015). Thermodynamic modelling of alkali-activated slag cements. *Applied Geochemistry*, *61*, 233–247. https://doi.org/10.1016/j.apgeochem.2015.06.006

Nixon, P. J., Collins, R. J., & Rayment, P. L. (1979). The concentration of alkalies by moisture migration in concrete—A factor influencing alkali aggregate reaction. *Cement and Concrete Research*, *9*(4), 417–423. https://doi.org/10.1016/0008-8846(79)90038-3

Nixon, P. J., & Sims, I. (2015). RILEM Recommended Test Method: AAR-4.1—Detection of Potential Alkali-Reactivity—60 °C Test Method for Aggregate Combinations Using Concrete Prisms. In *RILEM Recommendations for the Prevention of Damage by Alkali-Aggregate Reactions in New Concrete Structures: State-of-the-Art Report of the RILEM Technical Committee 219-ACS* (pp. 99-116). Springer Netherlands. https://link.springer.com/chapter/10.1007/978-94-017-7252-5_6

Nixon, P. J., & Sims, I. (2016). RILEM Recommended Test Method:AAR-1.1—Detection of Potential Alkali-Reactivity—Part 1: Petrographic Examination Method. In *RILEM Recommendations for the Prevention of Damage by Alkali-Aggregate Reactions in New Concrete Structures: State-of-the-Art Report of the RILEM Technical Committee 219-ACS* (pp. 35–60). Springer Netherlands. https://doi.org/10.1007/978-94-017-7252-5_3

Oberholster, R. E., Brandt, M. P., & Weston, A. C. (1978). Cement-aggregate reaction and the deterioration of concrete structures in the Cape Peninsula. *Civil Engineering (Die Siviele Ingenieur in Suid-Afrika), 7,* 161-166

Pekov, I. V., Zubkova, N. V., Filinchuk, Ya. E., Chukanov, N. V., Zadov, A. E., Pushcharovsky, D. Yu., & Gobechiya, E. R. (2010). Shlykovite $KCa[Si_4O_9(OH)]\cdot 3H_2O$ and cryptophyllite $K_2Ca[Si_4O_{10}]\cdot 5H_2O$, new mineral species

from the Khibiny alkaline pluton, Kola Peninsula, Russia. *Geology of Ore Deposits*, *52*(8), 767–777. https://doi.org/10.1134/S1075701510080088

Peterson, K., Gress, D., Van Dam, T., & Sutter, L. (2006). Crystallized alkali-silica gel in concrete from the late 1890s. *Cement and Concrete Research*, *36*(8), 1523–1532. https://doi.org/10.1016/j.cemconres.2006.05.017

Plusquellec, G., Geiker, M. R., Lindgård, J., & De Weerdt, K. (2018). Determining the free alkali metal content in concrete – Case study of an ASR-affected dam. *Cement and Concrete Research*, *105*, 111–125. https://doi.org/10.1016/j.cemconres.2018.01.003

Poole, A. B. (1991). Introduction to alkali-aggregate reaction in concrete. In *The alkali-silica reaction in concrete* (pp. 17–45). CRC Press.

Powers, T. C., & Steinour, H. H. (1955). An interpretation of some published researches on the alkali-aggregate reaction. Part 1—The chemical reactions and mechanism of expansion. *J. Am. Concr. Inst.*, *6*, 497–516.

Poyet, S., Sellier, A., Capra, B., Foray, G., Torrenti, J.-M., Cognon, H., & Bourdarot, E. (2007). Chemical modelling of alkali silica reaction: Influence of the reactive aggregate size distribution. *Materials and Structures*, *40*(2), 229–239. https://doi.org/10.1617/s11527-006-9139-3

Provis, J. L. (2018). Alkali-activated materials. *Cement and Concrete Research*, *114*, 40–48. https://doi.org/10.1016/j.cemconres.2017.02.009

Provis, J. L., & Bernal, S. A. (2014). Geopolymers and related alkali-activated materials. *Annual Review of Materials Research*, *44*(1), 299–327. https://doi.org/10.1146/annurev-matsci-070813-113515

Provis, J. L., Palomo, A., & Shi, C. (2015). Advances in understanding alkali-activated materials. *Cement and Concrete Research*, *78*, 110–125. https://doi.org/10.1016/j.cemconres.2015.04.013

Puertas, F., Fernández-Jiménez, A., & Blanco-Varela, M. T. (2004). Pore solution in alkali-activated slag cement pastes. Relation to the composition and structure of calcium silicate hydrate. *Cement and Concrete Research*, *34*(1), 139–148. https://doi.org/10.1016/S0008-8846(03)00254-0

Rajabipour, F., Giannini, E., Dunant, C., Ideker, J. H., & Thomas, M. D. A. (2015). Alkali-silica reaction: Current understanding of the reaction mechanisms and the knowledge gaps. *Cement and Concrete Research*, *76*, 130–146. https://doi.org/10.1016/j.cemconres.2015.05.024

Rajabipour, F., Maraghechi, H., & Fischer, G. (2010). Investigating the alkali-silica reaction of recycled glass aggregates in concrete materials. *Journal of Materials in Civil Engineering*, *22*(12), 1201–1208. Scopus. https://doi.org/10.1061/(ASCE)MT.1943-5533.0000126

Ramanathan, S., Moon, H., Croly, M., Chung, C.-W., & Suraneni, P. (2019). Predicting the degree of reaction of supplementary cementitious materials in cementitious pastes using a pozzolanic test. *Construction and Building Materials*, *204*, 621–630. https://doi.org/10.1016/j.conbuildmat.2019.01.173

Ramlochan, T., Thomas, M. D. A., & Hooton, R. D. (2004). The effect of pozzolans and slag on the expansion of mortars cured at elevated temperature: Part II: Microstructural and microchemical investigations. *Cement and Concrete Research*, *34*(8), 1341–1356. https://doi.org/10.1016/j.cemconres.2003.12.026

Rashad, A. M., Bai, Y., Basheer, P. A. M., Milestone, N. B., & Collier, N. C. (2013). Hydration and properties of sodium sulfate activated slag. *Cement and Concrete Composites*, *37*, 20–29. https://doi.org/10.1016/j.cemconcomp.2012.12.010

Rasheeduzzafar, & Ehtesham Hussain, S. (1991). Effect of microsilica and blast furnace slag on pore solution composition and alkali-silica reaction. *Cement and Concrete Composites*, *13*(3), 219–225. https://doi.org/10.1016/0958-9465(91)90023-B

Richardson, I. G., Brough, A. R., Groves, G. W., & Dobson, C. M. (1994). The characterization of hardened alkali-activated blast-furnace slag pastes and the nature of the calcium silicate hydrate (C-S-H) phase. *Cement and Concrete Research*, *24*(5), 813–829. https://doi.org/10.1016/0008-8846(94)90002-7

Rodrigue, A., Duchesne, J., Fournier, B., Champagne, M., & Bissonnette, B. (2020). Alkali-silica reaction in alkali-activated combined slag and fly ash concretes: The tempering effect of fly ash on expansion and cracking. *Construction and Building Materials*, *251*, 118968. https://doi.org/10.1016/j.conbuildmat.2020.118968

Šachlová, Š., Přikryl, R., & Pertold, Z. (2010). Alkali-silica reaction products: Comparison between samples from concrete structures and laboratory test specimens. *Materials Characterization*, *61*(12), 1379–1393. https://doi.org/10.1016/j.matchar.2010.09.010

Scrivener, K. L., & Kirkpatrick, R. J. (2008). Innovation in use and research on cementitious material. *Cement and Concrete Research*, *38*(2), 128–136. https://doi.org/10.1016/j.cemconres.2007.09.025

Shayan, A., Diggins, R. G., Ivanusec, I., & Westgate, P. L. (1988). Accelerated testing of some Australian and overseas aggregates for alkali-aggregate reactivity. *Cement and Concrete Research*. *18*(4), 843–851. https://doi.org/10.1016/0008-8846(88)90020-8

Shehata, M. H., & Thomas, M. D. A. (2000). Effect of fly ash composition on the expansion of concrete due to alkali-silica reaction. *Cement and Concrete Research*, *30*(7), 1063–1072. https://doi.org/10.1016/S0008-8846(00)00283-0

Shehata, M. H., & Thomas, M. D. A. (2002). Use of ternary blends containing silica fume and fly ash to suppress expansion due to alkali-silica reaction in concrete. *Cement and Concrete Research*, *32*(3), 341–349. https://doi.org/10.1016/S0008-8846(01)00680-9

Shehata, M. H., & Thomas, M. D. A. (2006). Alkali release characteristics of blended cements. *Cement and Concrete Research*, *36*(6), 1166–1175. https://doi.org/10.1016/j.cemconres.2006.02.015

Shi, C., Shi, Z., Hu, X., Zhao, R., & Chong, L. (2015). A review on alkali-aggregate reactions in alkali-activated mortars/concretes made with alkali-reactive aggregates. *Materials and Structures*, *48*(3), 621–628. https://doi.org/10.1617/s11527-014-0505-2

Shi, Z., Geng, G., Leemann, A., & Lothenbach, B. (2019). Synthesis, characterization, and water uptake property of alkali-silica reaction products. *Cement and Concrete Research*, *121*, 58–71. https://doi.org/10.1016/j.cemconres.2019.04.009

Shi, Z., Leemann, A., Rentsch, D., & Lothenbach, B. (2020). Synthesis of alkali-silica reaction product structurally identical to that formed in field concrete. *Materials & Design*, *190*, 108562. https://doi.org/10.1016/j.matdes.2020.108562

Shi, Z., & Lothenbach, B. (2019). The role of calcium on the formation of alkali-silica reaction products. *Cement and Concrete Research*, *126*, 105898. https://doi.org/10.1016/j.cemconres.2019.105898

Shi, Z., & Lothenbach, B. (2020). The combined effect of potassium, sodium and calcium on the formation of alkali-silica reaction products. *Cement and Concrete Research*, *127*, 105914. https://doi.org/10.1016/j.cemconres.2019.105914

Shi, Z., Ma, B., & Lothenbach, B. (2021). Effect of Al on the formation and structure of alkali-silica reaction products. *Cement and Concrete Research*, *140*, 106311. https://doi.org/10.1016/j.cemconres.2020.106311

Shi, Z., Shi, C., Wan, S., & Zhang, Z. (2018). Effects of alkali dosage and silicate modulus on alkali-silica reaction in alkali-activated slag mortars. *Cement and Concrete Research*, *111*, 104–115. https://doi.org/10.1016/j.cemconres.2018.06.005

Shi, Z., Shi, C., Zhang, J., Wan, S., Zhang, Z., & Ou, Z. (2018). Alkali-silica reaction in waterglass-activated slag mortars incorporating fly ash and metakaolin. *Cement and Concrete Research*, *108*, 10–19. https://doi.org/10.1016/j.cemconres.2018.03.002

Shi, Z., Shi, C., Zhao, R., & Wan, S. (2015). Comparison of alkali–silica reactions in alkali-activated slag and Portland cement mortars. *Materials and Structures*, *48*(3), 743–751. https://doi.org/10.1617/s11527-015-0535-4

Siddique, R. (2011). Utilization of silica fume in concrete: Review of hardened properties. *Resources, Conservation and Recycling*, *55*(11), 923–932. https://doi.org/10.1016/j.resconrec.2011.06.012

Sims, I., & Nixon, P. (2003). RILEM recommended test method AAR-0: Detection of alkali-reactivity potential in concrete—Outline guide to the use of RILEM methods in assessments of aggregates for potential alkali-reactivity. *Materials and Structures/Materiaux et Constructions*, *36*(261), 472–479. https://doi.org/10.1617/14059

Sjöberg, S. (1996). Silica in aqueous environments. *Journal of Non-Crystalline Solids*, *196*, 51–57. https://doi.org/10.1016/0022-3093(95)00562-5

Skalny, J. P., Gebauer, J., & Odler, I. (2001). *Materials Science of Concrete, Special Volume: Calcium Hydroxide in Concrete*. John Wiley & Sons.

Smaoui, N., Bérubé, M. A., Fournier, B., Bissonnette, B., & Durand, B. (2005). Effects of alkali addition on the mechanical properties and durability of concrete. *Cement and Concrete Research*, *35*(2), 203–212. https://doi.org/10.1016/j.cemconres.2004.05.007

Song, S., & Jennings, H. M. (1999). Pore solution chemistry of alkali-activated ground granulated blast-furnace slag. *Cement and Concrete Research*. *29*(2), 159-170.

Stanton, S., Porter, O. J., Meder, L. C., & Nicol, A. (1942). California experience with the expansion of concrete through reaction between cement and aggregate. *ACI Journal Proceedings*, *38*, 209–236. https://doi.org/10.14359/8598

Sun, G. K., Young, J. F., & Kirkpatrick, R. J. (2006). The role of Al in C–S–H: NMR, XRD, and compositional results for precipitated samples. *Cement and Concrete Research*, *36*(1), 18–29. https://doi.org/10.1016/j.cemconres.2005.03.002

Swaddle, T. W. (2001). Silicate complexes of aluminum(III) in aqueous systems. *Coordination Chemistry Reviews*, *219–221*, 665–686. https://doi.org/10.1016/S0010-8545(01)00362-9

Talling, B., & Brandstetr, J. (1989). Present state and future of alkali-activated slag concretes. *ACI Special Publication*, *114*, 1519–1546.

Tänzer, R., Jin, Y., & Stephan, D. (2017). Effect of the inherent alkalis of alkali activated slag on the risk of alkali silica reaction. *Cement and Concrete Research*, *98*, 82–90. https://doi.org/10.1016/j.cemconres.2017.04.009

Tapas, M. J., Sofia, L., Vessalas, K., Thomas, P., Sirivivatnanon, V., & Scrivener, K. (2021). Efficacy of SCMs to mitigate ASR in systems with higher alkali contents assessed by pore solution method. *Cement and Concrete Research*, *142*, 106353. https://doi.org/10.1016/j.cemconres.2021.106353

Thomas, M. (2001). The role of calcium hydroxide in alkali recycling in concrete. In *Materials Science of Concrete Special Volume on Calcium Hydroxide in Concrete* (pp. 269–280). American Ceramic Society, Westerville, OH.

Thomas, M. (2011). The effect of supplementary cementing materials on alkali-silica reaction: A review. *Cement and Concrete Research*, *41*(12), 1224–1231. https://doi.org/10.1016/j.cemconres.2010.11.003

Tremblay, C., Bérubé, M. A., Fournier, B., Thomas, M. D., & Folliard, K. J. (2010). Experimental investigation of the mechanisms by which LiNO is effective against ASR. *Cement and Concrete Research*, *40*(4), 583–597. https://doi.org/10.1016/j.cemconres.2009.09.022

Vivian, H. E. (1947). *Studies in cement-aggregate reaction*. Council for Scientific and Industrial Research. Melbourne, Australia.

Vollpracht, A., Lothenbach, B., Snellings, R., & Haufe, J. (2016). The pore solution of blended cements: A review. *Materials and Structures*, *49*(8), 3341–3367. https://doi.org/10.1617/s11527-015-0724-1

Wagner, T., Kulik, D. A., Hingerl, F. F., & Dmytrieva, S. V. (2012). GEM-Selektor geochemical modeling package: TSolMod library and data interface for multicomponent phase models. *The Canadian Mineralogist*, *50*(5), 1173–1195. https://doi.org/10.3749/canmin.50.5.1173

Walkley, B., Ke, X., Hussein, O., & L. Provis, J.L. (2021). Thermodynamic properties of sodium aluminosilicate hydrate (N–A–S–H). *Dalton Transactions*, *50*(39), 13968–13984. https://doi.org/10.1039/D1DT02202D

Walther, J. V., & Helgeson, H. C. (1977). Calculation of the thermodynamic properties of aqueous silica and the solubility of quartz and its polymorphs at high pressures and temperatures. *American Journal of Science*, *277*(10), 1315–1351. https://doi.org/10.2475/ajs.277.10.1315

Wang, H., & Gillott, J. E. (1991). Mechanism of alkali-silica reaction and the significance of calcium hydroxide. *Cement and Concrete Research*, *21*(4), 647–654. https://doi.org/10.1016/0008-8846(91)90115-X

Wang, W., & Noguchi, T. (2020). Alkali-silica reaction (ASR) in the alkali-activated cement (AAC) system: A state-of-the-art review. *Construction and Building Materials*, *252*, 119105. https://doi.org/10.1016/j.conbuildmat.2020.119105

Wang, W., Noguchi, T., & Maruyama, I. (2022). Mechanism understanding of alkali-silica reaction in alkali-activated materials system. *Cement and Concrete Research*, *156*, 106768. https://doi.org/10.1016/j.cemconres.2022.106768

West, T. R. (2010). *Geology Applied to Engineering*. Waveland Press.

Williams, A., Markandeya, A., Stetsko, Y., Riding, K., & Zayed, A. (2016). Cracking potential and temperature sensitivity of metakaolin concrete. *Construction and Building Materials*, *120*, 172–180. https://doi.org/10.1016/j.conbuildmat.2016.05.087

Winnefeld, F., Gluth, G. J. G., Bernal, S. A., Bignozzi, M. C., Carabba, L., Chithiraputhiran, S., Dehghan, A., Dolenec, S., Dombrowski-Daube, K., Dubey, A., Ducman, V., Jin, Y., Peterson, K., Stephan, D., & Provis, J. L. (2020). RILEM TC 247-DTA round robin test: Sulfate resistance, alkali-silica reaction and freeze–thaw resistance of alkali-activated concretes. *Materials and Structures/Materiaux et Constructions*, *53*(6), 140. https://doi.org/10.1617/s11527-020-01562-0

Yan, Y., Ma, B., Miron, G. D., Kulik, D. A., Scrivener, K., & Lothenbach, B. (2022). Al uptake in calcium silicate hydrate and the effect of alkali hydroxide. *Cement and Concrete Research*, *162*, 106957. https://doi.org/10.1016/j.cemconres.2022.106957

Yang, C., Pu, X., & Wu, F. (1999a). A study on alkali-aggregate reaction of alkali-clinker-slag cement concrete. *Chongqing Jianzhu Daxue Xuebao/Journal of Chongqing Jianzhu University*, *21*(1), 14–19.

Yang, C., Pu, X., & Wu, F. (1999b). Research on alkali aggregate reaction expansion of alkali-slag mortar (In Chinese). *Journal of the Chinese Ceramic Society*. *1304*, 651–657.

Zachariasen, W. H. (1932). The atomic arrangement in glass. *Journal of the American Chemical Society*, *54*(10), 3841–3851. https://doi.org/10.1021/ja01349a006

Zhang, C., & Wang, A. (2008). Effect of mineral admixtures on alkali-silica reaction. *Journal of Wuhan University of Technology-Mater. Sci. Ed.*, *23*(1), 16–19. https://doi.org/10.1007/s11595-006-1016-y

Zhou, J., Chen, L., Liu, Z., He, F., & Zheng, K. (2022). Effect of transitional aluminas on Portland cement hydration, phase assemblage and the correlation to ASR preventing effectiveness. *Cement and Concrete Research*, *151*, 106622. https://doi.org/10.1016/J.CEMCONRES.2021.106622

Zhou, J., Chen, L., Zheng, K., Liu, Z., Yuan, Q., & He, F. (2022). Formulating Portland cement–reactive alumina blend through thermodynamic modeling to prevent the alkali–silica reaction. *Journal of the American Ceramic Society*, *105*(2), 1533–1547. https://doi.org/10.1111/jace.18151

Zhou, J., Zheng, K., Liu, Z., Chen, L., & Lippiatt, N. (2019). Use of γ-Al_2O_3 to prevent alkali-silica reaction by altering solid and aqueous compositions of hydrated cement paste. *Cement and Concrete Research*, *124*, 105817. https://doi.org/10.1016/j.cemconres.2019.105817

Zubkova, N. V., Filinchuk, Y. E., Pekov, I. V., Pushcharovsky, D., & Yu. Gobechiya, E. R. (2010). Crystal structures of shlykovite and cryptophyllite: Comparative crystal chemistry of phyllosilicate minerals of the mountainite family. *European Journal of Mineralogy*, *22*(4), 547–555. https://doi.org/10.1127/0935-1221/2010/0022-2041

Zuo, Y., Nedeljković, M., & Ye, G. (2019). Pore solution composition of alkali-activated slag/fly ash pastes. *Cement and Concrete Research, 115*, 230–250. https://doi.org/10.1016/j.cemconres.2018.10.010

Appendix A Supporting information for Chapter 4

Table A-1 The amount of ions and dissolved neutral species in the pore solution after cement hydration when incorporating different contents of slag and silica fume /mol/L

	cement	*20%slag*	*30%slag*	*40%slag*	*50%slag*	*5%SF*	*10%SF*	*15%SF*
AlO_2^-	4.56E-06	5.74E-06	5.50E-06	5.24E-06	7.53E-06	1.38E-06	6.83E-07	4.02E-07
AlO_2H	3.09E-13	4.76E-13	5.09E-13	5.42E-13	8.55E-13	1.20E-13	7.22E-14	5.02E-14
$AlSiO_5^{3-}$	2.64E-09	1.96E-09	1.43E-09	1.03E-09	1.13E-09	4.59E-10	1.43E-10	5.67E-11
$CaCO_3$	1.92E-11	2.94E-11	3.68E-11	4.60E-11	5.59E-11	3.34E-11	5.18E-11	7.48E-11
CaSO4	4.92E-08	4.62E-08	4.89E-08	5.16E-08	2.13E-08	9.72E-08	1.44E-07	1.92E-07
Ca^{2+}	5.73E-06	8.70E-06	1.08E-05	1.33E-05	1.58E-05	8.40E-06	1.14E-05	1.48E-05
$CaOH^+$	7.41E-06	1.01E-05	1.17E-05	1.36E-05	1.53E-05	9.43E-06	1.14E-05	1.35E-05
$Ca(HSiO_3)^+$	1.28E-10	1.75E-10	2.07E-10	2.43E-10	2.69E-10	1.80E-10	2.30E-10	2.81E-10
$CaSiO_3$	2.72E-07	3.18E-07	3.44E-07	3.70E-07	3.80E-07	3.13E-07	3.43E-07	3.69E-07
FeO_2^-	1.44E-10	1.02E-10	9.68E-11	9.13E-11	5.93E-11	2.82E-10	3.75E-10	4.34E-10
FeO_2H	3.83E-15	3.32E-15	3.51E-15	3.70E-15	2.64E-15	9.60E-15	1.55E-14	2.12E-14
$K(SO_4)^-$	5.88E-06	2.96E-06	2.20E-06	1.60E-06	4.88E-07	5.68E-06	4.87E-06	4.14E-06
K^+	0.003686	0.003279	0.002986	0.002674	0.002443	0.002936	0.002509	0.00222
KOH	0.000228	0.000173	0.000145	0.000119	0.000101	0.00015	0.00011	8.52E-05
Mg^{2+}	3.09E-13	4.05E-13	5.01E-13	6.18E-13	6.00E-13	7.39E-13	1.32E-12	2.08E-12
$MgOH^+$	8.74E-12	1.03E-11	1.19E-11	1.38E-11	1.27E-11	1.82E-11	2.90E-11	4.16E-11
$MgSiO_3$	1.85E-13	1.86E-13	2.01E-13	2.17E-13	1.81E-13	3.47E-13	5.00E-13	6.55E-13

$Na(CO_3)^-$	2.90E-10	2.91E-10	2.95E-10	2.99E-10	2.97E-10	2.70E-10	2.44E-10	2.17E-10
$NaHCO_3$	4.52E-15	5.55E-15	6.28E-15	7.11E-15	7.76E-15	5.41E-15	5.94E-15	6.24E-15
$Na(SO_4)^-$	1.68E-06	1.03E-06	8.85E-07	7.57E-07	2.55E-07	1.78E-06	1.53E-06	1.26E-06
Na^+	0.00149	0.001614	0.001696	0.001781	0.001806	0.001299	0.001113	0.000954
$NaOH$	0.000176	0.000163	0.000157	0.000151	0.000143	0.000126	9.27E-05	6.98E-05
$HSiO_3^-$	9.33E-08	8.93E-08	8.68E-08	8.39E-08	7.85E-08	8.41E-08	7.61E-08	6.95E-08
SiO_2	1.48E-11	1.73E-11	1.87E-11	2.02E-11	2.07E-11	1.70E-11	1.87E-11	2.01E-11
SiO_3^{2-}	4.12E-07	3.09E-07	2.62E-07	2.22E-07	1.85E-07	2.75E-07	1.96E-07	1.47E-07
CO_3^{2-}	6.91E-10	6.79E-10	6.68E-10	6.55E-10	6.47E-10	6.96E-10	7.04E-10	7.07E-10
HCO_3^-	1.56E-13	1.96E-13	2.21E-13	2.47E-13	2.74E-13	2.13E-13	2.72E-13	3.34E-13
O_2	1.61E-05	1.86E-05	1.99E-05	2.12E-05	2.23E-05	1.68E-05	1.75E-05	1.82E-05
SO_4^{2-}	1.49E-05	8.96E-06	7.45E-06	6.16E-06	2.07E-06	1.70E-05	1.64E-05	1.52E-05
OH^-	0.005152	0.004893	0.004691	0.004475	0.004283	0.004217	0.003616	0.00318
H^+	6.99E-16	9.51E-16	1.11E-15	1.29E-15	1.45E-15	8.92E-16	1.08E-15	1.28E-15

Table A-2 The amount of ions and dissolved neutral species in the pore solution after cement hydration when incorporating different contents of metakaolin and fly ash /mol/L

	5%MK	*10%MK*	*15%MK*	*20%FAS*	*40%FAS*	*20%FAC*	*40%FAC*
AlO_2^-	6.20E-06	6.21E-06	1.77E-05	8.44E-06	1.07E-05	7.86E-06	9.54E-06
AlO_2H	4.50E-13	4.89E-13	1.41E-12	5.63E-13	7.14E-13	5.40E-13	6.70E-13
$AlSiO_5^{3-}$	2.96E-09	2.40E-09	6.12E-09	4.98E-09	6.34E-09	4.29E-09	4.98E-09
$CaCO_3$	2.26E-11	2.73E-11	2.91E-11	1.86E-11	1.86E-11	1.75E-11	1.63E-11
$CaSO_4$	4.43E-08	4.78E-08	4.16E-09	5.60E-08	7.11E-08	5.36E-08	6.63E-08
Ca^{2+}	6.88E-06	8.36E-06	8.75E-06	7.68E-06	9.74E-06	7.69E-06	9.79E-06
$CaOH^+$	8.57E-06	9.95E-06	1.04E-05	1.00E-05	1.27E-05	9.88E-06	1.24E-05
$Ca(HSiO_3)^+$	1.47E-10	1.72E-10	1.66E-10	1.70E-10	2.15E-10	1.68E-10	2.13E-10
$CaSiO_3$	2.95E-07	3.24E-07	3.09E-07	3.65E-07	4.63E-07	3.53E-07	4.40E-07
FeO_2^-	1.12E-10	1.11E-10	4.34E-11	1.55E-10	1.96E-10	1.43E-10	1.73E-10
FeO_2H	3.19E-15	3.44E-15	1.36E-15	4.04E-15	5.13E-15	3.85E-15	4.75E-15
$K(SO_4)^-$	4.42E-06	3.76E-06	3.31E-07	7.07E-06	8.96E-06	4.96E-06	4.34E-06
K^+	0.003807	0.003786	0.004043	0.005191	0.006573	0.003864	0.003514
KOH	0.000223	0.000208	0.00022	0.000325	0.000412	0.000236	0.000212
Mg^{2+}	3.21E-13	3.90E-13	2.44E-13	3.59E-13	4.56E-13	3.60E-13	4.58E-13
$MgOH^+$	8.76E-12	1.01E-11	6.31E-12	1.03E-11	1.30E-11	1.01E-11	1.27E-11
$MgSiO_3$	1.74E-13	1.90E-13	1.08E-13	2.15E-13	2.73E-13	2.08E-13	2.59E-13
$Na(CO_3)^-$	2.76E-10	2.68E-10	2.41E-10	2.86E-10	2.88E-10	3.73E-10	4.41E-10
$NaHCO_3$	4.61E-15	4.87E-15	4.43E-15	4.39E-15	4.42E-15	5.91E-15	7.12E-15

$Na(SO_4)^-$	1.22E-06	1.06E-06	7.77E-08	1.94E-06	2.50E-06	2.58E-06	4.05E-06
Na^+	0.001487	0.001506	0.001339	0.002018	0.002586	0.002841	0.00463
$NaOH$	0.000166	0.000158	0.000139	0.000241	0.000309	0.000331	0.000531
$HSiO_3^-$	9.47E-08	9.59E-08	9.03E-08	1.27E-07	1.62E-07	1.19E-07	1.46E-07
SiO_2	1.60E-11	1.76E-11	1.68E-11	1.98E-11	2.51E-11	1.91E-11	2.39E-11
SiO_3^{2-}	3.85E-07	3.52E-07	3.26E-07	5.73E-07	7.28E-07	5.17E-07	6.17E-07
CO_3^{2-}	7.01E-10	7.05E-10	7.30E-10	6.95E-10	6.93E-10	6.09E-10	5.43E-10
HCO_3^-	1.72E-13	1.91E-13	2.01E-13	1.54E-13	1.53E-13	1.40E-13	1.28E-13
O_2	1.76E-05	1.92E-05	1.98E-05	2.20E-05	2.80E-05	2.12E-05	2.62E-05
SO_4^{2-}	1.15E-05	1.03E-05	8.75E-07	1.75E-05	2.23E-05	1.57E-05	1.85E-05
OH^-	0.005281	0.005286	0.00539	0.007181	0.009123	0.006683	0.00812
H^+	8.09E-16	9.40E-16	9.78E-16	9.47E-16	1.20E-15	9.32E-16	1.17E-15

Table A-3 Phases formed after cement hydration with different SCMs/g per 100 g blended cement

	cement	*20%slag*	*30%slag*	*40%slag*	*50%slag*	*5%SF*	*10%SF*	*15%SF*	*5%MK*	*10%MK*	*15%MK*	*20%FAS*	*40%FAS*	*20%FAC*	*40%FAC*
aqueous	14.26	16.24	17.01	17.97	18.76	14.45	14.83	15.34	15.35	16.57	17.08	19.25	24.37	18.62	23.10
$C_3(AF)S_{0.84}H$	13.00	10.68	9.49	8.29	7.11	12.03	10.89	9.72	12.50	11.92	11.38	22.23	31.40	13.05	13.03
CNKASNH	53.78	57.00	58.62	60.24	61.83	65.14	76.61	88.13	54.93	56.10	57.21	48.63	43.51	50.68	47.58
ettringite	13.50	7.94	4.86	1.78	0.00	12.85	12.20	11.55	7.99	1.86	0.00	11.11	8.10	8.86	3.58
Portlandite	43.12	31.45	25.48	19.52	13.72	33.30	23.51	13.69	36.65	29.92	23.49	25.36	7.32	30.19	17.00
Hydrotalcite	7.75	8.24	8.49	8.73	8.98	7.44	7.12	6.80	7.37	6.98	6.59	6.40	5.05	7.49	7.23
AFm phase	0.00	8.07	12.60	17.14	20.37	0.00	0.00	0.00	8.38	16.94	22.03	0.24	1.49	4.34	9.73

Table A-4 The amount of end-members of C-S-H formed after cement hydration/mol per 100 g blended cement

	5CA	***5CNA***	***INFCA***	***INFCK***	***INFCKA***	***INFCN***	***INFCNA***	***T2C***	***T5C***	***TobH***	***K-containing endmembers***	***Na-containing endmembers***
cement	0.0721	0.0047	0.0022	0.0307	0.0028	0.0065	0.0018	0.1462	0.0225	0.0001	0.0335	0.0130
20%slag	0.0861	0.0050	0.0027	0.0251	0.0026	0.0059	0.0018	0.1549	0.0238	0.0001	0.0277	0.0128
30%slag	0.0899	0.0049	0.0029	0.0227	0.0023	0.0058	0.0018	0.1618	0.0250	0.0001	0.0250	0.0126
40%slag	0.0936	0.0049	0.0030	0.0202	0.0020	0.0058	0.0018	0.1687	0.0261	0.0001	0.0222	0.0124
50%slag	0.1035	0.0051	0.0034	0.0175	0.0019	0.0054	0.0018	0.1705	0.0263	0.0001	0.0194	0.0123
5%SF	0.0765	0.0041	0.0023	0.0325	0.0021	0.0071	0.0014	0.1933	0.0304	0.0002	0.0347	0.0126
10%SF	0.0832	0.0038	0.0024	0.0336	0.0018	0.0072	0.0012	0.2395	0.0382	0.0002	0.0354	0.0121
15%SF	0.0901	0.0035	0.0026	0.0344	0.0016	0.0072	0.0010	0.2860	0.0460	0.0003	0.0360	0.0117
5%MK	0.0813	0.0049	0.0026	0.0284	0.0030	0.0058	0.0018	0.1462	0.0224	0.0001	0.0315	0.0125
10%MK	0.0841	0.0047	0.0027	0.0269	0.0028	0.0056	0.0017	0.1513	0.0232	0.0001	0.0297	0.0120
15%MK	0.1022	0.0053	0.0034	0.0242	0.0035	0.0046	0.0020	0.1439	0.0217	0.0001	0.0277	0.0119
20%FAS	0.0710	0.0046	0.0022	0.0273	0.0029	0.0055	0.0018	0.1275	0.0194	0.0001	0.0302	0.0119
40%FAS	0.0634	0.0041	0.0020	0.0246	0.0026	0.0050	0.0016	0.1140	0.0174	0.0001	0.0272	0.0107
20%FAC	0.0746	0.0058	0.0024	0.0242	0.0025	0.0073	0.0024	0.1340	0.0205	0.0001	0.0267	0.0155
40%FAC	0.0707	0.0062	0.0022	0.0189	0.0019	0.0082	0.0027	0.1270	0.0194	0.0001	0.0208	0.0171

Table A-5 The atoms contained in the C-S-H/mol per 100 g blended cement

	Al	*Ca*	*K*	*Na*	*Si*	*Al/Si*	*(Na+K)/Si*
cement	0.021328	0.387496	0.021113	0.007622	0.315145	0.067678	0.09118
20%slag	0.025010	0.414335	0.017465	0.007463	0.331017	0.075555	0.075308
30%slag	0.025872	0.428008	0.015739	0.007357	0.339023	0.076314	0.068126
40%slag	0.026735	0.441664	0.014029	0.007248	0.347030	0.07704	0.061311
50%slag	0.029401	0.454560	0.012273	0.007190	0.355012	0.082815	0.054824
5%SF	0.021951	0.474301	0.021808	0.007427	0.378472	0.057999	0.077244
10%SF	0.023417	0.562117	0.022249	0.007191	0.442155	0.052962	0.066582
15%SF	0.024999	0.650386	0.022569	0.006911	0.505886	0.049415	0.058274
5%MK	0.023872	0.396857	0.019846	0.007343	0.320775	0.074421	0.084762
10%MK	0.024456	0.406739	0.018748	0.007027	0.326544	0.074893	0.078932
15%MK	0.029641	0.414948	0.017503	0.006880	0.332247	0.089214	0.073388
20%FAS	0.021063	0.349942	0.019076	0.006968	0.285047	0.073892	0.091367
40%FAS	0.018839	0.312991	0.017164	0.006261	0.255088	0.073854	0.091832
20%FAC	0.022369	0.365976	0.016855	0.009093	0.296023	0.075566	0.087658
40%FAC	0.021373	0.344875	0.013136	0.010083	0.277040	0.077147	0.083808

Table A-6 The volume of two ASR products with total volume formed in the process of ASR/cm^3 per 100g blended cement

	K-shlykovite	*Na-shlykovite*	*Total*
cement	0.7174	0.2734	0.9908
20%slag	0.6281	0.2914	0.9195
30%slag	0.5676	0.3038	0.8714
40%slag	0.5044	0.3167	0.8211
50%slag	0.4577	0.3192	0.7769
5%SF	0.5617	0.2338	0.7954
10%SF	0.4739	0.1976	0.6715
15%SF	0.4142	0.1677	0.5819
5%MK	0.7055	0.2711	0.9766
10%MK	0.6871	0.2528	0.9399
15%MK	0.6549	0.2422	0.8972
20%FAS	1.0056	0.3724	1.3780
40%FAS	1.2767	0.4807	1.7573
20%FAC	0.7524	0.5125	1.2649
40%FAC	0.6851	0.8289	1.5140

Table A-7 The amounts of atoms in the pore solution after cement hydration, and the amount of alkalis inputted into modelling/mol per 100g blended cement

	Al	*Ca*	*Fe*	*K*	*Mg*	*Na*	*S*	*Si*	*K inputted*	*Na inputted*
cement	0.000252	0.001029	1.16E-08	0.25127	7.66E-10	0.124088	0.001565	5.23E-05	0.024681	0.009355
20%slag	0.000341	0.00127	6.08E-09	0.195794	7.11E-10	0.11451	0.000711	4.25E-05	0.020638	0.00929
30%slag	0.000309	0.001427	5.45E-09	0.167526	7.78E-10	0.112375	0.000551	3.91E-05	0.018617	0.009258
40%slag	0.00028	0.001607	4.88E-09	0.141438	8.51E-10	0.11063	0.000427	3.64E-05	0.016596	0.009226
50%slag	0.000368	0.001789	3.15E-09	0.121343	7.70E-10	0.107228	0.000148	3.34E-05	0.014574	0.009194
5%SF	8.48E-05	0.001329	2.03E-08	0.19926	1.45E-09	0.101809	0.001627	4.51E-05	0.024723	0.008887
10%SF	4.26E-05	0.00164	2.55E-08	0.167001	2.20E-09	0.083418	0.001473	4.07E-05	0.024766	0.008419
15%SF	2.49E-05	0.001967	2.85E-08	0.144444	3.06E-09	0.068878	0.00131	3.80E-05	0.023553	0.009048
5%MK	0.000384	0.001103	6.95E-09	0.239303	6.37E-10	0.111763	0.00097	4.75E-05	0.022426	0.008742
10%MK	0.000356	0.001207	6.38E-09	0.220005	6.83E-10	0.104113	0.000797	4.41E-05	0.021298	0.008435
15%MK	0.000917	0.001253	2.47E-09	0.219781	4.31E-10	0.091284	6.98E-05	3.96E-05	0.024502	0.009426
20%FAF	0.000416	0.001002	7.62E-09	0.261742	5.91E-10	0.120689	0.001198	5.17E-05	0.024323	0.009497
40%FAF	0.000418	0.000995	7.67E-09	0.263402	5.88E-10	0.121263	0.001216	5.21E-05	0.020569	0.012093
20%FAC	0.000408	0.001026	7.43E-09	0.201359	6.02E-10	0.175982	0.001121	5.09E-05	0.016458	0.014831
40%FAC	0.000406	0.001034	7.34E-09	0.147845	6.06E-10	0.22951	0.001087	5.08E-05	0.024809	0.007952

Appendix B Supporting information for Chapter 5

Table B-1 The amounts of ions and dissolved neutral species in the pore solution after blast furnace slag hydration when activated by NaOH /mol/L

Dosage of NaOH	*2%*	*4%*	*6%*	*8%*
AlO^{+}	2.39E-19	9.06E-20	3.03E-20	9.71E-21
AlO_2^{-}	3.88E-05	2.14E-04	3.31E-04	0.000318
AlO_2H	3.27E-12	4.46E-12	3.00E-12	1.55E-12
$AlOH^{2+}$	3.48E-26	3.87E-27	6.66E-28	1.30E-28
$AlHSiO_3^{2+}$	1.97E-32	1.97E-33	0.00E+00	0.00E+00
$AlSiO_5^{3-}$	6.02E-08	6.03E-06	3.60E-05	7.17E-05
$Ca(SO_4)$	8.27E-09	9.79E-09	1.22E-08	7.44E-09
Ca^{2+}	2.54E-05	1.73E-06	5.27E-07	2.76E-07
$CaOH^{+}$	1.19E-05	2.68E-06	1.50E-06	1.20E-06
$Ca(HSiO_3)^{+}$	2.84E-10	5.71E-11	1.91E-11	8.20E-12
$CaSiO_3$	3.31E-07	2.48E-07	1.75E-07	1.31E-07
$Fe(HSO_4)^{+}$	4.12E-25	3.20E-26	6.47E-27	9.57E-28
$Fe(SO_4)$	6.22E-13	1.80E-13	7.69E-14	1.99E-14
Fe^{2+}	2.15E-09	3.56E-11	3.72E-12	8.28E-13
$FeOH^{+}$	1.92E-06	1.05E-07	2.03E-08	6.85E-09
FeO^{+}	1.22E-13	8.42E-15	1.82E-15	6.07E-16
FeO_2^{-}	0.004507	0.004509	0.004509	0.004509
FeO_2H	1.49E-07	3.69E-08	1.60E-08	8.61E-09

$FeOH^{2+}$	1.24E-22	2.51E-24	2.79E-25	5.66E-26
$FeHSiO_3^{2+}$	2.40E-29	4.35E-31	2.87E-32	3.15E-33
$K(SO_4)^-$	6.40E-08	6.83E-07	3.42E-06	5.32E-06
K^+	0.000496	0.000257	0.000266	0.000314
KOH	1.62E-05	3.03E-05	6.28E-05	1.20E-04
Mg^{2+}	2.65E-11	1.97E-12	5.70E-13	2.63E-13
$MgOH^+$	2.71E-10	6.69E-11	3.56E-11	2.50E-11
$MgSO_4$	1.01E-14	1.31E-14	1.55E-14	8.31E-15
$Mg(HSiO_3)^+$	5.89E-16	1.30E-16	4.11E-17	1.56E-17
$MgSiO_3$	4.34E-12	3.56E-12	2.38E-12	1.57E-12
$Na(SO_4)^-$	2.68E-06	8.45E-05	5.96E-04	1.02E-03
Na^+	0.029326	0.044922	0.065426	0.085455
$NaOH$	0.001829	0.010081	0.029426	0.06215
$HSiO_3^-$	1.30E-07	4.47E-07	5.19E-07	4.18E-07
$Si_4O_{10}^{4-}$	8.53E-17	2.23E-14	1.05E-13	1.14E-13
SiO_2	2.65E-11	2.34E-11	1.24E-11	5.83E-12
SiO_3^{2-}	6.74E-07	1.02E-05	2.97E-05	4.73E-05
H_2	1.32E-09	8.27E-10	5.86E-10	5.24E-10
$S_2O_3^{2-}$	2.74E-15	1.71E-14	4.49E-14	3.88E-14
HSO_3^-	2.17E-20	7.76E-20	1.33E-19	9.65E-20
SO_3^{2-}	1.45E-13	2.28E-12	9.79E-12	1.41E-11
HSO_4^-	2.93E-18	1.61E-17	3.29E-17	2.15E-17
SO_4^{2-}	3.35E-06	8.05E-05	4.14E-04	5.34E-04

H_2S	5.92E-09	1.47E-09	6.36E-10	3.43E-10
HS^-	0.020134	0.020134	0.020132	0.02013
S^{2-}	2.24E-07	9.82E-07	2.46E-06	4.86E-06
OH^-	0.005196	0.020042	0.039123	0.058399
H^+	1.66E-15	4.40E-16	1.86E-16	9.24E-17
H_2O	1.235126	1.361415	1.429914	1.455378

Table B-2 The amounts of ions and dissolved neutral species in the pore solution after blast furnace slag hydration when activated by Na_2SO_4 /mol/L

Dosage of Na_2SO_4	*2%*	*4%*	*6%*	*8%*
AlO^+	1.25E-18	9.88E-20	1.04E-20	6.50E-21
AlO_2^-	1.54E-05	5.75E-05	5.47E-05	3.21E-05
AlO_2H	4.64E-12	2.39E-12	6.59E-13	3.57E-13
$AlOH^{2+}$	6.83E-25	8.72E-27	3.72E-28	2.56E-28
$AlHSiO_3^{2+}$	2.48E-30	1.03E-32	0	0
$AlSiO_5^{3-}$	1.27E-08	9.91E-07	6.87E-06	4.09E-06
$Ca(SO_4)$	8.56E-08	6.23E-08	1.05E-07	2.44E-07
Ca^{2+}	5.87E-05	2.51E-06	3.47E-07	3.68E-07
$CaOH^+$	7.28E-06	1.88E-06	5.74E-07	4.85E-07
$Ca(HSiO_3)^+$	1.11E-09	9.30E-11	1.18E-11	7.53E-12
$CaSiO_3$	3.54E-07	1.98E-07	7.35E-08	4.65E-08
$Fe(HSO_4)^+$	2.43E-22	1.92E-24	3.27E-25	8.45E-25
$Fe(SO_4)$	1.00E-10	5.29E-12	2.64E-12	6.75E-12
Fe^{2+}	7.69E-08	2.39E-10	9.84E-12	1.14E-11
$FeOH^+$	1.82E-05	3.41E-07	3.10E-08	2.87E-08
FeO^+	1.61E-12	3.42E-14	3.80E-15	4.03E-15
FeO_2^-	0.00449	0.004508	0.004509	0.004509
FeO_2H	5.30E-07	7.36E-08	2.13E-08	1.97E-08
$FeOH^{2+}$	6.13E-21	2.10E-23	9.43E-25	1.11E-24
$FeHSiO_3^{2+}$	7.60E-27	8.46E-30	1.57E-31	1.40E-31

$K(SO_4)^-$	1.39E-07	1.94E-06	3.17E-05	0.000119
K^+	0.000229	0.000161	0.000155	0.000222
KOH	2.03E-06	9.30E-06	2.34E-05	2.91E-05
Mg^{2+}	2.18E-10	5.83E-12	7.97E-13	8.93E-13
$MgOH^+$	5.93E-10	9.57E-11	2.88E-11	2.57E-11
$MgSO_4$	3.74E-13	1.70E-13	2.82E-13	6.94E-13
$Mg(HSiO_3)^+$	8.25E-15	4.32E-16	5.40E-17	3.64E-17
$MgSiO_3$	1.66E-11	5.82E-12	2.13E-12	1.42E-12
$Na(SO_4)^-$	1.09E-05	0.000272	0.007052	0.027542
Na^+	0.025413	0.031816	0.048818	0.072581
$NaOH$	0.00043	0.003513	0.014045	0.018178
$HSiO_3^-$	1.77E-07	3.37E-07	2.33E-07	1.14E-07
$Si_4O_{10}^{4-}$	7.68E-16	2.92E-14	1.44E-13	5.81E-14
SiO_2	1.30E-10	3.53E-11	7.92E-12	4.08E-12
SiO_3^{2-}	2.64E-07	3.92E-06	1.11E-05	6.41E-06
H_2	5.30E-10	3.43E-10	1.24E-10	6.43E-11
$S_2O_3^{2-}$	4.87E-14	1.60E-13	1.23E-12	4.05E-12
HSO_3^-	1.51E-19	2.97E-19	6.99E-19	1.09E-18
SO_3^{2-}	2.89E-13	4.44E-12	4.28E-11	7.87E-11
HSO_4^-	3.89E-17	9.61E-17	3.01E-16	5.44E-16
SO_4^{2-}	1.27E-05	0.000245	0.003142	0.006706
H_2S	2.12E-08	2.93E-09	8.47E-10	7.84E-10
HS^-	0.020132	0.020134	0.020132	0.020132

S^{2-}	6.40E-08	5.00E-07	2.04E-06	2.41E-06
OH^-	0.00111	0.006508	0.010863	0.007028
H^+	4.67E-15	5.80E-16	1.07E-16	7.39E-17
H_2O	0.975888	0.908399	0.749276	0.769943

Table B-3 The amounts of ions and dissolved neutral species in the pore solution after blast furnace slag hydration when activated by silicate activators with dosage of 2% Na_2O_{eq} /mol/L

Modulus	*0.5*	*1*	*1.5*	*2*
AlO^+	2.40E-19	5.52E-19	1.92E-18	5.68E-18
AlO_2^-	3.50E-05	2.57E-05	1.55E-05	7.74E-06
AlO_2H	3.09E-12	4.07E-12	5.95E-12	7.28E-12
$AlOH^{2+}$	3.73E-26	1.49E-25	1.21E-24	8.62E-24
$AlHSiO_3^{2+}$	2.13E-32	2.07E-31	5.41E-30	7.53E-29
$AlSiO_5^{3-}$	5.04E-08	2.68E-08	8.46E-09	1.35E-09
$Ca(SO_4)$	7.89E-09	3.94E-08	1.12E-07	1.67E-07
Ca^{2+}	2.72E-05	4.10E-05	8.93E-05	0.000312
$CaOH^+$	1.19E-05	1.04E-05	9.72E-06	1.42E-05
$Ca(HSiO_3)^+$	2.85E-10	6.10E-10	1.82E-09	5.20E-09
$CaSiO_3$	3.14E-07	3.82E-07	4.78E-07	5.63E-07
$Fe(HSO_4)^+$	4.69E-25	1.19E-23	4.34E-22	6.15E-21
$Fe(SO_4)$	6.69E-13	9.64E-12	1.47E-10	8.62E-10
Fe^{2+}	2.59E-09	1.13E-08	1.31E-07	1.81E-06
$FeOH^+$	2.16E-06	5.47E-06	2.73E-05	0.000156
FeO^+	1.36E-13	4.27E-13	2.45E-12	1.41E-11
FeO_2^-	0.004506	0.004503	0.004481	0.004349
FeO_2H	1.56E-07	2.80E-07	6.74E-07	1.60E-06
$FeOH^{2+}$	1.48E-22	8.01E-22	1.08E-20	1.49E-19
$FeHSiO_3^{2+}$	2.88E-29	3.80E-28	1.64E-26	4.44E-25

$K(SO_4)^-$	5.56E-08	1.19E-07	1.02E-07	4.60E-08
K^+	0.000477	0.00032	0.000216	0.000232
KOH	1.47E-05	5.63E-06	1.60E-06	7.11E-07
Mg^{2+}	2.84E-11	7.79E-11	3.75E-10	2.04E-09
$MgOH^+$	2.72E-10	4.34E-10	8.93E-10	2.02E-09
$MgSO_4$	9.65E-15	8.79E-14	5.54E-13	1.28E-12
$Mg(HSiO_3)^+$	5.92E-16	2.31E-15	1.52E-14	6.77E-14
$MgSiO_3$	4.12E-12	9.14E-12	2.53E-11	4.62E-11
$Na(SO_4)^-$	2.38E-06	7.12E-06	8.51E-06	3.36E-06
Na^+	0.028798	0.026937	0.025351	0.023923
$NaOH$	0.001692	0.000904	0.000358	0.00014
$HSiO_3^-$	1.17E-07	1.63E-07	2.20E-07	1.80E-07
$Si_4O_{10}^{4-}$	7.02E-17	2.23E-16	6.40E-16	2.55E-16
SiO_2	2.51E-11	6.25E-11	2.04E-10	4.08E-10
SiO_3^{2-}	5.82E-07	4.45E-07	2.44E-07	8.10E-08
H_2	1.28E-09	8.47E-10	6.52E-10	6.61E-10
$S_2O_3^{2-}$	2.65E-15	1.46E-14	4.34E-14	4.34E-14
HSO_3^-	2.01E-20	7.46E-20	1.74E-19	1.78E-19
SO_3^{2-}	1.29E-13	2.63E-13	2.48E-13	1.03E-13
HSO_4^-	2.66E-18	1.52E-17	4.70E-17	4.86E-17
SO_4^{2-}	2.91E-06	9.16E-06	1.15E-05	4.80E-06
H_2S	6.22E-09	1.11E-08	2.70E-08	6.60E-08
HS^-	0.020134	0.020134	0.020131	0.020115

S^{2-}	2.15E-07	1.18E-07	4.78E-08	1.93E-08
OH^-	0.004658	0.002665	0.001123	0.000469
H^+	1.66E-15	2.97E-15	7.21E-15	1.78E-14
H_2O	1.176565	1.175988	1.176851	1.18905

Table B-4 The amounts of ions and dissolved neutral species in the pore solution after blast furnace slag hydration when activated by silicate activators with dosage of 4% Na_2O_{eq} /mol/L

Modulus	*0.5*	*1*	*1.5*	*2*
AlO^+	8.69E-20	1.04E-19	2.22E-19	5.56E-19
AlO_2^-	0.000187	0.000167	0.000101	4.99E-05
AlO_2H	4.07E-12	4.24E-12	4.99E-12	5.70E-12
$AlOH^{2+}$	3.93E-27	5.40E-27	2.01E-26	1.07E-25
$AlHSiO_3^{2+}$	2.01E-33	3.52E-33	2.55E-32	2.54E-31
$AlSiO_5^{3-}$	4.93E-06	4.05E-06	1.12E-06	1.70E-07
$Ca(SO_4)$	9.01E-09	1.35E-08	4.24E-08	8.54E-08
Ca^{2+}	1.75E-06	1.87E-06	4.03E-06	1.32E-05
$CaOH^+$	2.57E-06	2.39E-06	3.01E-06	4.67E-06
$Ca(HSiO_3)^+$	5.50E-11	6.54E-11	1.60E-10	4.65E-10
$CaSiO_3$	2.27E-07	2.33E-07	3.10E-07	4.05E-07
$Fe(HSO_4)^+$	3.61E-26	8.53E-26	1.23E-24	1.75E-23
$Fe(SO_4)$	1.93E-13	3.94E-13	3.08E-12	1.97E-11
Fe^{2+}	4.21E-11	6.12E-11	3.29E-10	3.41E-09
$FeOH^+$	1.17E-07	1.49E-07	4.67E-07	2.31E-06
FeO^+	9.26E-15	1.24E-14	4.35E-14	2.21E-13
FeO_2^-	0.004509	0.004509	0.004508	0.004506
FeO_2H	3.85E-08	4.49E-08	8.69E-08	2.02E-07
$FeOH^{2+}$	2.91E-24	4.49E-24	2.75E-23	2.98E-22
$FeHSiO_3^{2+}$	5.08E-31	9.98E-31	1.19E-29	2.40E-28

$K(SO_4)^-$	5.54E-07	6.19E-07	6.46E-07	3.45E-07
K^+	0.000227	0.000183	0.000145	0.000138
KOH	2.54E-05	1.78E-05	7.81E-06	3.37E-06
Mg^{2+}	2.00E-12	2.51E-12	8.09E-12	3.81E-11
$MgOH^+$	6.42E-11	7.03E-11	1.32E-10	2.96E-10
$MgSO_4$	1.21E-14	2.13E-14	1.00E-13	2.90E-13
$Mg(HSiO_3)^+$	1.25E-16	1.75E-16	6.40E-16	2.68E-15
$MgSiO_3$	3.27E-12	3.95E-12	7.82E-12	1.48E-11
$Na(SO_4)^-$	7.30E-05	9.47E-05	0.000105	5.09E-05
Na^+	0.042275	0.039653	0.033423	0.028654
$NaOH$	0.009013	0.007342	0.003424	0.001338
$HSiO_3^-$	3.91E-07	4.22E-07	4.72E-07	4.11E-07
$Si_4O_{10}^{4-}$	1.80E-14	2.43E-14	2.09E-14	7.33E-15
SiO_2	2.14E-11	2.68E-11	5.70E-11	1.14E-10
SiO_3^{2-}	8.60E-06	7.88E-06	4.34E-06	1.56E-06
H_2	7.76E-10	6.83E-10	5.97E-10	6.00E-10
$S_2O_3^{2-}$	1.66E-14	2.62E-14	5.94E-14	7.03E-14
HSO_3^-	7.04E-20	9.87E-20	2.05E-19	2.55E-19
SO_3^{2-}	1.99E-12	2.38E-12	2.43E-12	1.24E-12
HSO_4^-	1.41E-17	2.21E-17	5.87E-17	7.86E-17
SO_4^{2-}	6.81E-05	9.09E-05	0.000119	6.54E-05
H_2S	1.53E-09	1.79E-09	3.46E-09	8.03E-09
HS^-	0.020134	0.020134	0.020134	0.020134

S^{2-}	9.46E-07	8.05E-07	3.95E-07	1.63E-07
OH^-	0.017435	0.014726	0.008479	0.003948
H^+	4.21E-16	4.77E-16	9.62E-16	2.28E-15
H_2O	1.251122	1.210991	1.234752	1.251524

Table B-5 The amounts of ions and dissolved neutral species in the pore solution after blast furnace slag hydration when activated by silicate activators with dosage of 6% Na_2O_{eq} /mol/L

Modulus	*0.5*	*1*	*1.5*	*2*
AlO^+	4.89E-20	7.91E-20	9.03E-20	2.02E-19
AlO_2^-	0.000333	0.000292	0.000235	0.000125
AlO_2H	3.89E-12	4.77E-12	4.63E-12	5.29E-12
$AlOH^{2+}$	1.33E-27	2.80E-27	3.74E-27	1.57E-26
$AlHSiO_3^{2+}$	0	1.39E-33	2.20E-33	1.82E-32
$AlSiO_5^{3-}$	2.70E-05	1.40E-05	8.95E-06	1.71E-06
$Ca(SO_4)$	1.07E-08	9.96E-09	1.27E-08	3.93E-08
Ca^{2+}	6.38E-07	1.03E-06	1.26E-06	3.37E-06
$CaOH^+$	1.50E-06	1.90E-06	2.00E-06	2.93E-06
$Ca(HSiO_3)^+$	2.50E-11	3.97E-11	4.94E-11	1.43E-10
$CaSiO_3$	1.81E-07	2.14E-07	2.24E-07	3.22E-07
$Fe(HSO_4)^+$	1.18E-26	2.27E-26	4.55E-26	7.36E-25
$Fe(SO_4)$	1.11E-13	1.58E-13	2.67E-13	2.15E-12
Fe^{2+}	7.46E-12	1.83E-11	2.96E-11	2.07E-10
$FeOH^+$	3.35E-08	6.44E-08	8.96E-08	3.43E-07
FeO^+	2.93E-15	5.39E-15	7.64E-15	3.20E-14
FeO_2^-	0.004509	0.004509	0.004509	0.004508
FeO_2H	2.07E-08	2.89E-08	3.48E-08	7.46E-08
$FeOH^{2+}$	5.54E-25	1.33E-24	2.21E-24	1.74E-23
$FeHSiO_3^{2+}$	7.49E-32	2.26E-31	4.43E-31	6.85E-30

$K(SO_4)^-$	1.88E-06	8.95E-07	7.60E-07	6.08E-07
K^+	0.000211	0.000187	0.000155	0.000124
KOH	4.02E-05	2.69E-05	1.90E-05	7.75E-06
Mg^{2+}	7.37E-13	1.22E-12	1.64E-12	6.41E-12
$MgOH^+$	3.80E-11	4.93E-11	5.70E-11	1.22E-10
$MgSO_4$	1.45E-14	1.39E-14	1.95E-14	8.79E-14
$Mg(HSiO_3)^+$	5.76E-17	9.39E-17	1.28E-16	5.41E-16
$MgSiO_3$	2.64E-12	3.19E-12	3.67E-12	7.71E-12
$Na(SO_4)^-$	0.000353	0.000166	0.000155	0.000124
Na^+	0.056083	0.048957	0.044734	0.035659
$NaOH$	0.020336	0.013455	0.01044	0.00426
$HSiO_3^-$	5.28E-07	5.18E-07	5.06E-07	5.40E-07
$Si_4O_{10}^{4-}$	9.92E-14	5.84E-14	5.05E-14	2.85E-14
SiO_2	1.61E-11	2.15E-11	2.51E-11	5.59E-11
SiO_3^{2-}	2.28E-05	1.55E-05	1.24E-05	5.77E-06
H_2	6.10E-10	7.09E-10	6.73E-10	6.37E-10
$S_2O_3^{2-}$	3.76E-14	2.58E-14	3.06E-14	5.63E-14
HSO_3^-	1.18E-19	9.80E-20	1.12E-19	2.08E-19
SO_3^{2-}	6.59E-12	3.77E-12	3.53E-12	2.86E-12
HSO_4^-	2.82E-17	2.19E-17	2.61E-17	5.98E-17
SO_4^{2-}	0.000268	0.000144	0.000141	0.000141
H_2S	8.23E-10	1.15E-09	1.38E-09	2.97E-09
HS^-	0.020133	0.020133	0.020133	0.020134

S^{2-}	1.86E-06	1.29E-06	1.05E-06	4.60E-07
OH^-	0.030301	0.023683	0.019525	0.010601
H^+	2.31E-16	3.33E-16	3.89E-16	8.85E-16
H_2O	1.338413	1.337231	1.286174	1.32318

Table B-6 The amounts of ions and dissolved neutral species in the pore solution after blast furnace slag hydration when activated by silicate activators with dosage of 8% Na_2O_{eq} /mol/L

Modulus	*0.5*	*1*	*1.5*	*2*
AlO^+	2.00E-20	3.13E-20	5.23E-20	4.92E-20
AlO_2^-	0.000428	0.000377	0.000329	8.19E-05
AlO_2H	2.64E-12	3.21E-12	4.02E-12	2.04E-12
$AlOH^{2+}$	3.27E-28	6.63E-28	1.47E-27	2.51E-27
$AlHSiO_3^{2+}$	0	0	0	3.28E-33
$AlSiO_5^{3-}$	8.98E-05	4.95E-05	2.50E-05	4.16E-06
$Ca(SO_4)$	8.15E-09	1.18E-08	1.06E-08	6.11E-08
Ca^{2+}	2.59E-07	4.11E-07	6.83E-07	1.12E-06
$CaOH^+$	9.46E-07	1.20E-06	1.56E-06	1.46E-06
$Ca(HSiO_3)^+$	9.89E-12	1.60E-11	2.68E-11	8.01E-11
$CaSiO_3$	1.27E-07	1.54E-07	1.87E-07	2.91E-07
$Fe(HSO_4)^+$	2.48E-27	6.66E-27	1.28E-26	4.60E-25
$Fe(SO_4)$	4.13E-14	8.29E-14	1.16E-13	2.16E-12
Fe^{2+}	1.47E-12	3.23E-12	8.36E-12	4.44E-11
$FeOH^+$	1.02E-08	1.81E-08	3.64E-08	1.10E-07
FeO^+	9.30E-16	1.65E-15	3.17E-15	1.20E-14
FeO_2^-	0.004509	0.004509	0.004509	0.004509
FeO_2H	1.09E-08	1.51E-08	2.16E-08	4.40E-08
$FeOH^{2+}$	1.06E-25	2.44E-25	6.19E-25	4.24E-24
$FeHSiO_3^{2+}$	9.01E-33	2.64E-32	8.65E-32	1.89E-30

$K(SO_4)^-$	4.24E-06	3.02E-06	1.27E-06	1.78E-06
K^+	0.000222	0.000184	0.000156	6.96E-05
KOH	7.00E-05	4.52E-05	2.86E-05	6.89E-06
Mg^{2+}	2.88E-13	4.65E-13	7.91E-13	3.76E-12
$MgOH^+$	2.30E-11	2.98E-11	3.95E-11	1.07E-10
$MgSO_4$	1.07E-14	1.57E-14	1.44E-14	2.41E-13
$Mg(HSiO_3)^+$	2.20E-17	3.61E-17	6.20E-17	5.38E-16
$MgSiO_3$	1.78E-12	2.19E-12	2.73E-12	1.23E-11
$Na(SO_4)^-$	0.000993	0.000748	0.00032	0.000793
Na^+	0.073367	0.064523	0.05534	0.043759
$NaOH$	0.044144	0.030152	0.019379	0.008263
$HSiO_3^-$	5.04E-07	5.25E-07	5.33E-07	9.62E-07
$Si_4O_{10}^{4-}$	2.23E-13	1.54E-13	9.42E-14	4.77E-13
SiO_2	8.64E-12	1.20E-11	1.69E-11	5.98E-11
SiO_3^{2-}	4.42E-05	3.22E-05	2.20E-05	1.83E-05
H_2	4.84E-10	5.18E-10	6.26E-10	4.49E-10
$S_2O_3^{2-}$	5.21E-14	5.56E-14	3.56E-14	1.95E-13
HSO_3^-	1.22E-19	1.44E-19	1.16E-19	4.82E-19
SO_3^{2-}	1.38E-11	1.14E-11	6.14E-12	1.18E-11
HSO_4^-	2.93E-17	3.66E-17	2.74E-17	1.83E-16
SO_4^{2-}	0.000565	0.000494	0.000248	0.000768
H_2S	4.34E-10	6.00E-10	8.60E-10	1.75E-09
HS^-	0.020131	0.020132	0.020133	0.020134

S^{2-}	3.77E-06	2.64E-06	1.77E-06	8.20E-07
OH^-	0.046029	0.037734	0.029589	0.016726
H^+	1.12E-16	1.63E-16	2.44E-16	5.22E-16
H_2O	1.343625	1.347699	1.346144	1.349305

Table B-7 The amounts of ions and dissolved neutral species in the pore solution after blast furnace slag hydration when activated by Na_2CO_3 /mol/L

Dosage of Na_2CO_3	*2%*	*4%*	*6%*	*8%*
AlO^+	8.41E-18	1.11E-19	1.45E-20	6.76E-21
AlO_2^-	6.00E-06	2.98E-05	6.98E-05	0.000103
AlO_2H	7.93E-12	1.91E-12	9.71E-13	7.55E-13
$AlSiO_5^{3-}$	6.37E-10	4.46E-07	1.11E-05	3.97E-05
$Ca(CO_3)$	8.48E-08	8.79E-08	7.59E-08	6.80E-08
$Ca(HCO_3)^+$	2.04E-11	1.13E-12	2.38E-13	1.20E-13
$Ca(SO_4)$	1.93E-07	2.18E-07	1.64E-08	5.17E-09
Ca^{2+}	0.000462	3.63E-06	3.78E-07	1.65E-07
$CaOH^+$	1.59E-05	2.08E-06	7.48E-07	5.10E-07
$Ca(HSiO_3)^+$	7.65E-09	2.51E-10	3.41E-11	1.38E-11
$CaSiO_3$	6.06E-07	3.72E-07	2.08E-07	1.48E-07
$Fe(CO_3)$	5.19E-09	1.96E-10	3.15E-11	1.42E-11
$Fe(HCO_3)^+$	6.84E-13	1.38E-15	5.40E-17	1.37E-17
$Fe(HSO_4)^+$	7.16E-21	1.58E-23	5.36E-26	4.81E-27
$Fe(SO_4)$	7.34E-10	3.03E-11	4.23E-13	6.72E-14
Fe^{2+}	1.97E-06	5.66E-10	1.09E-11	2.41E-12
$FeOH^+$	0.000129	6.16E-07	4.13E-08	1.42E-08
FeO^+	1.17E-11	7.37E-14	4.13E-15	1.31E-15
FeO_2^-	0.001889	0.004508	0.004509	0.004509
FeO_2H	9.79E-07	1.13E-07	2.46E-08	1.30E-08

$FeOH^{2+}$	1.64E-19	6.10E-23	9.33E-25	1.79E-25
$FeHSiO_3^{2+}$	6.42E-25	5.99E-29	3.46E-31	3.91E-32
$K(SO_4)^-$	4.28E-08	3.07E-06	3.20E-06	4.03E-06
K^+	0.000294	0.00012	0.000138	0.000211
KOH	6.63E-07	4.98E-06	2.22E-05	5.64E-05
$Mg(CO_3)$	3.76E-13	2.79E-13	1.89E-13	1.39E-13
$Mg(HCO_3)^+$	1.46E-16	5.78E-18	9.54E-19	3.95E-19
Mg^{2+}	3.60E-09	2.03E-11	1.65E-12	5.92E-13
$MgOH^+$	2.71E-09	2.53E-10	7.15E-11	4.00E-11
$MgSO_4$	1.76E-12	1.43E-12	8.42E-14	2.18E-14
$Mg(HSiO_3)^+$	1.19E-13	2.79E-15	2.98E-16	9.84E-17
$MgSiO_3$	5.95E-11	2.61E-11	1.14E-11	6.70E-12
$Na(CO_3)^-$	4.15E-07	0.000107	0.001816	0.005774
$Na(HCO_3)$	1.26E-10	1.58E-09	5.82E-09	9.78E-09
$Na(SO_4)^-$	2.13E-06	0.0006	0.000886	0.000993
Na^+	0.020687	0.033226	0.054036	0.073593
$NaOH$	8.89E-05	0.002614	0.016511	0.037449
$HSiO_3^-$	1.73E-07	8.26E-07	1.17E-06	1.10E-06
$Si_4O_{10}^{4-}$	1.67E-16	1.96E-13	2.76E-12	5.07E-12
SiO_2	5.46E-10	1.29E-10	4.22E-11	2.24E-11
SiO_3^{2-}	5.35E-08	5.84E-06	4.28E-05	8.14E-05
CO_2	6.31E-16	2.53E-16	1.27E-16	8.46E-17
CO_3^{2-}	1.78E-07	3.28E-05	0.000372	0.000886

HCO_3^-	5.72E-10	4.63E-09	1.02E-08	1.20E-08
CH_4	1.45E-11	6.41E-13	1.52E-12	2.14E-12
H_2	6.72E-10	3.62E-10	4.47E-10	4.69E-10
$S_2O_3^{2-}$	4.14E-14	4.44E-13	1.17E-13	6.15E-14
HSO_3^-	1.81E-19	9.29E-19	2.68E-19	1.39E-19
SO_3^{2-}	7.22E-14	8.46E-12	1.26E-11	1.32E-11
HSO_4^-	4.98E-17	4.39E-16	8.39E-17	3.49E-17
SO_4^{2-}	3.40E-06	0.000683	0.000674	0.000566
H_2S	9.15E-08	4.50E-09	9.78E-10	5.17E-10
HS^-	0.019807	0.020134	0.020133	0.020131
S^{2-}	1.31E-08	3.04E-07	1.57E-06	3.17E-06
OH^-	0.000342	0.006528	0.024546	0.039097
H^+	2.49E-14	1.25E-15	2.64E-16	1.33E-16
H_2O	1.181467	1.238539	1.291065	1.353811

Table B-8 Phases formed after blast furnace slag hydration when activated by NaOH/g per 100 g AAS

Dosage of NaOH	*Aqueous*	*CKNASH*	*Strätlingite*	*MgAl-OH-LDH*	C_3AH_6	Ca_4AsH_{12}
2%	22.677	18.575	7.009	4.079	1.736	0.483
4%	24.901	18.761	2.056	4.104	4.641	0.433
6%	26.107	18.858	0	4.059	6.107	0.170
8%	26.576	18.751	0	3.982	6.331	0

Table B-9 Phases formed after blast furnace slag hydration when activated by Na_2SO_4/g per 100 g AAS

Dosage of Na_2SO_4	*Aqueous*	*CKNASH*	*Strätlingite*	*Ettringite*	*MgAl-OH-LDH*	*Ca_4AsH_{12}*	*Brucite*	*Natrolite*
2%	18.008	17.488	7.021	7.965	4.137	0	0	0
4%	16.776	16.489	0	11.729	4.085	4.895	0	2.344
6%	14.061	15.687	0	19.131	3.980	2.149	0	2.438
8%	14.869	14.170	0	19.487	0	4.196	1.907	3.714

Table B-10 Phases formed after blast furnace slag hydration when activated by Na_2CO_3/g per 100 g AAS

Dosage of Na_2CO_3	*Aqueous*	*CKNASH*	*MgAl-OH-LDH*	*C4AcH11*	*Calcite*	*Brucite*	*Natrolite*
2%	21.714	17.562	4.161	7.799	0	0	1.626
4%	22.747	16.169	4.022	9.520	1.036	0	2.378
6%	23.638	15.150	3.953	9.424	2.165	0	2.790
8%	24.749	13.133	0	10.185	3.084	1.907	4.651

Table B-11 Phases formed after blast furnace slag hydration when activated by silicate activators/g per 100 g AAS

Dosage and modulus of silicate activators	*Aqueous*	*CKNASH*	*Strätlingite*	*Ettringite*	*MgAl-OH-LDH*	*C_3AH_6*	*Ca_4AsH_{12}*	*Natrolite*
2% / 0.5	21.621	19.083	8.794	0	4.078	0.428	0.483	0
2% / 1	21.618	19.552	9.018	0	4.106	0	0.480	0
2% / 1.5	21.638	20.010	8.772	0.364	4.140	0	0	0
2% / 2	21.856	20.510	7.594	0.371	4.155	0	0	0.657
4% / 0.5	22.919	19.784	5.365	0	4.104	2.183	0.441	0
4% / 1	22.204	20.777	8.293	0	4.111	0	0.427	0
4% / 1.5	22.656	21.664	6.385	0	4.123	0	0.415	1.464
4% / 2	22.977	22.577	4.387	0.341	4.131	0	0	3.073
6% / 0.5	24.468	20.429	0	0	4.095	4.598	0.291	1.201
6% / 1	24.456	21.930	0	0	4.114	3.020	0.388	2.667
6% / 1.5	23.547	23.410	3.599	0	4.114	0	0.393	3.076
6% / 2	24.245	24.739	0.506	0	4.121	0	0.402	5.524
8% / 0.5	24.566	21.068	0	0	4.052	4.568	0	1.141
8% / 1	24.634	23.083	0	0	4.074	2.592	0.098	2.995
8% / 1.5	24.607	25.072	0	0	4.097	0.490	0.308	4.937
8% / 2	24.712	26.408	0	0	4.022	0	0	6.769